

Changes to Lipid Ordering and Lipid Interactions Following Oxidative Damage to Lung Surfactant - a Molecular Dynamics Study

Merril Mathew

Supervisor: Dr. Katherine Thompson

Degree course: MSc. Bioinformatics with Systems
Biology



Department of Biological Sciences
Birkbeck, University of London
Malet Street, London WC1E 7HX
United Kingdom

Abstract

Lung surfactant is a mixture of lipid and proteins arranged into a monolayer. Lung surfactant has important biological roles in pulmonary health and disease and its primary function is to reduce the surface tension at the air-liquid interface, hence preventing alveolar collapse during the gaseous exchange. Lung surfactant serves as the first contact point between air and the inside of the body, consequently any pollutants found in the air can interact with lung surfactant components and potentially contribute to the respiratory diseases. Unsaturated lung surfactant lipids are susceptible to oxidation which can affect the normal function of the lung. In this research, oxidation product (PonPG) of 1-palmitoyl-2-oleoyl-*sn*-glycero-3-phospho-(1'-*rac*-glycerol) (POPG) following the reaction with ozone is systematically studied by means of molecular dynamics simulations. United-atom molecular dynamics simulations of various systems involving 1,2-dipalmitoyl-*sn*-glycero-3-phosphocholine (DPPC), POPG and the oxidised lipid reveal structural and functional changes of the lung surfactant monolayer which includes acyl-chain reversal of oxidised lipid, change in surface pressure, membrane thickness and increased fluidity and water penetration of the monolayer. The change in function of the monolayers is correlated with the presence and concentration of oxidised lipid and much of the effect is induced by the orientation and localisation of polar groups introduced by the oxidised lipid. Overall this study shows that the oxidation of lung surfactant lipids negatively affect the normal functions of the lung surfactant and shows the ability of molecular dynamic simulation as an important tool in pulmonary research to elicit important atomic level insight which maybe crucial for the understanding and impact on the respiratory health.

Contents

Abstract	2
List of figures	5
List of tables	6
List of abbreviations	7
Acknowledgements	9
1. Introduction	10
1.1 Lung surfactant	10
1.1.1 Lung structure and gaseous exchange	10
1.1.2 Lung surfactant and hypophase	10
1.1.3 Surface tension	11
1.1.4 Lung surfactant production	11
1.1.5 Lung surfactant functions	12
1.2 Lung surfactant composition	13
1.3 Lung surfactant lipids	13
1.4 Lung surfactant proteins	14
1.4.1 Surfactant protein A	15
1.4.2 Surfactant protein D	15
1.4.3 Surfactant protein C	15
1.4.4 Surfactant protein B	16
1.5 Functions of lipids in Lung surfactant	16
1.5.1 Role of DPPC and POPG in lung surfactant	17
1.6 Oxidative stress on lung surfactant	18
1.6.1 Ozonolysis	19
1.6.2 Oxidation of POPG to form PonPG	19
1.7 Functions of oxidised lipid in the lung surfactant	19
1.8 Research purpose	21
1.9 Molecular dynamics theory	21
1.10 Molecular dynamics simulations of monolayers	23
2. Materials and methods	23
2.0 Simulation	23
2.1 Simulated systems	23

2.2 Forcefield parameters	24
2.3 Simulation parameters	25
2.4 Analysis	27
2.4.1 Order parameter	27
2.4.2 Area per lipid	28
2.4.3 Monolayer thickness	28
2.4.4 Surface tension	28
2.4.5 Movement of lipid head groups	29
2.4.6 Acyl-chain reversal	29
3. Results	30
3.1 Standard results	31
3.2 Simulation specific results	33
3.2.1 Snapshots of monolayers at $80 \text{ \AA}^2 \text{ area lipid}^{-1}$	33
3.2.2 Snapshots of monolayers at $63 \text{ \AA}^2 \text{ area lipid}^{-1}$	36
3.2.3 Surface pressure	39
3.2.4 Monolayer thickness	43
3.2.5 Order parameter	44
3.2.6 Movement of lipid head groups	49
3.2.7 Movement of aldehyde group	53
3.2.8 Acyl-chain reversal	54
4. Discussion	56
5. Conclusion	62
6. References	64
7. Supplementary information	74

List of figures

Figure 1	Lung structure and mechanism of gas exchange	10
Figure 2	Alveolus and air-liquid interface	10
Figure 3	Surface tension of liquids	11
Figure 4	Surfactant production and film formation	12
Figure 5	Human lung surfactant composition of molecules	13
Figure 6	Chemical structure of phospholipids, DPPC, POPC and POPG	14
Figure 7	Surfactant associated proteins and different phases of monolayer	17
Figure 8	Formation of PonPG following the reaction with ozone	19
Figure 9	Order parameter of lipid acyl chains	27
Figure 10	Configuration of air-liquid interface at various stages of the simulation	30
Figure 11	Partial density of water in simulation	31
Figure 12	Plots of standard results – potential, temperature and pressure	32
Figure 13	Snapshots of monolayers at $80 \text{ \AA}^2 \text{ area lipid}^{-1}$	33
Figure 14	Snapshots of monolayers at $63 \text{ \AA}^2 \text{ area lipid}^{-1}$	36
Figure 15	Simulated surface tension of air-water interface	39
Figure 16	Simulated surface tension of air-lipid interface	39
Figure 17	Order parameter of <i>sn</i> -1 chains of DPPC at $80 \text{ \AA}^2 \text{ area lipid}^{-1}$	45
Figure 18	Order parameter of <i>sn</i> -1 chains of DPPC at $63 \text{ \AA}^2 \text{ area lipid}^{-1}$	45
Figure 19	Order parameter of <i>sn</i> -2 chains of DPPC at $80 \text{ \AA}^2 \text{ area lipid}^{-1}$	46
Figure 20	Order parameter of <i>sn</i> -2 chains of DPPC at $63 \text{ \AA}^2 \text{ area lipid}^{-1}$	46
Figure 21	Order parameter of <i>sn</i> -1 chains of POPG at $80 \text{ \AA}^2 \text{ area lipid}^{-1}$	47
Figure 22	Order parameter of <i>sn</i> -1 chains of POPG at $63 \text{ \AA}^2 \text{ area lipid}^{-1}$	47
Figure 23	Order parameter of <i>sn</i> -2 chains of POPG at $80 \text{ \AA}^2 \text{ area lipid}^{-1}$	48
Figure 24	Order parameter of <i>sn</i> -2 chains of POPG at $63 \text{ \AA}^2 \text{ area lipid}^{-1}$	48
Figure 25	Lipid head group movement in simulation	50
Figure 26	Movement of aldehyde group in simulation	53
Figure 27	Head group – aldehyde group distance of PonPG	54
Figure 28	Acyl-chain reversal of <i>sn</i> -2 chain of PonPG	54
Figure 29	Largest distance between the acyl chains of DPPC, POPG, and PonPG	57
Figure 30	Partial density of sodium ion in different systems	59
Figure 31	Sodium ion movement in simulation	60

List of tables

Table 1	Average surface tension and pressure of simulated systems	40
Table 2	Average surface tension/pressure at 0.5 ns intervals at 80 \AA^2 area lipid $^{-1}$	41
Table 3	Average surface tension/pressure at 0.5 ns intervals at 63 \AA^2 area lipid $^{-1}$	42
Table 4	Monolayer thickness of simulated systems	43
Table 5	Average head group movement of lipids in simulations at 80 \AA^2 area lipid $^{-1}$	50
Table 6	Average head group movement of lipids in simulations at 63 \AA^2 area lipid $^{-1}$	51
Table 7	Average movement of aldehyde group in simulations	53
Table 8	Percentage of lipids that carry out acyl-chain reversal	55
Table 9	Average movement of aldehyde group at 0.5 ns intervals at 80 \AA^2 area lipid $^{-1}$	55
Table 10	Average movement of aldehyde group at 0.5 ns intervals at 63 \AA^2 area lipid $^{-1}$	56

List of abbreviations

Å	Angstrom
ARDS	Acute Respiratory Distress Syndrome
Chol	Cholesterol
COM	Centre of mass
CRD	Carbohydrate recognition domain
CSV	Comma separated value
DlinPC	dilinolenoyl-sn-glycero-3-phosphocholine
DLPC	1,2-dilinoleoyl-sn-glycero-3-phosphocholine
DOPC	1,2-dioleoyl-sn-glycero-3-phosphocholine
DOPG	dioleoylphosphatidylglycerol
DPPC	Dipalmitoyl phosphatidylcholine
fs	femtosecond
GROMACS	GRO ningen M achine for C hemical S imulations
GROMOS	GRO ningen Molecular Simulation
IPF	Idiopathic pulmonary fibrosis
IRDS	Infant Respiratory Distress Syndrome
K	Kelvin
L _c	Liquid-condensed
L _e	Liquid-expanded
LINCS	LINEar Constraint Solver
L _o	Liquid-ordered
MD	Molecular Dynamics
NaCl	sodium chloride
NL	Neutral lipids
nm	nanometer
NMR	Nuclear Magnetic Resonance
NPT	Isothermal-isobaric ensemble
ns	nanosecond
NVT	Canonical ensemble
PBC	Periodic boundary conditions
PC	Phosphatidylcholine
PE	Phosphatidylethanolamine

PG	Phosphatidylglycerol
PI	phosphatidylinositol
PL	Phospholipids
PME	Particle-Mesh Ewald
POPC	Palmitoyl-oleoyl phosphatidylcholine
POPG	1-palmitoyl-2-oleoyl- <i>sn</i> -glycero-3-phospho-(1'- <i>rac</i> -glycerol)
ps	Picosecond
RDS	Respiratory distress syndrome
SP – A	Surfactant protein – A
SP – B	Surfactant protein – B
SP – C	Surfactant protein – C
SP – D	Surfactant protein – D
SPC	Single point charge
UFF	Universal Forcefield
WHO	World Health Organisation

Acknowledgements

I would first like to thank my supervisor Dr. Katherine Thompson for her expert knowledge and support. Thank you for the guidance and teaching me so much throughout the project.

I would like to thank all my lecturers who taught me over the past two years for teaching me some essential skills and knowledge which have become useful in completing this project. I would also like to thank my colleagues for all the helpful discussions and most importantly good laughs throughout the course.!

I would like to thank my family and friends for constant encouragement and source of motivation in completing my study. Thanks to my brother Melvin, mother Jolly and sister-in law Tonia for all the happy moments.

Finally I would like to thank my friend Dr. Steven Hutt for all the intellectual and philosophical conversations as well as laughter, banter and free drinks.!

1. Introduction

1.1.1. Lung structure and gaseous exchange

In the lungs, thin walled structures known as alveoli found at the end of the respiratory tree are the site of gas exchange. Gaseous exchange occurs through diffusion from a fine mesh of capillaries covering the alveolus (figure 1).

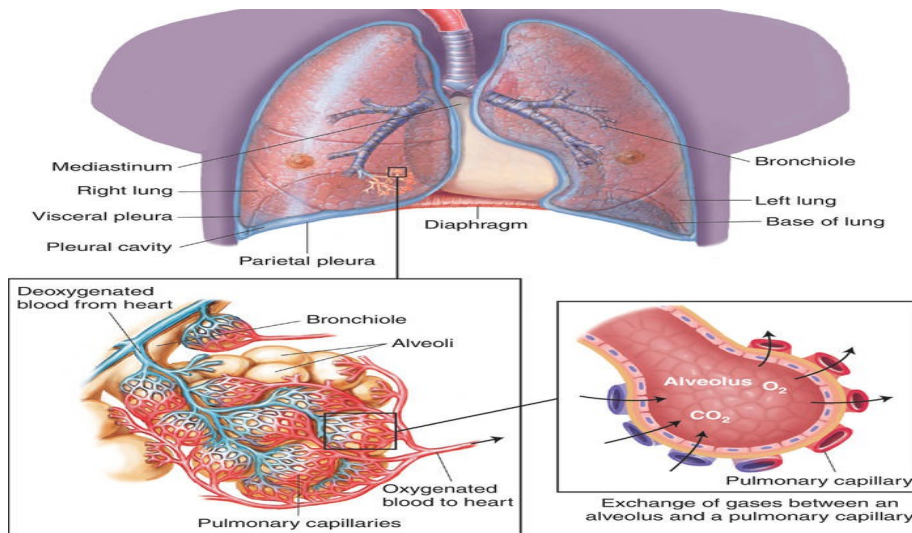
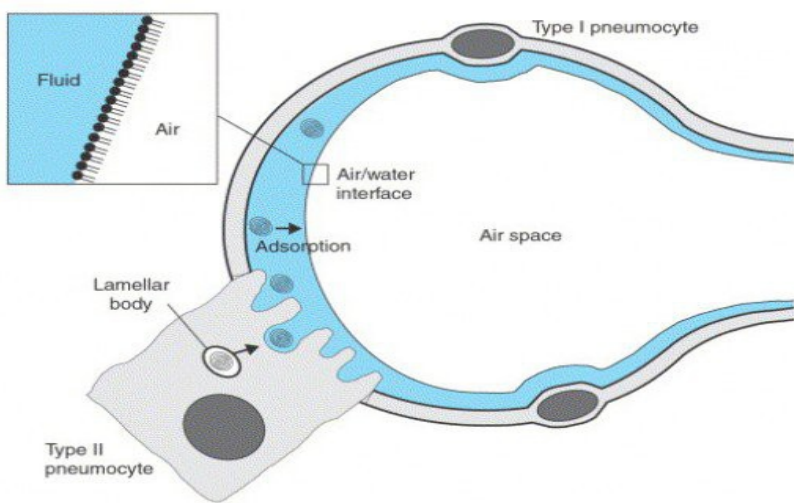


Figure 1. Showing the structure of the lungs and the mechanism of gaseous exchange. Image taken from Medical Dictionary <http://medical-dictionary.thefreedictionary.com/Alveoli>.

1.1.2. Lung surfactant and hypophase

Mammalian lungs have a large internal surface area and much of it is lined by a thin liquid film called alveolar hypophase (figure 2). The hypophase introduces surface tension due to the restricted movement of liquid molecules at the surface of the liquid.



Current Opinion in Structural Biology

Figure 2. Showing an alveolus. The blue lining is the alveolar hypophase. Figure also showing surfactant producing type 2 cells and the arrangement of surfactant monolayer at the air/liquid interphase. Image taken from <https://owlcation.com/stem/Surfactant-Lowering-Pulmonary-Surface-Tension>.

1.1.3. Surface tension

Restricted movement of liquid molecules at the surface happens in order to maintain the hydrogen bonds existing between the liquid molecules. At the surface of the liquid, liquid molecules have negligible van der Waals interaction with air molecules above, hence even the smallest rotational movement can cause them to lose hydrogen bonds. Surface tension means that it is relatively difficult to break the bonds that exist on the surface of the liquid. This implies that the bonds on the surface of liquid are strong and the liquid molecules on the surface can exert a force when there is force applied on them (figure 3). [1]

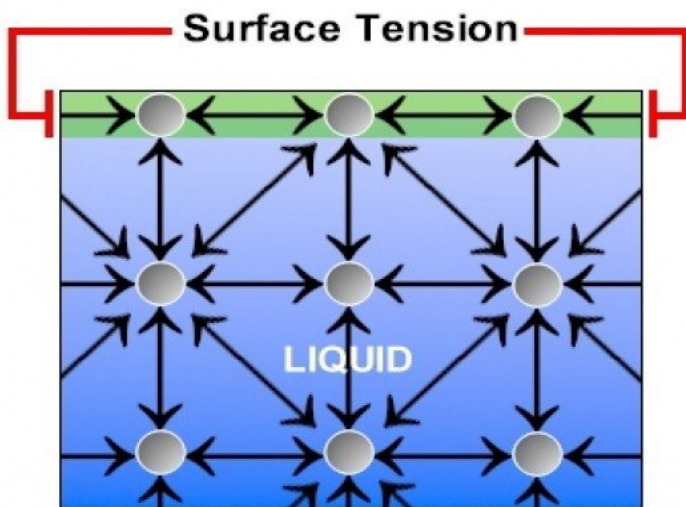


Figure 3. Showing the interaction of liquid molecules in the bulk and at the interface. Blue region represents the bulk region of the liquid and the green region is the liquid/air interface. Gas phase (above the green section) is more dilute than liquid, therefore gas molecules exert minimal attraction on interfacial molecules. This causes an inward attractive force on interfacial molecules that leads to the surface to seek a minimal surface area, generating surface tension. Image taken from <https://owlcation.com/stem/Surfactant-Lowering-Pulmonary-Surface-Tension>.

1.1.4. Lung surfactant production

Type 2 alveolar cells synthesise a mixture of lipoproteins called surfactant which is then secreted continuously into the alveolar liquid/air interphase. Pulmonary surfactant is packaged in lamellar bodies and are secreted into the alveolar hypophase by the type 2 cells. In the hypophase lamellar bodies form a cross hatched structure called tubular myelin consists of lipids and proteins. Tubular myelin is the source of the lipids that form the surfactant layer and the reservoir (figure 4). [2]

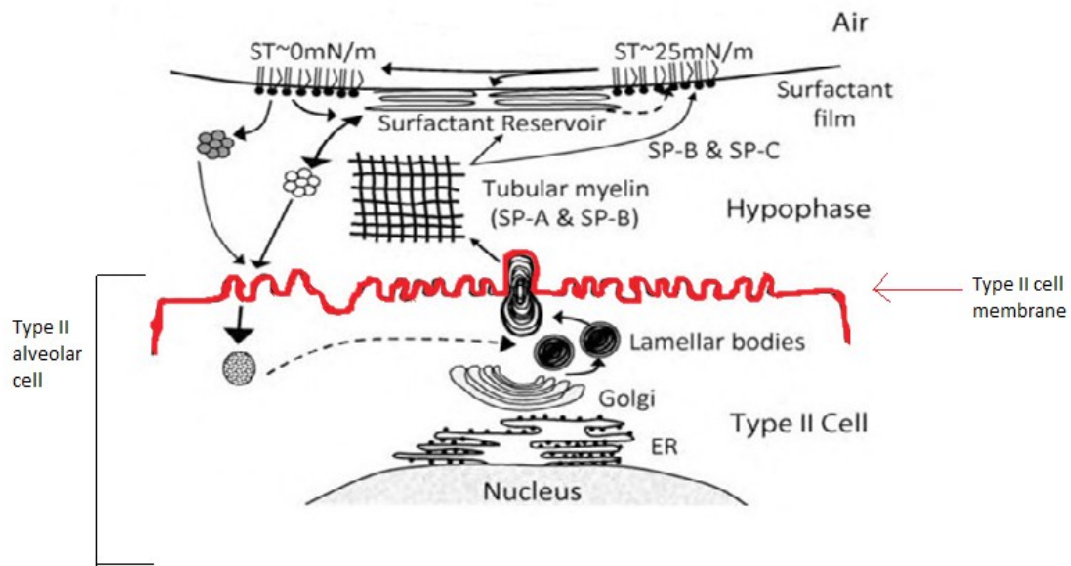


Figure 4. Schematic representation of surfactant production. Image adapted from S. Orgeig et al (2010). [3]

1.1.5. Lung surfactant functions

Two major functions of lung surfactant is to reduce the pressure needed to expand the alveoli during inhalation and to prevent alveoli from collapsing on themselves during exhalation. [4] Pulmonary surfactant does this by reducing the surface tension at the air/liquid interface from 70 mN m^{-1} to near 0 surface tension. Surfactant molecules align along the surface of the liquid such that their polar head group point towards the water and their non-polar tails point towards air. This causes the liquid molecule near the surface to interact with the polar head groups of surfactant, therefore can freely rotate and move compared to liquid/air interface, hence this lowers their ability withstand forces resulting in reduced surface tension. [5] Numerous physiological functions are associated with pulmonary surfactant, which can be divided into surface tension related and non-surface tension related. Surface tension related physiological functions of pulmonary surfactant are, maintaining a large gas transfer area, alveoli stabilization on expiration, increasing lung compliance on inspiration, stabilizing airway, anti-adhesion agent, anti-edema effects, epithelial cell protection in airway reopening, facilitation of mucociliary transport, dispersal of fluids and removal of particles. Non-surface tension related functions are, specific and non-specific host defence, pathogen barrier, antibacterial/antiviral activity and smooth muscle relaxation. [4][6][7][8]

1.2. Lung surfactant composition

Lung surfactant contains phospholipids, neutral lipids, fatty acids and surfactant proteins. Lung surfactant consists of approximately 90% lipids and 10% proteins (figure 5). [9]

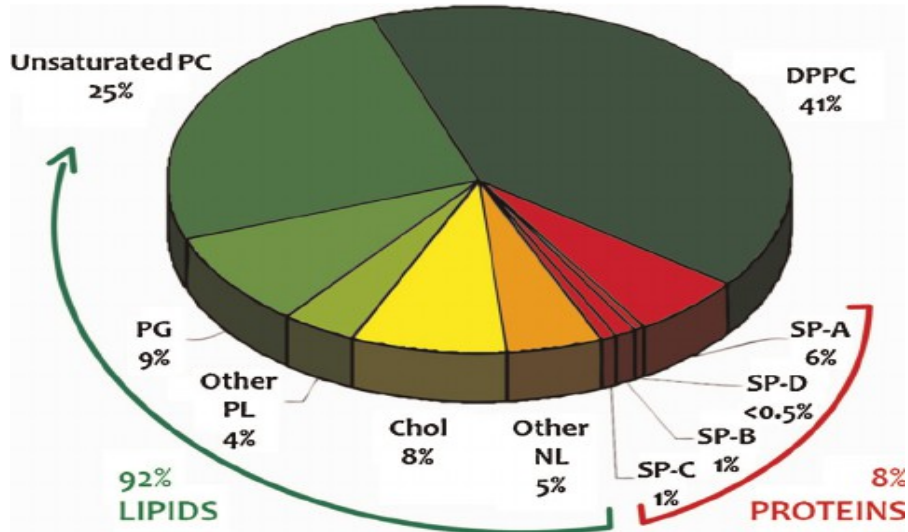


Figure 5. Showing the percentage of molecules in human lung surfactant. PC- Phosphatidylcholine, PG- Phosphatidylglycerol, PL- Phospholipids, Chol-Cholesterol, NL - Neutral lipids. Image taken from, E.Parra et al (2015). [9]

1.3. Lung surfactant lipids

Lung surfactant membranes contain approximately equivalent proportion of saturated and unsaturated lipid species. [9] Zwitterionic phosphatidylcholines and anionic phospholipids such as phosphatidylglycerol, cholesterol and neutral lipids make up majority of surfactant lipid composition in mammals. Zwitterionic phosphatidylcholines (PC) is approximated to be 60-70% by surfactant mass. In human lung surfactant the most prevalent PC is the long chained disaturated zwitterionic phospholipid dipalmitoyl phosphatidylcholine (DPPC) accounting for 30-60% of the PCs. Other major PC component in the mammalian surfactant are all unsaturated, eg. Palmitoyloleoyl phosphatidylcholine (POPC). Approximately 20% of phospholipids are primarily unsaturated and anionic, such as phosphatidyl-glycerol (PG), lyso-bis-phosphatidic acid and phosphatidylinositol (PI). Non-PC zwitterionic PL such as phosphatidylethanolamine (PE) and sphingomyeline and neutral lipids mainly cholesterol in small amounts are also present. [10][8] In the unsaturated lipids, cis-double bond (C=C) moiety introduces a kink in the alkyl chain of unsaturated lipids and reduces the van der Waals interaction with other lipids, therefore increases the fluidity of the lipid membranes. [11]

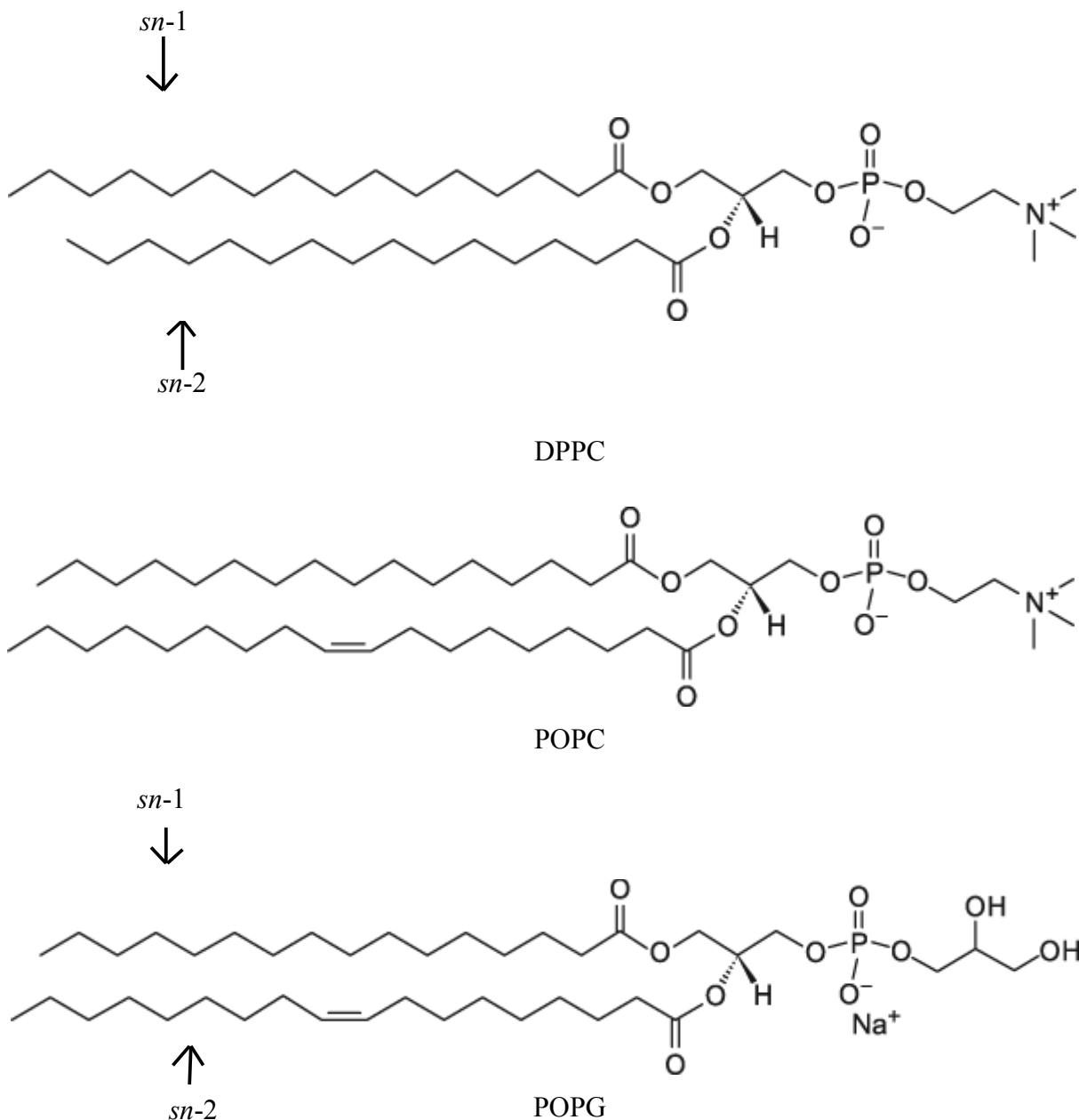


Figure 6. Showing different structures of phospholipids. Saturated phosphatidylcholine (DPPC), unsaturated phosphatidylcholine (POPC) and the unsaturated 1-palmitoyl-2-oleoyl-*sn*-glycero-3-phospho-(1'-*rac*-glycerol) (POPG) are all present in the human lung surfactant. Images adapted from <https://avantilipids.com/product>

1.4. Lung surfactant proteins

Lung surfactant proteins can be classified into two groups: SP-A and SP-D (hydrophilic) and SP-B and SP-C (hydrophobic). SP-A and SP-D are known to be involved in the innate defence mechanisms at the alveoli due to their trimeric subunits capable of recognising, inhibiting and inactivating a broad spectrum of pathogens. SP-A is an integral part of the surfactant system and known to bind phospholipids avidly and found in tubular myelin and lamellar bodies. [12] whereas SP-D is not usually associated with membranes. [13] SP-B and SP-C are crucial for the biophysical

function of the surfactant as they are associated with the surfactant lipid film at the air-water interface. [9] SP-B and SP-C regulate the initial adsorption of the lipids to the interface, the reversible sequestration of the lipids into the surfactant reservoir, and lipid recruitment from the reservoir to the surfactant film (figure 4). [8]

1.4.1.SP-A

SP-A is able to bind to multiple ligands such as sugars, Ca^{2+} , and phospholipids, which allows the protein to bind to multiple pathogens such as bacteria, viruses and fungi. [14] It has been proposed that SP-A associates with surfactant membranes and promote membrane-membrane aggregation. [15] It has also been proposed that the SP-A is able to recognize liquid-ordered phases [16] and the boundaries between ordered and disordered phases in monolayers. [17]

1.4.2. SP-D

SP-D is homologous to SP-A and have similar roles in respiratory system. Like SP-A, SP-D is a collagen containing calcium dependent lectins called collectins and significantly contributes to the surfactant homoeostasis and pulmonary immunity. Their immune functions include neutralization of viruses, removal of bacteria, fungi, apoptotic and necrotic cells, down regulating allergic reactions and resolving inflammations. The basic structure of these proteins include a triple-helical region and a C-terminal homo-trimeric lectin or carbohydrate recognition domain (CRD). The CRD can recognise carbohydrates or charge patterns on microbes, allergens and dying cells, whereas the collagen region can interact with the receptors of immune cells to coordinate clearance mechanism. [18]

1.4.3. SP-C

As with SP-B, SP-C is highly expressed in lung tissue, and the mature SP-C is stored in the lamellar body and secreted out by exocytosis by alveolar type II cells along with phospholipids and SP-B. Although surfactant phospholipids are the principle components in reducing surface tension, the addition of either SP-B or SP-C to exogenous surfactant preparations has been shown to rapidly lower the surface tension in vitro and effectively treating respiratory distress syndrome (RDS) in experimental animals. [19] SP-C as well as SP-B has been reported to be partitions into disordered regions in both bilayers and monolayers. [20] SP-C has been shown to promote phospholipid exchange between membranes [21] and between membranes and air/water monolayers, resulting in rapid formation of interfacial films, [22] and aids in spreading of the DPPC across air/water interface. [20]

1.4.4.SP-B

SP-B is thought to be the most important protein in lung surfactant. In-vitro studies have shown that the SP-B is involved in the transfer of the surface active phospholipid species from membranes into air-liquid interface. [23] SP-B is permanently associated with the membrane due to its high hydrophobicity. SP-B has a net positive charge of 7+ at physiological pH and is thought to promote selective interaction with anionic phospholipids, particularly PG. [24] SP-B distributes preferentially in disordered regions of membranes and air/water interface. [25] It is thought that the amphipathic helices of SP-B cause membrane perturbation and is important for the transit of phospholipids from surfactant membranes into the surface active interfacial monolayers. [26]

1.5. Functions of lipids in lung surfactant

At the air/water interface the phospholipids form the monolayers by extending the hydrophobic fatty acid groups into the air and the polar head groups oriented towards the aqueous phase as a result of an energetically favourable configuration. The number of water molecules exposed to air depends on the the number of phospholipid molecules assembled and the area per lipid at which the lipids arrange at the interface, therefore an increase in phospholipid concentration reduces the surface tension. [27] DPPC is the main phospholipid species that reduce the surface tension due to its ability to pack at a high density at the air/water interface. This is achieved by a tight packing of DPPC's saturated fatty acid chain at physiological temperatures. [28] A kink in the chains of unsaturated phospholipid makes it impossible to pack the molecules together beyond a threshold therefore to sustain a low surface tension. [29] The packing capability of a phospholipid also depends on the temperature, presence of other lipids, and the state of compression at the interface. Packing at the interface can be defined by the changes in the surface available for the molecules to redistribute, for example inspiration and expiration of breathing cycles. During inspiration the surface area available for lipid molecules is higher, therefore a low packing density and more configurational freedom at the interface, which is known as the liquid-expanded phase (L_e). [30] At high compression levels, i.e during expiration, the phospholipids reach highly packed structure known as liquid-condensed phase (L_c) (figure 5). [31] Packing of the surfactant is influenced by the the presence of cholesterol and it decreases the packing and increase the mobility of phospholipids in the liquid-condensed phase maintaining a certain order of the acyl chains. In the presence of cholesterol the monolayer is known as liquid-ordered phase (L_o). [32]

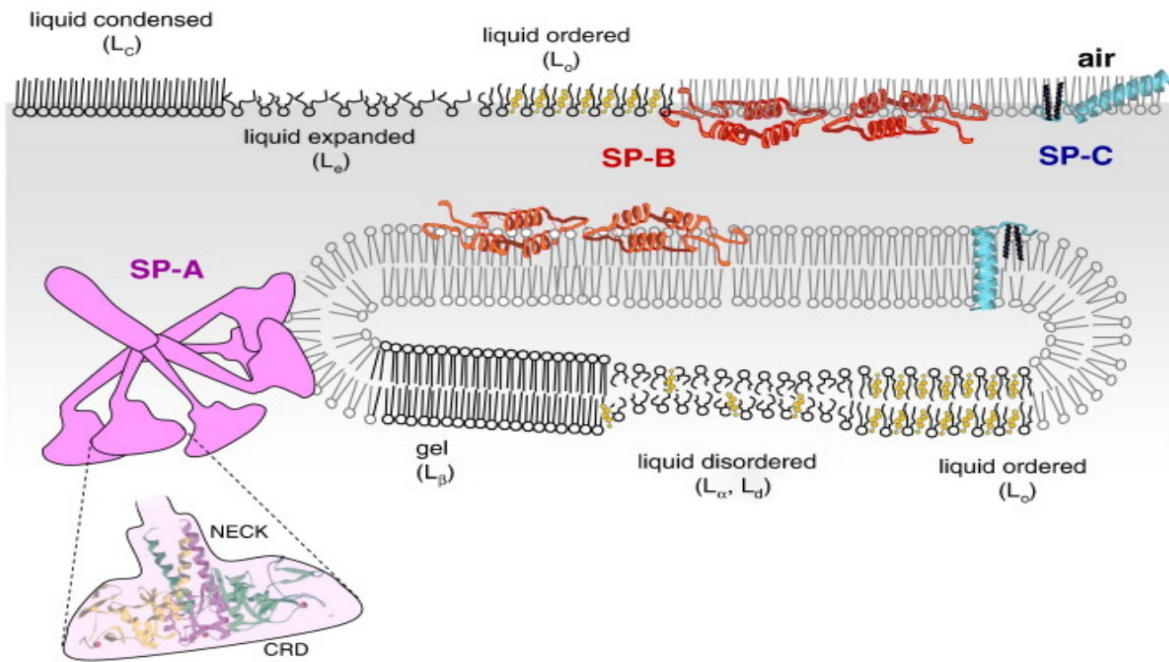


Figure 7. Showing different phases and SP-B and SP-C proteins at the interface. Cholesterol is coloured in yellow. The bottom part of the image shows the surfactant reservoir and the current model of the three proteins and its proposed function found in the interface. Image taken from, J.Perez-Gil (2008). [33]

1.5.1. Role of DPPC and POPG in lung surfactant

An effective lung surfactant has the ability to compress to near zero surface tension rapidly at the end of expiration and rapidly re-spread during inhalation. The role of DPPC is to reduce the surface tension to near 0 mN m^{-1} as it exhibits a liquid-condensed phase (L_c) under physiological conditions, hence poor respreadability. Monolayers of unsaturated phospholipids collapse near the equilibrium surface tension of $\sim 24 \text{ mN m}^{-1}$. [34] Unsaturated phospholipids such as palmitoyloleoylphosphatidylglycerol (POPG) are thought to fluidize the lung surfactant by re-spreading of the film increasing the adsorption to the interface. [35] These physical properties of DPPC and POPG are related to their chemical nature of the head group and the fatty acid chains which determines the molecular shape and the temperature of the melting transition from ordered to disordered state. [36] DPPC has a melting temperature of 41°C (315 K), which is higher than rest of the phospholipids in the surfactant due to the rigidity and high packing properties of the fatty acid chains. [37] POPG has a melting temperature of -4°C (269 K), due to the double bond in the fatty acid chains occupying larger area causing lower packing potential. [38] At physiological temperatures the DPPC would be in liquid condensed state. [36] In the liquid condensed state the phospholipids are restricted of motion than liquid expanded. [39] Phosphatidylglycerol (PG) is the

second most abundant phospholipid in the lung surfactant. Majority of the 9% phosphatidylglycerol class in the lung surfactant is palmitoyl-oleoyl-PG (POPG). [40] POPG is reported to have a major regulatory role in the innate immunity of the lungs and anti-viral properties. [41] The Infant Respiratory Distress Syndrome (IRDS) and the Acute Respiratory Distress Syndrome (ARDS) are the two most prevalent diseases associated with surfactant dysfunction. [42] It has been generally accepted that the presence of PG is crucial for the mature lung surfactant in human neonates and once PG is detected respiratory distress syndrome (RDS) will not occur. [43] Impairment of lung surfactant function has been reported with altered fatty acid composition of lung surfactant phospholipids. A lower relative content of oleic acid in the phosphatidylglycerol profile and higher level of saturated fatty acids has been reported in patients with idiopathic pulmonary fibrosis (IPF), suggesting that PG lipids play an important role in the lung surfactant function. [44]

1.6. Oxidative stress on lung surfactant

Oxidative alterations and dysfunction of surfactant may lead to lung diseases such as acute lung injury and acute respiratory distress syndrome (ARDS). Patients with ARDS show evidence of increased oxidative damage to lipids and proteins and biophysical modifications of lung surfactant. [45] Reactive oxygen species such as superoxide anion (O_2^-) and hydroxyl radical ($\cdot OH$) have shown to have inhibitory effects on surface tension parameters, including adsorption, minimum surface tension, percentage film area change and compressibility. [46] Decreased surface activity, including prolonged adsorption times and elevated surface tension have been reported on various studies. [45]

The disruptive effects of reactive oxygen species on surfactant function is thought to be caused by the alterations to lipids and proteins in the surfactant. Lipid oxidation is involved in number of diseases including, Parkinson's, Alzheimers's, cardiac arrhythmia, hypertension, inflammatory diseases, schizophrenia and cancer. [47] Air pollution is associated with an increase in the risk of acute and chronic diseases and death. Air pollutants cause oxidative stress in cells and tissues that they contact. The world health organisation (WHO) guideline of safe level of ozone exposure is $100 \mu\text{g m}^{-3}$ for 8-hour mean. However roughly third of the major cities in the world exceed the harmful threshold for ozone [48]

1.6.1. Ozonolysis

Ozone is particularly interesting as it's an extremely reactive oxygen species and reacts readily with the carbon-carbon double bond of phospholipids and cleaves the alkene through a process called ozonolysis. Ozone addition at the double bond results in the intermediate cyclic molozonide, this is then isomerised to form trioxolane. Trioxolane is hydrolysed to form the oxidative or reductive species which gives rise to ketone, aldehyde or acid products. [49]

1.6.2. Oxidation of POPG to form PonPG

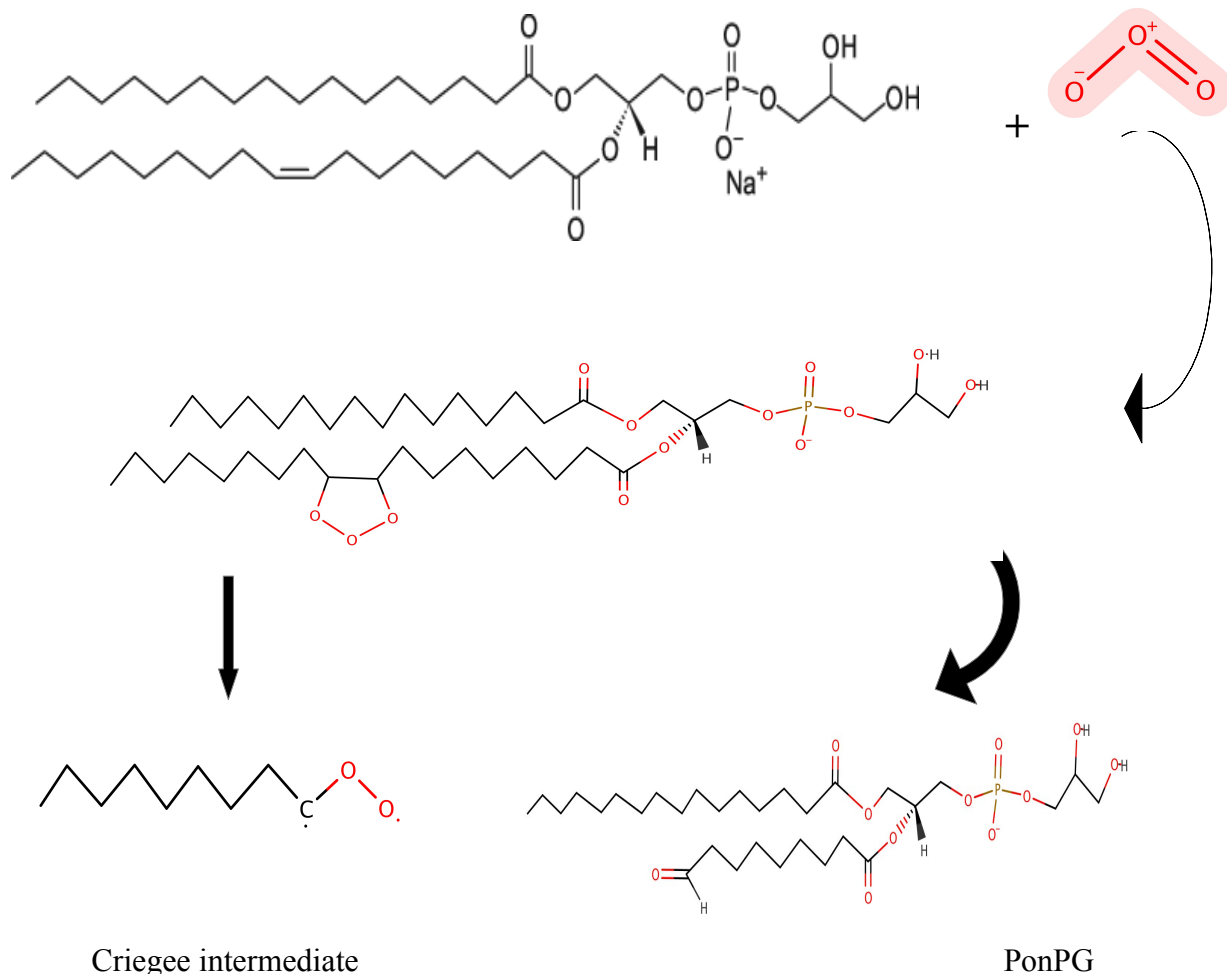


Figure 8. Shows the steps in the formation of the oxidised product PonPG. The reaction of ozone happens at the double bond of the POPG which leads to the formation of PonPG and Criegee intermediate.

1.7. Functions of oxidised lipid in the lung surfactant

It has been suggested that the hydrophilic group bearing sn-2 acyl chains in the oxidised lipid would reverse the direction (acyl chain reversal) to accommodate the polar moieties into the vicinity of the lipid head groups, hence locating closer to the interface than the unoxidised chains thus explaining

the expansion of the monolayer. The L_c - L_e transition and a shift to L_e state is noted in the presence of oxidised lipids. Monolayer expansion is dependent on the length of the acyl chains, with shorter chains forming more fluid and expanded monolayers. Acyl chain reversal towards the interface decreases its length and increasing the volume available for *sn*-1 chain which remains perpendicular to the membrane plane. At constant temperature and pressure oxidised lipid/DPPC mixed monolayers are less ordered compared to pure DPPC, hence the disappearance of the L_c - L_e coexistence phase and transition into L_e state. [47]

Membrane perturbation of the structure and modifications of properties such as fluidity, permeability and thickness have been shown in bilayer structures, as well as a direct relationship between lipid oxidation and membrane leakiness. Some studies report a decrease in lipid tail order parameter, whereas some report an increase or no change upon oxidation. [51] Experimental study of pure POPC monolayer has been reported to be unstable in extremely low level ozone, where the C=C moieties in the oleyl chain of POPC were selectively modified to produce nonanal and oxidized lipids POnPC and PazPC. Nonanal is thought to evaporate from the surface and the oxidised lipids remain in the monolayer and reorientate towards water surface and gradually dissolve. In mixed DPPC:POPC monolayer the lipids phase-separate but strongly interact with each other. The oxidation rate of POPC was decreased in the presence of DPPC and the oxidised lipids gradually dissolve into the water. [52]

Solubilization of the oxidised molecules was reported when the monolayer was compressed significantly. [47] It has been shown that ozone reacting with monolayer of 1-palmitoyl-2-oleoyl-*sn*-glycero-3-phosphocholine (POPC) results in surface pressure elevation followed by surface pressure reduction below the initial level. The POPC damage was due to direct contact with ozone than exposure to oxidation products. [50] Similar results were also reported for langmuir monolayers of unsaturated phospholipids, 1,2-dioleoyl-*sn*-glycero-3-phosphocholine (DOPC), 1,2-dilinoleoyl-*sn*-glycero-3-phosphocholine (DLPC), and dilinolenoyl-*sn*-glycero-3-phosphocholine (DlinPC) when exposed to laboratory air. [53] The initial increase in surface pressure was suggested as a result of accumulation of oxidation products and the slow decrease in surface pressure due to the volatile oxidation products gradually leaving the monolayer. [50][53]

1.8. Research purpose

The complex action of lung surfactant remains poorly understood despite various research. This research aims to find the effect of oxidative lipid on the properties of lung surfactant. Various simulations with DPPC, POPG and oxidised lipid PonPG formed from POPG decomposition was used to study the physical, structural and dynamics of monolayers. Although there have been some experimental [54][55][47] and computational [56] studies using oxidised phospholipids in the monolayers, there have been no research experimental or molecular dynamics studies carried out with the oxidised species of POPG on a monolayer to the best of knowledge. Computational study of the oxidised lipid used dioleoylphosphatidylcholine (DOPC), which is not found in the lung surfactant whereas POPG is. The consequence of oxidised species derived from POPG on monolayer simulation offers insight into structure and dynamics of the monolayer at small spatial and temporal scales not accessible on experimental research.

This study focuses on the effect of PonPG, which is formed after the reaction of POPG with ozone, on the lung surfactant monolayers. Molecular dynamics simulations are carried out using GROMACS (**GRO**ningen **M**achine for **C**hemical **S**imulations) software package.

1.9 Molecular Dynamics Theory

There are different methods to describe the dynamics of macromolecular systems. Quantum mechanical methods give the most accurate result, however these are computationally expensive and are limited to short time scales involving very few atoms. Molecular dynamics are methods that use simplified classical mechanics, where the momenta and the positions of all particles in a system are calculated as a function of time. Molecular dynamics integrate Newton's equation of motion simultaneously for all atoms in discrete time steps.

$$F=ma \quad (1)$$

where F is the force acting on the particle, m is the mass of the particle and a is the acceleration. This research uses leap-frog integrator algorithm to integrate equations of motion. [57] Forces between atoms are calculated using a force field which is a set of mathematical functions and parameters that describe the interaction between different types of atoms in different chemical environment.

The forcefields used in this study are GROMOS53A6 [58] and Berger lipid. [59] United-atom forcefields which subsumes non-polar hydrogen atoms into their adjacent carbon atom, were chosen to be used in this study due to its distinct advantage in membrane simulations, reducing the number of particles by up to 60% when compared with all-atom forcefield, thus reducing the computing

time. [60] For example united-atom model of DPPC is composed of 50 atoms whereas the all-atom model consists of 130 particles. Berger lipid forcefield, which is a hybrid between GROMOS and OPLS [61] forcefields is compatible with the parameters used to describe molecules in GROMACS (**see supplementary information S2**). The DPPC molecules are parametrised using Berger lipids and the POPG molecules are parametrised using a modified GROMOS forcefield [62] due to reported problems associated with 53A6 forcefield distribution for DPPC lipid model [60] and Berger lipid and GROMOS representation for PG head groups. [63] The PonPG molecules are parameterised by editing the forcefield of POPG (see section 2.2 for detailed description).

The intramolecular and intermolecular interactions described by the forcefield is used to calculate the potential energy (V) of the system.

$$V = \Sigma_{\text{bonded}} + \Sigma_{\text{non-bonded}} \quad (2)$$

Bonded interactions included in the forcefield are bond lengths and strength, angles, and dihedrals. Non-bonded interactions include electrostatic interactions incorporated by coulomb potentials involving atom charges and van der Waals interactions modelled by Lennard-Jones potential. Periodic boundary conditions (PBC) are applied to the simulating systems to minimize the edge effects, thus in theory there are no boundaries of the system. PBC is achieved by putting the atoms of the system into a space-filling box which is surrounded by translated copies of itself, hence artefacts caused by boundaries is replaced by artefacts of periodic conditions. Using PBC combined with minimum image convention, only one – the nearest image of each atom is considered for short range electrostatics and van der Waals interactions. The minimum image convention uses a cut-off radius to truncate non-bonded interactions that exceed half the shortest box vector. Long range non-bonded interactions are modelled by Particle Mesh Ewald summation method.

An NVT ensemble, constant number of particles, volume and temperature is used to represent the possible micro-state of the system in thermal equilibrium with the surrounding environment. An NVT ensemble is preferred for this study over NPT (constant pressure, particles and temperature) due to distortion of the monolayer structures introduced by the pressure applied on the system, hence allowing the simulations of monolayers at constant area per molecule. Energy minimization step is applied to the system before the simulations to remove large forces and kinetic energy that can cause the simulation to crash. For detailed explanation of the theories and calculations used for simulating biological systems, readers are referred to GROMACS manual. [64]

1.10. Molecular dynamics simulations of monolayers

Molecular dynamics simulations of lipid monolayers are carried out using atomistic models, coarse grained models or united atom models. Atomistic simulations of zwitterionic and anionic lipid mixtures [65] and mixtures with surfactant proteins [66][67] as well as coarse grained simulations have been reported previously. [68] [69] [35] United-atom models using lipids and surfactant proteins have been reported previously. [70][71][72] The choice of simulation package, temperature (323 K), box dimensions, simulation time scale, lipid species, algorithms and simulation parameters are adapted from previously reported successful simulations. [70] [73]

2. Materials and methods

2.0. Simulation

All simulations were performed using GROMACS software v5.0.4. 15 out of the 17 systems, including pure water were simulated using computing resource of intel Xeon (CPU) and Nvidia Titan X – Maxwell (GPU). The average simulation time of the 14 systems were 6 hours and 34 minutes. 2 out of 17 simulations were carried out using an Intel Core i7 CPU 950 (CPU) and Nvidia GeForce GTX 580. The average simulation time of the 2 systems were 24 hours and 43 minutes.

2.1. Simulated systems

Simulated system consisted of three types of phospholipids in monolayers. Monolayers were created using water slab method, where two monolayers are created either side of a water box. The monolayers were simulated at different area per lipid density at $\sim 63\text{\AA}^2$ and $\sim 80\text{\AA}^2\text{lipid}^{-1}$.

1. DPPC with 53 lipids
2. POPG with 53 lipids
3. DPPC/PonPG with 48 DPPC lipids and 5 PonPG lipids
4. POPG/PonPG with 48 POPG lipids and 5 PonPG lipids
5. DPPC/POPG with 42 DPPC lipids and 11 POPG lipids
6. DPPC/POPG/PonPG with 42 DPPC lipids, 6 POPG lipids and 5 PonPG lipids.
7. DPPC/PonPG/POPG with 36 DPPC lipids, 11 PonPG lipids and 6 POPG lipids
8. PonPG with 53 lipids

2.2. Forcefield parameters

The DPPC lipid coordinate and parameter files were obtained from a DPPC bilayer from Peter Tieleman's website. [74] The POPG files were obtained from lipidbook. [75] The d-popg lipids are used in this simulation. The monolayers using slab geometry were built with Packmol. [76] (**see supplementary information S3**). PonPG is the oxidised POPG where the double bond in the oleyl chain is replaced with an aldehyde group and the remaining atoms in the sn-2 chains were removed. The editing was done using Avogadro molecular editing tool. [77]

The structure is optimised using Universal Force Field (UFF) with Molecular Dynamics 300 K algorithm available in Avogadro. UFF uses forcefield parameters estimated based on the element, hybridization and connectivity to put the collection of atoms in space whose bond length and angle are arranged such that the net inter-atomic force on each atom is close to zero. [78] Performing geometry optimization of a molecule aims to find the molecule's structure that correspond to the structure found in nature, hence can be used in experimental and computational study of the molecule more confidently.

The parameters for the oxidised lipids were derived from editing the parameters of POPG obtained from lipidbook as detailed below. [79] Forcefield editing of a phospholipid to derive oxidised version of the molecule's forcefield is an approach that has been successfully used to simulate lipid monolayer [56] and bilayer [51] studies.

The deleted atoms from the structure was removed from the **[atoms]** directive and corresponding parameters for the deleted atoms were also removed from **[bonds]**, **[pairs]**, **[angles]** and **[dihedrals]** directive. The newly added aldehyde group on the oleyl chain was parameterised using propanal [80] and oleic acid. [81] The partial charges for the aldehyde group was derived from propanal and the bonded and non bonded parameters were derived from the oleic acid for the oxidised lipid PonPG.

Newly added lines in **[atoms]**:

30	LC	1	OPO	C30	18	0.530	12.0110	; Ekkabut et al (2007)
38	LO	1	OPO	O38	19	-0.530	15.9994	: Ekkabut et al (2007)

[bonds]

30	38	1	0.12300E+00	502080.0	; from olicc.itp, M.I. Hoopes (2011)
----	----	---	-------------	----------	--------------------------------------

[pairs]

28 38 1 ; pair with new carbonyl oxygen

[angles]

29 30 38 1 121.0 502.1 ; from oleic.itp, M.I. Hoopes (2011)

[dihedrals]

28 29 30 38 1 0.0 0.42 6 ; from oleic.itp, M.I. Hoopes (2011)

For the full forcefield file for PonPG, see appendix (**See supplementary information S13**)

2.3. Simulation parameters

The different areas per lipid to simulate different packing density of the monolayer ($L_c - L_e$ phases) was achieved by adjusting the box vectors in x and y dimensions when packing the lipids using packmol. $\sim 63 \text{ \AA}^2 \text{ lipid}^{-1}$ is achieved by packing 53 lipids in 58 Å for x and y directions. $\sim 80 \text{ \AA}^2 \text{ lipid}^{-1}$ is achieved by packing 53 lipids in 65 Å for x and y directions. The z direction was 210 Å for the box and the water slab which initially contained 4000 water molecule was 100 Å. This made sure that there was a vacuum layer above the monolayers. Energy minimization is performed on the system using steepest descent algorithm which finds the nearest local minimum by systematically moving down the steepest local gradient. [82]

Additional single point charge (SPC) water molecules were added to maximise the number of water molecules in the box so as to fill the simulation box with a density of 1g cm⁻³, using the solvate module available in GROMACS. Water molecules added above the heads of the monolayers were removed using a perl script (**see supplementary information S11.2**). This resulted in different number of water molecules around $\sim 10,000$. Sodium counter ions were added to the systems containing negatively charged POPG and PonPG to neutralise the system by replacing a water molecule for each ion. An NVT, constant number of atoms (N), constant volume (V) and temperature (T) equilibration of the system was carried out using leap-frog integrator with a time step of 0.002 picosecond for 50000 steps giving an equilibration time of 100 ps. Position, velocity and energy was written to files every 100 steps or 0.2 ps. All simulations were run with constant temperature 323 K and maintained using Nose-Hoover thermostat. [83] DPPC has phase transition temperature of 315 K [84] therefore 323 K is used for the system to have a fluid monolayer. Since some simulations contain mostly DPPC, temperature of 323 K avoids the formation of liquid-condensed phase, therefore avoiding the restriction of motion of lipids imposed by this phase (see 1.5.1). The lipids were coupled together and the water and ions were coupled together in the thermostat. All bonds were constrained using constraint algorithm LINCS with fourth order

expansion and one iteration. [85]

Particle-Mesh Ewald method was used for long range electrostatic interaction. [86] Fourth order (cubic) interpolation was used with real space cutoff of 1.2 nm and grid spacing of 0.16 nm. The grid neighbour search was used with a cut-off distance for the short-range neighbour list of 1.2 nm. Short-range van der Waals cutoff distance of 1.4 nm was used. The neighbour list was updated every 5 time steps (10 fs). Periodic boundary conditions were applied in all X,Y and Z directions. Velocities were assigned from Maxwell distribution at 323 K with initial velocity generated randomly. Centre of mass (COM) motion removal is used for interfacial systems (membrane-water). The motion of the monolayers COM and the solvent COM is reset separately to avoid the phases moving in opposite direction. A 10 ps short MD run was conducted with strong position restraint on lipid molecules to allow water molecules to orient around the lipid heads. The short MD run and the final MD run of 5 ns was run with similar parameters except with a more accurate Nose-Hoover thermostat instead V-rescale thermostat, which is a modified Berendsen thermostat [87] used in NVT equilibration and without velocity generation (**see supplementary information S4-S9**).

2.4. Analysis

2.4.1. Order Parameter

Lipid order parameters are a measure for the orientational mobility of the C-D bond measured through ^2H NMR experiments. [88]

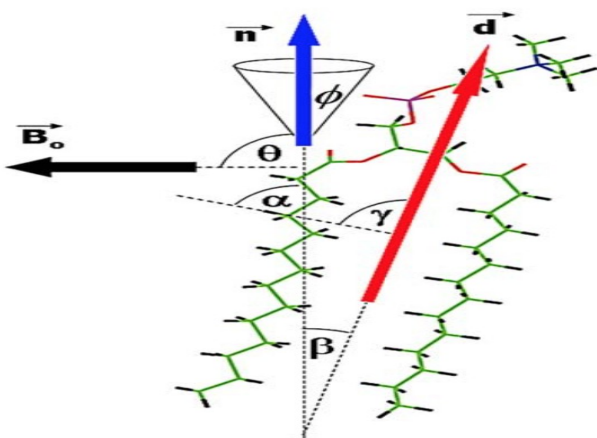


Figure 9. Showing the different contribution to the observed order parameter value in ^2H NMR experiments. The vector \mathbf{n} is the monolayer normal which is at an angle θ to the external magnetic field \mathbf{B}_0 . The CD vector is tilted at angle α with respect the monolayer normal. The angle ϕ is the possible wobbling of the \mathbf{n} within a cone. The molecular director is at angle β to the monolayer normal. The observed CD vector is at angle γ with respect to the molecular director. Image taken from, Vermeer et al (2007).

Order parameter is defined for every CH_2 group in the chain as:

$$S_{\text{CD}} = \frac{1}{2} (3 < \cos^2 \theta_{\text{CD}} > - 1)$$

Where θ_{CD} is the angle (α) between a CD-bond (experiment) or a CH-bond (simulation) and the membrane normal (\mathbf{n}). The S_{CD} for an atom C_i is calculated in GROMACS by using the vector C_{i-1} to C_{i+1} , this way the C-D bond vector is reconstructed and $C_{(i-1)} - C_{(i+1)}$ vector is taken as \mathbf{n} . [88] The CH-bonds are reconstructed for the three successive CH_2 groups assuming tetrahedral geometry of the CH_2 groups. The brackets represents the average of the two bonds in each CH_2 bonds, of all the selected lipid in the simulation and time. [89] The simulations used united-atom force field, therefore individual hydrogen atoms are not recognised, instead GROMACS treats carbon atoms as having the atomic weight of carbon plus the bonded hydrogen atoms. [73] This value is not valid for unsaturated bonds due to different geometry. [88]

Order parameters for POPG is calculated on *sn*-1 chain and all the CH_2 carbons up to the double

bond in *sn*-2 chain (**see supplementary information S10.2**).

2.4.2. Area per lipid

Area per lipid is calculated from the box dimension of the system in the X Y direction.

$$\text{BOX}_x * \text{BOX}_y / \text{no.lipids}$$

2.4.3. Monolayer thickness

Monolayer thickness can be calculated by examining electron density for the head group and tail group of the molecule of interest and calculating the difference between the peaks of the head group and tail (**see supplementary information S10.1**).

2.4.4. Surface tension

GROMACS calculates the average surface tension of the system by taking the difference of the normal (PN) and lateral pressures (PL) in the box (**see supplementary information S12.2**):

$\gamma_m = (PN - PL).Lz/2$, where $PL = (P_{xx} + P_{yy})/2$ and Lz is the box normal size. The term surface tension and surface pressure is interchangeable. The change in surface tension of the system as a function of the change in system can be used to measure the surface pressure introduced by the lipids at the air-liquid interface.

Surface pressure is defined as:

$\Pi(AL) = \gamma_{\text{aw}} - \gamma_m(AL)$, where γ_{aw} is the surface tension of the vacuum-water interface and $\gamma_m(AL)$ is the average surface tension in the monolayer.

To compare the experimental and calculated isotherms, γ_{aw} in the surface pressure equation is used as an adjustable parameter (γ_{aw}^*) derived from the vacuum-water interface calculated using the SPC model. The difference between the experimental value of the surface tension at the air-water interface and the value of the surface tension at the vacuum-water interface simulated can be compensated by using the adjustable parameter. The value of the adjustable parameter can change with a change in temperature and size of the simulation system.

2.4.5. Movement of lipid head group

Analysis of head group movement will be able to reflect the attraction of the hydrophilic region of the lipid molecules to the water. It will also be able to identify any difference in function of the air-liquid interface as a result of oxidised lipids present.

A Python script is developed to measure (**see supplementary information, S11.1**) the distance travelled by a reference atom of a lipid from initial configuration file(.gro) to the simulated configuration file. The script takes the two files and finds the difference in xyz coordinates. Since packmol arranges the molecules randomly in the defined box and the removal of water above the lipid/water interface, after solvating of the simulation box (Using a perl script), there is a cutoff distance set by the user where the chosen reference atom is expected to be within. The script then stores all the xyz coordinates of the reference atom and computes the difference between the coordinates from the two files. The script also identifies the direction of movement of the atom from the set planes of lipid/water interface. Since there are two monolayers on each side of the slab of water, an average distance moved by the reference atom of the lipid and the average direction of movement (towards or away from water) is printed out for each monolayer. Distance moved by individual molecules on each monolayer is printed to a CSV file. Any atom type and lipid molecule type within the system can be chosen to find the distance and direction of movement, provided that the reference atom type is associated with the molecule type (**see supplementary information S11**).

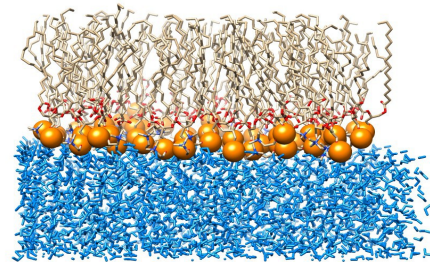
2.5.6. Acyl chain reversal

The python script used for head group movement of lipids is modified to calculate the acyl chain reversal. The reference atom is set to be the aldehyde oxygen and the plane in which the atom is expected to be found is set to a distance (~21Å) above the lipid/water interface where the atom is expected to be found after packing of the PonPG lipids. The percentage of oxidised lipids with acyl-chain reversal is calculated from the distance the aldehyde oxygen move towards the water above a threshold distance. The threshold distance is set be 16 Å and the number of lipids meet the threshold can be found from the output files of the python script (**see supplementary information S11**).

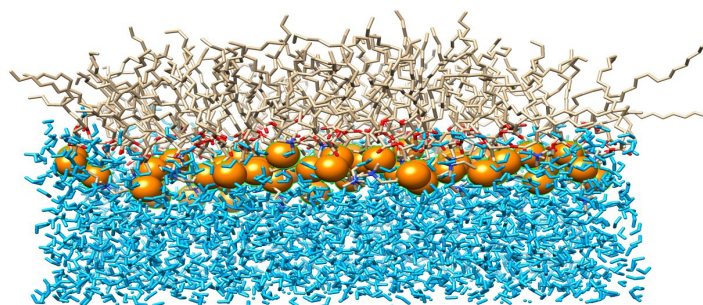
3. Results

3.1. Standard results

The standard behaviour of lipid/water monolayer where the hydrophobic tails extend towards air whereas the the hydrophilic head groups immerse in water [56] is observed for all simulated systems as seen from figure 10. The dimension of water slab remains same for all simulation as can be seen from the density profile of the water (figure 11), where the highest peak in density the initial Z-dimension of 5.4 nm and 15.8 nm.



A



B

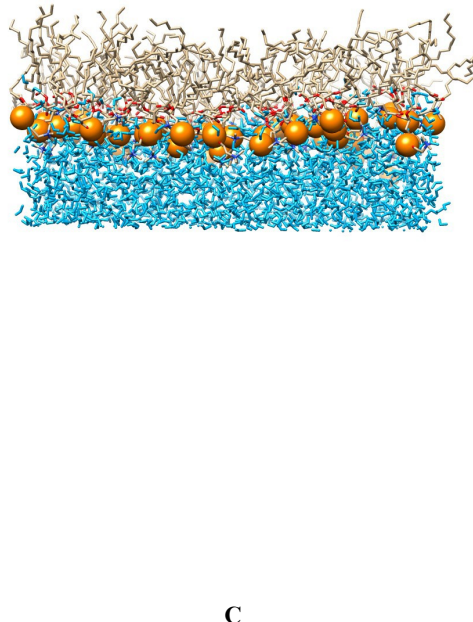


Figure 10. Showing representative configuration of water/lipid interface before equilibration (**A**), after equilibration at $t = 0$ ns (**B**) and after simulation at $t = 5$ ns (**C**). Only one monolayer from the two present in the simulation box is shown. Colour coding: Blue – water molecules, Gold – DPPC tails, orange balls – head group phosphorous atom of DPPC.

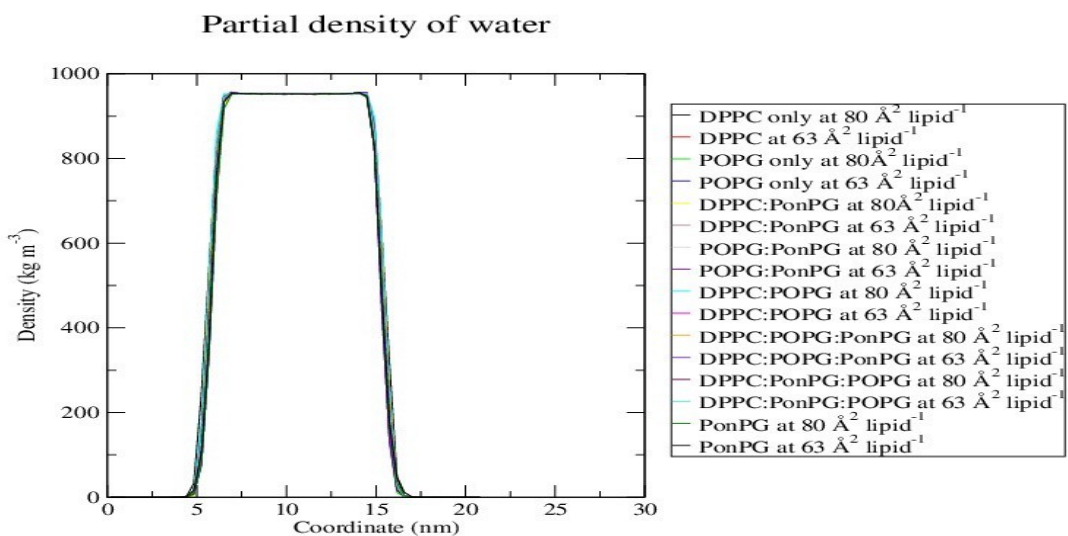
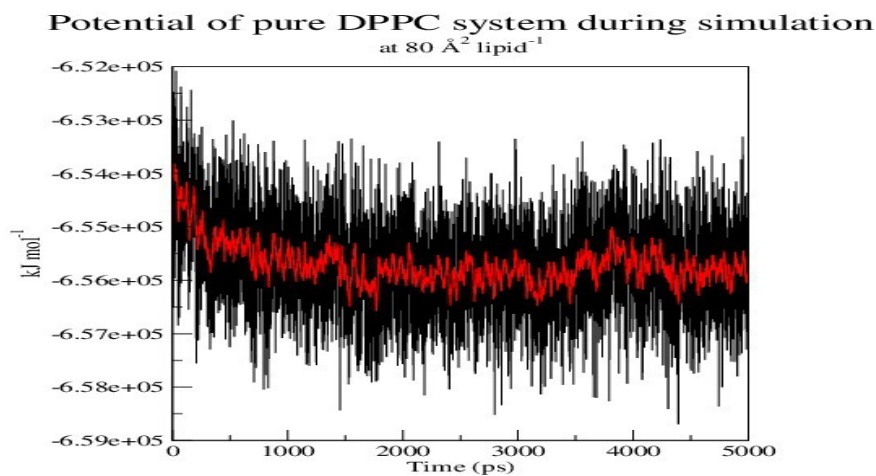


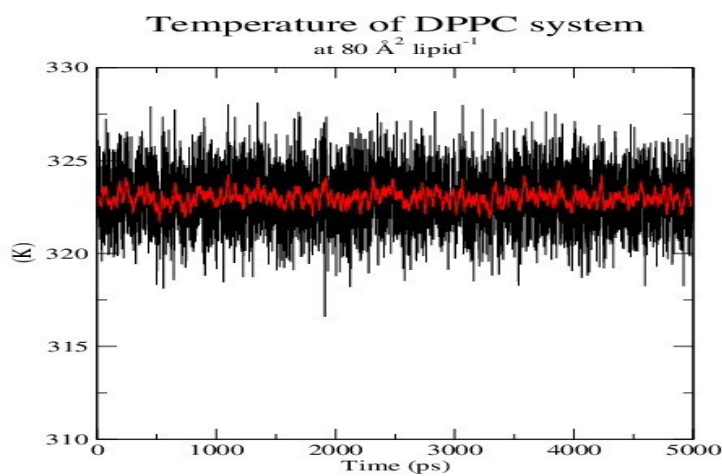
Figure 11. Showing the density profiles of water slabs from all simulations. Each curves are fitted on top of each other. The highest peaks are between 5.4 nm to 15.8 nm on Z-dimension. A steep curve shows a relative little movement of water molecules beyond the initial positions of water slab.

The simulated systems are stable as can be seen from the representative plots of energy minimization prior to equilibration, potential during simulation, temperature and pressure of the system after simulation.

A



B



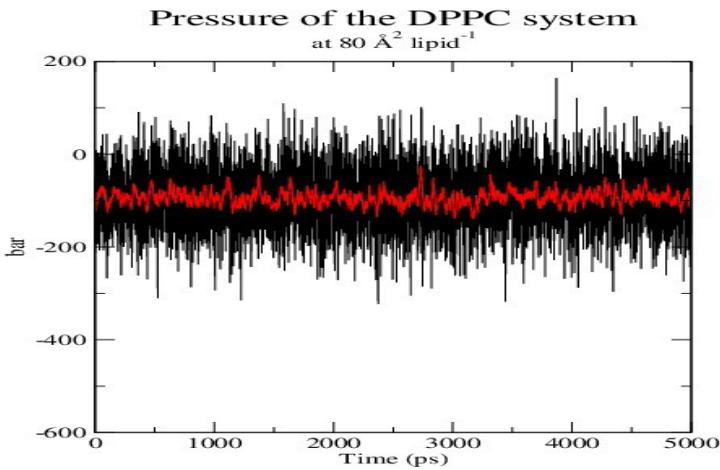
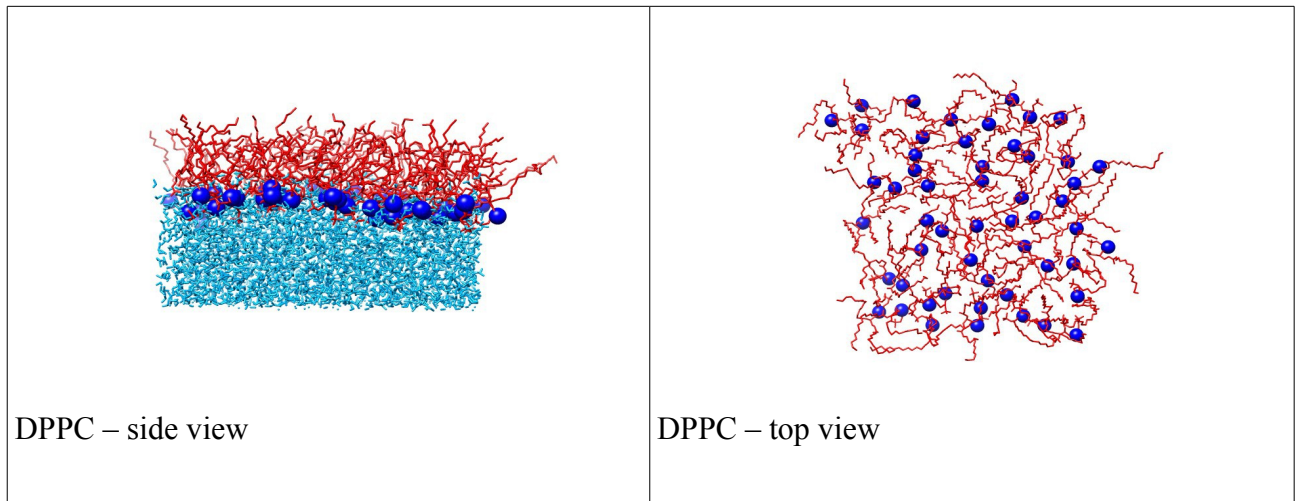
C

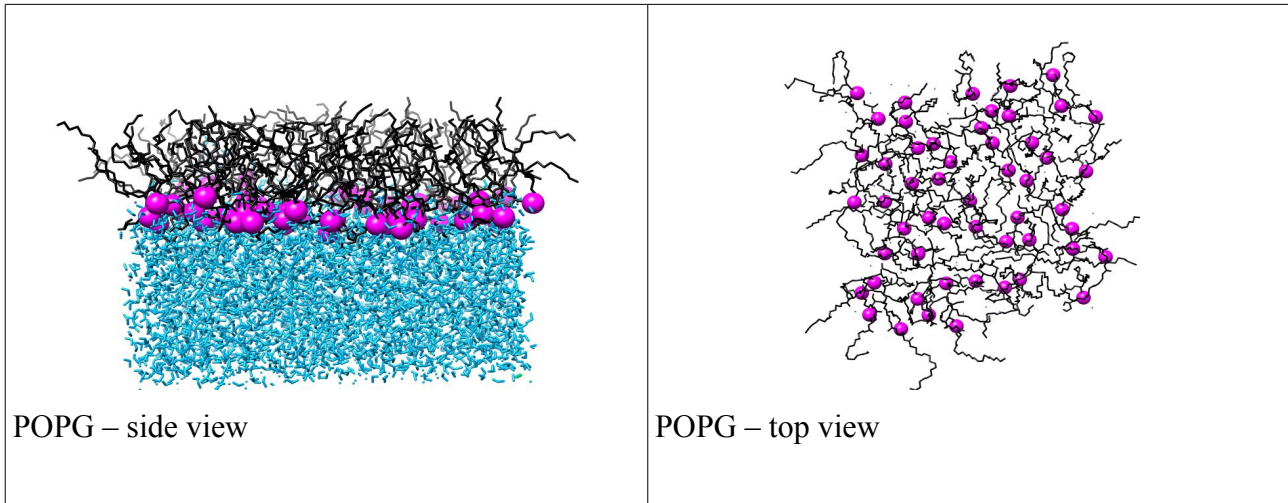
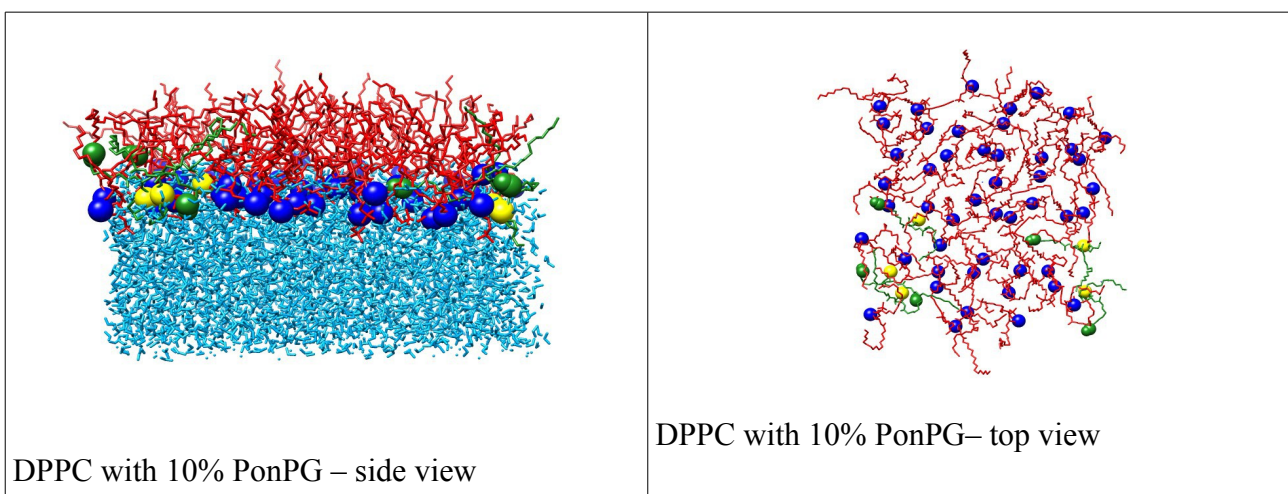
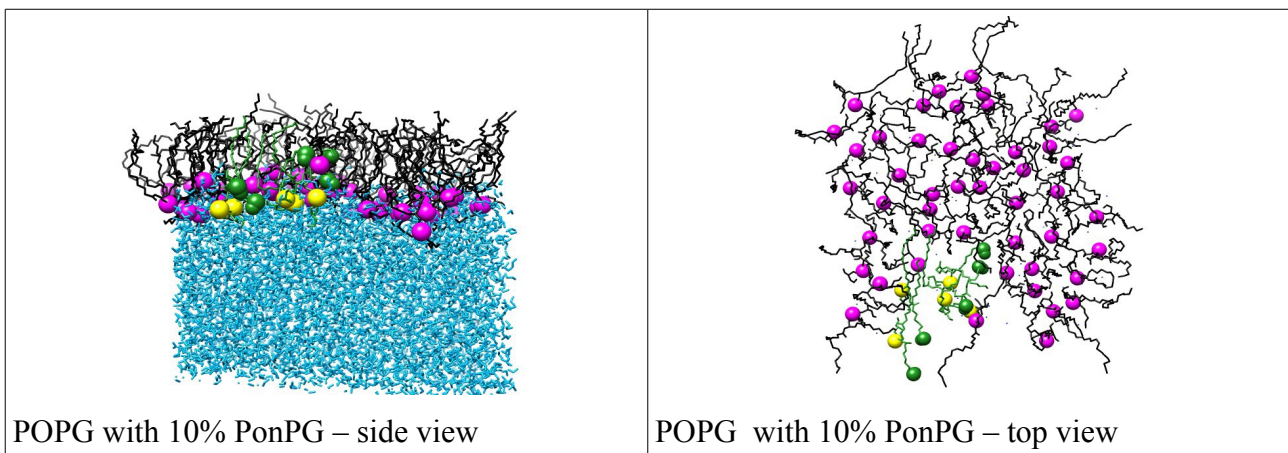
Figure 12. Showing the representative plots of potential over the simulation time (**A**) temperature over the simulation time (**B**) and pressure over the simulation time (**C**) of the simulated systems. The plots are derived from the pure DPPC simulation at $80 \text{ \AA}^2 \text{ area lipid}^{-1}$. The plots of temperature and pressure shows a large fluctuation, but it remains stable throughout the simulation. Black lines represents the value over time and the red lines represents the running average.

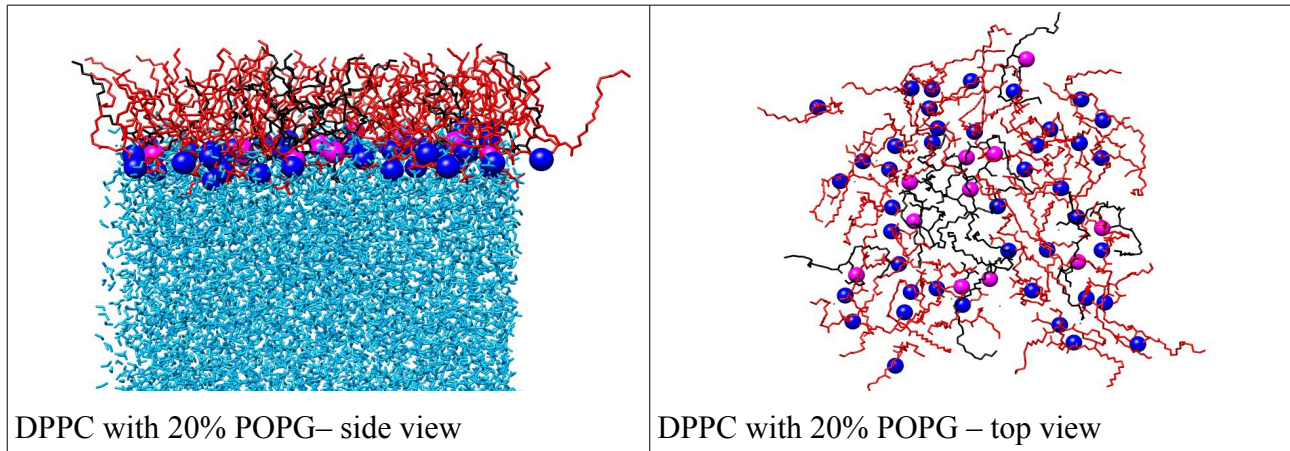
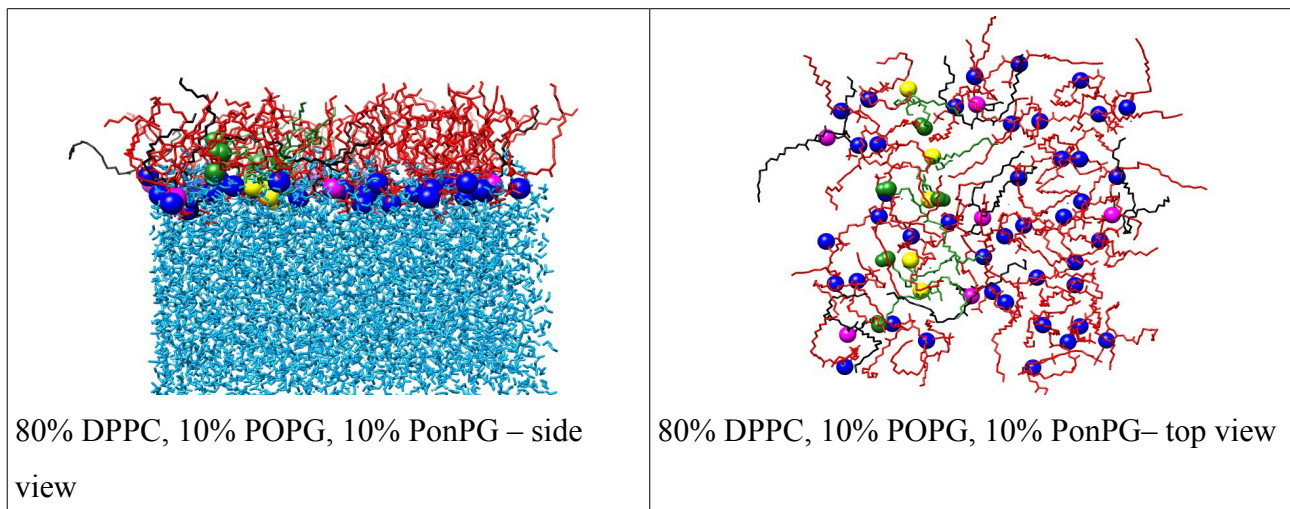
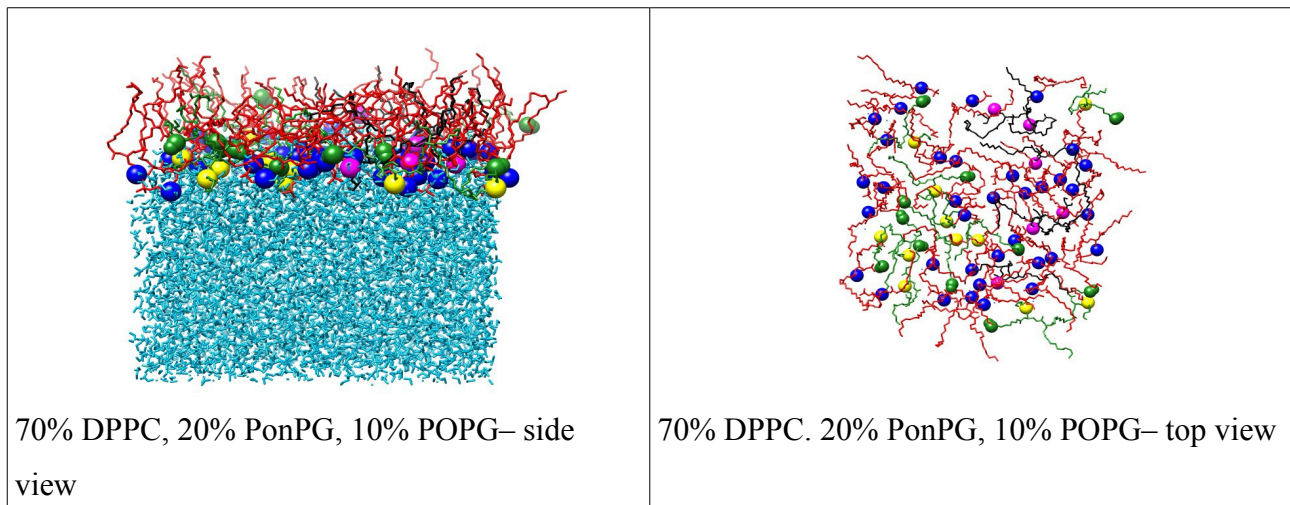
The parametrisation of the oxidised product PonPG produce a previously reported result [56] (see 3.2.8), suggesting that the forcefield editing of POPG to make oxidised product is working as expected within the simulations.

3.2. Simulation specific results

3.2.1. Snapshot of monolayers at $80 \text{ \AA}^2 \text{ area lipid}^{-1}$

A

B**C****D**

E**F****G**

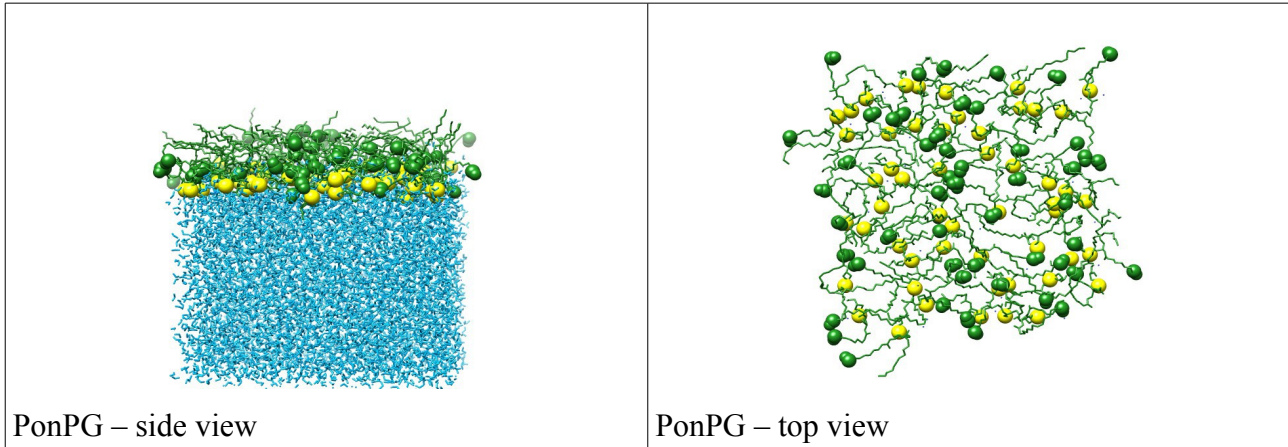
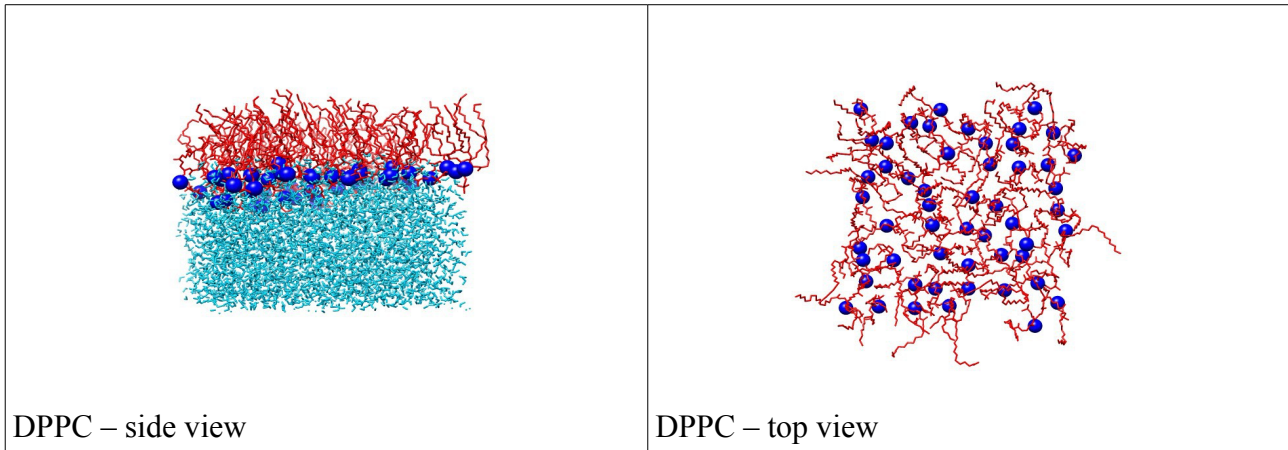
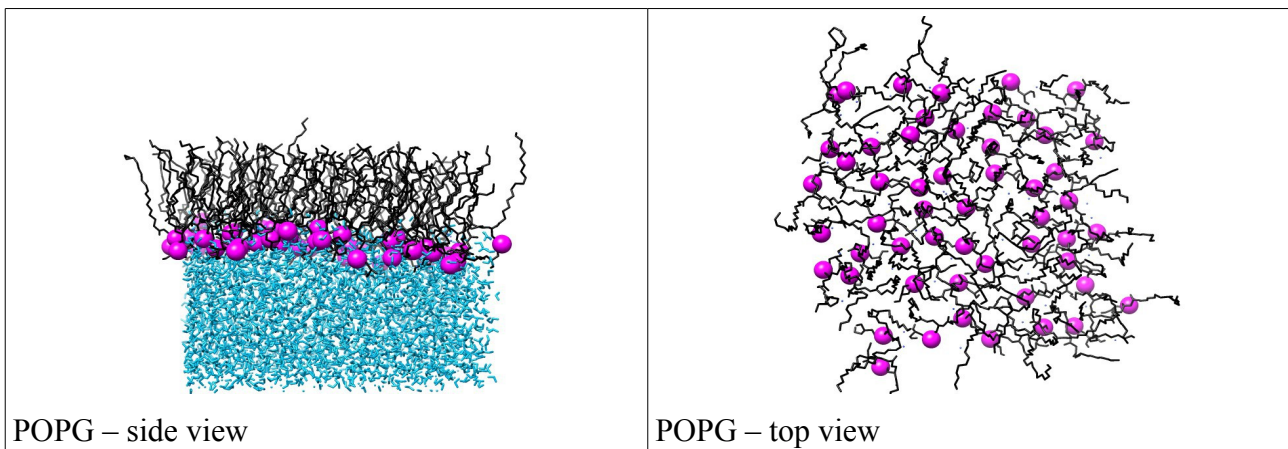
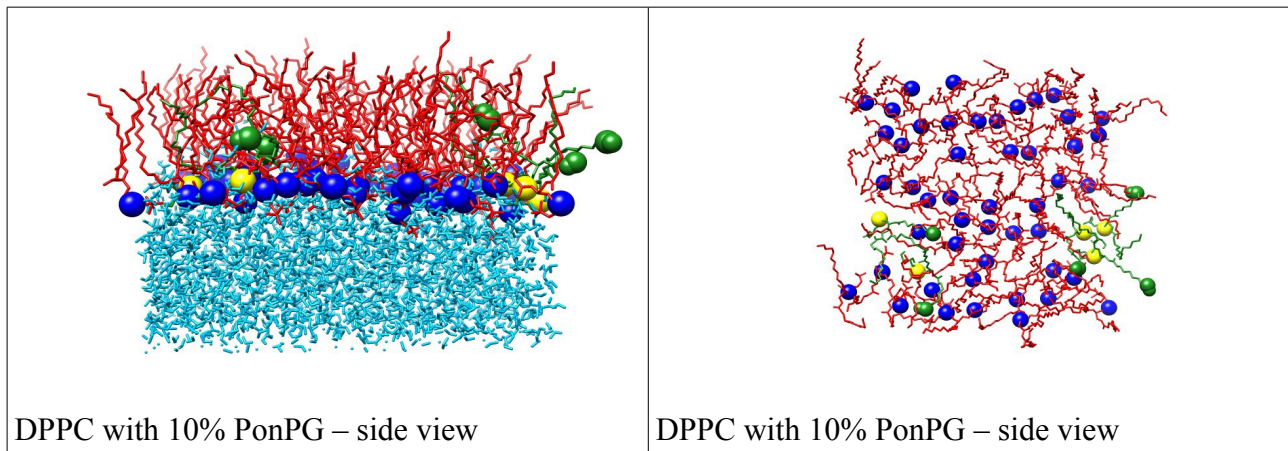
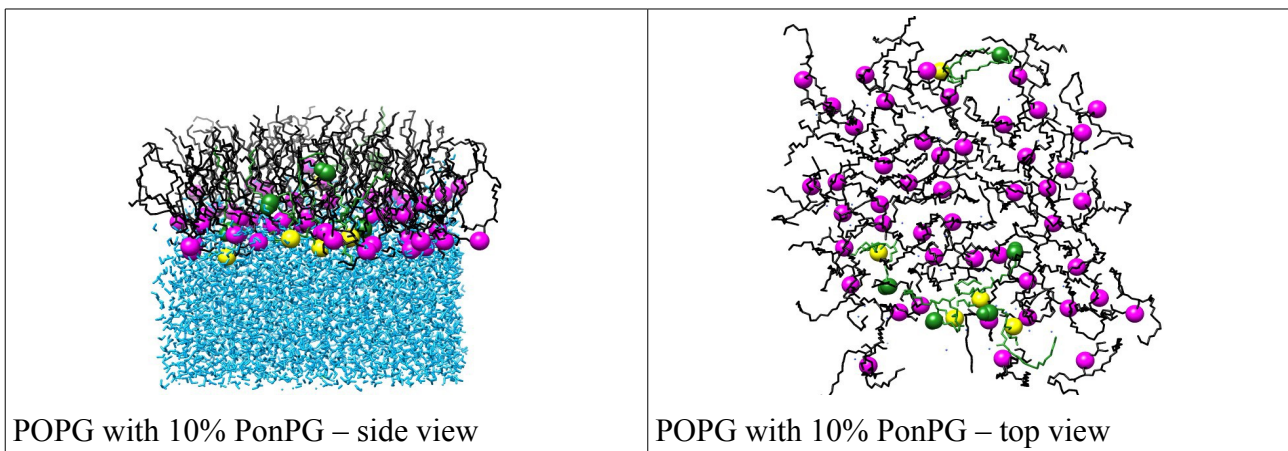
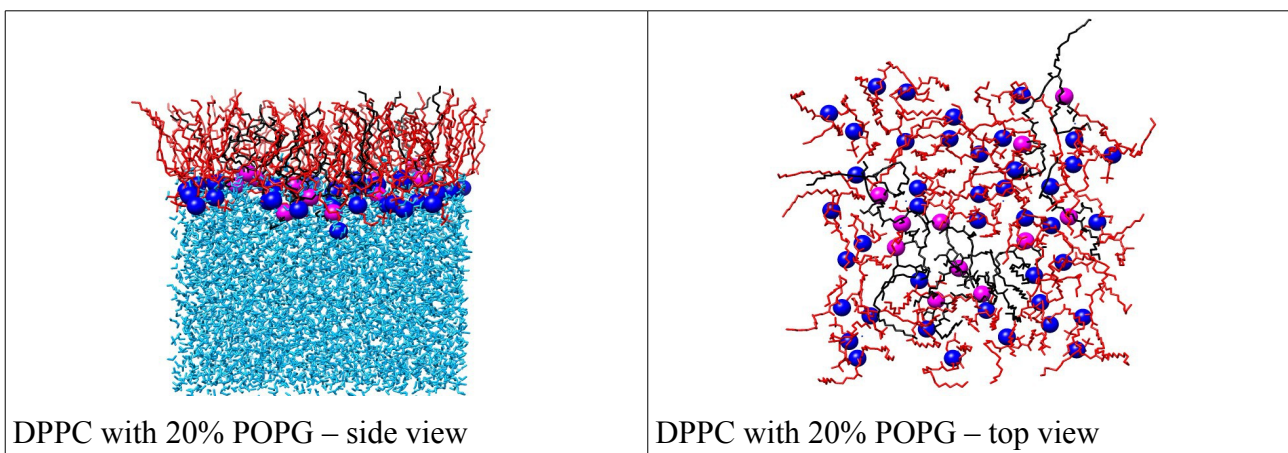
H

Figure 13. Showing snap shots of simulations at $80 \text{ \AA}^2 \text{ area lipid}^{-1}$. Colour scheme – DPPC (red stick), DPPC head group (phosphorus atom, dark blue sphere), POPG (black stick), POPG head (phosphorus atom, magenta sphere), PonPG (forest green stick), PonPG head (phosphorus atom, yellow sphere), PonPG aldehyde group (forest green sphere). Only one monolayer out of two is shown.

3.2.2. Snapshots of monolayers at $63 \text{ \AA}^2 \text{ area lipid}^{-1}$

A**B**

C**D****E****F**

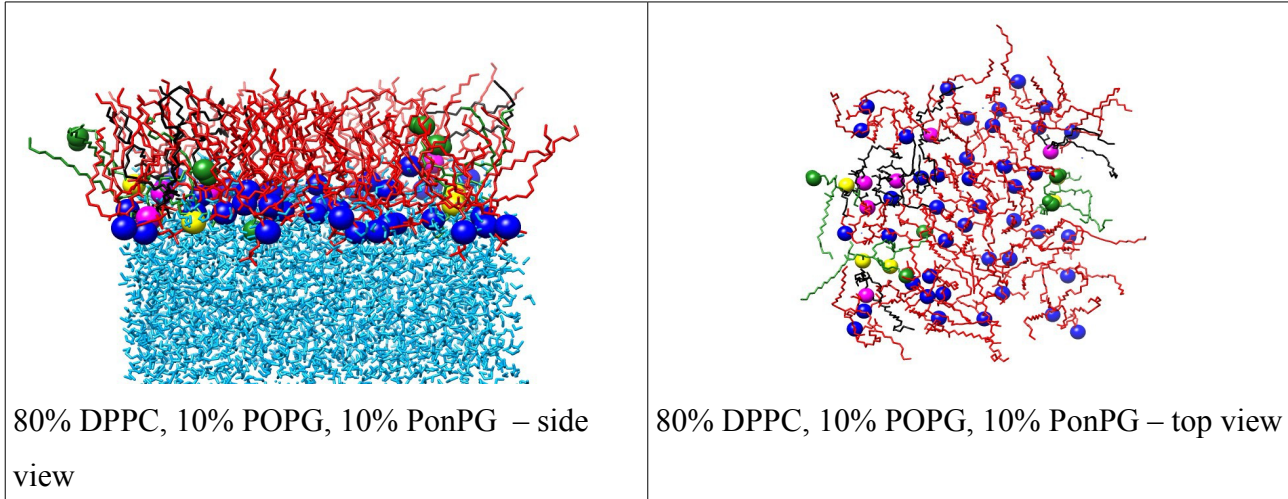
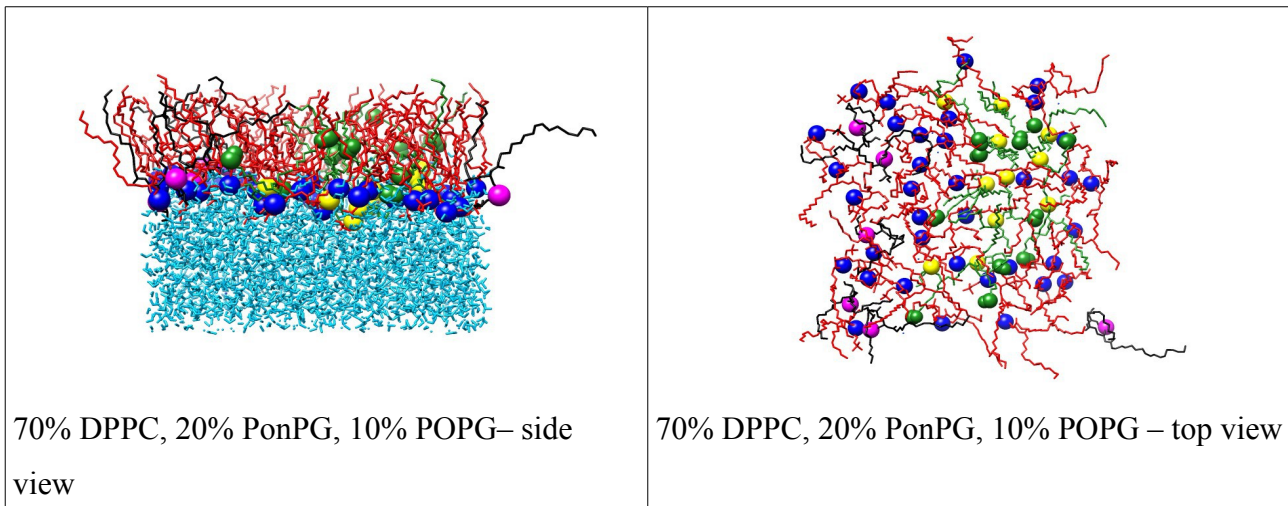
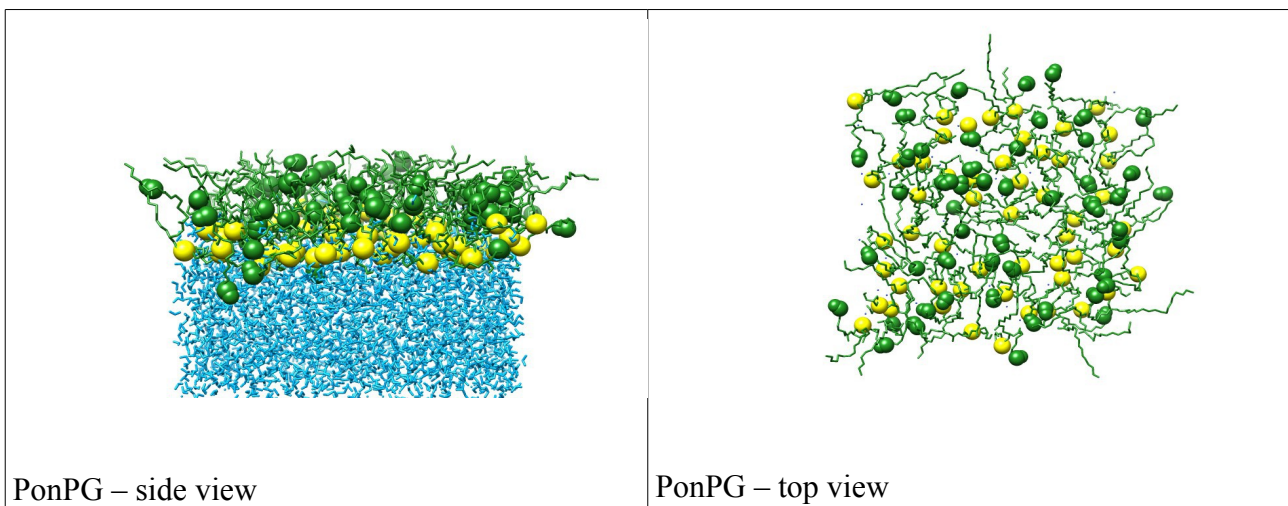
**G****H**

Figure 14. Showing snap shots of simulations at $63 \text{ \AA}^2 \text{ area lipid}^{-1}$. Colour scheme – DPPC (red stick), DPPC head group (phosphorus atom, dark blue sphere), POPG (black stick), POPG head group (phosphorus atom, magenta sphere), PonPG (forest green stick), PonPG head group (phosphorus atom, yellow sphere), PonPG aldehyde group (forest green sphere). Only one monolayer out of two is shown.

3.2.3. Surface pressure

The average surface pressure over the 5 ns simulations are given in table 1. The surface tension of the pure water using the same water box size as for the monolayer simulations at 323 K is 47 mN m^{-1} , which is lower than experimentally produced value of 67.6 mN m^{-1} at 323 K. [90] However there is a large fluctuation in the surface tension value over the simulation time for air/water interface (figure 15) and air/lipid interface (figure 16). To find the agreement between surface tension value observed for SPC water model used in this study and the literature, a 300 K simulation was run using the same box dimensions at $80 \text{ \AA}^2 \text{ lipid}^{-1}$ (see supplementary information S12.1) and found the surface tension value to be lower than the reported values in the literature by $\sim 3\text{-}4 \text{ mN m}^{-1}$. This difference maybe due to the difference in simulation parameters. Surface tension values of liquids are affected by surface area, density and the cutoff range used for inter and intra-molecular interactions in the simulated system. [91]

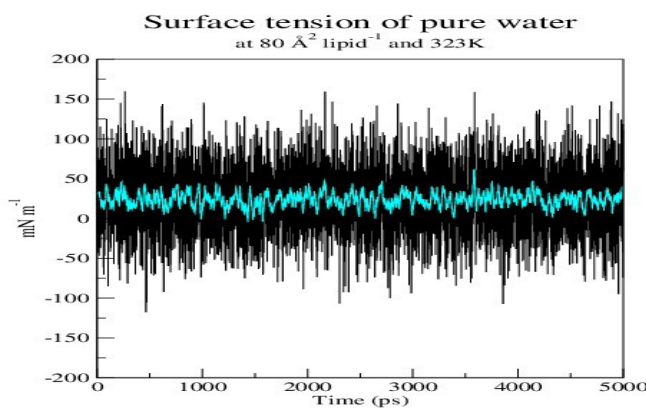


Figure 15. Showing the surface tension of air/water interface over 5 ns simulation at $80 \text{ \AA}^2 \text{ lipid}^{-1}$ and 323 K temperature. The surface tension value of air/water interface at $63 \text{ \AA}^2 \text{ lipid}^{-1}$ was found to be similar at 323 K temperature (data not shown). Blue line is the running average over the simulation time using 20 data points.

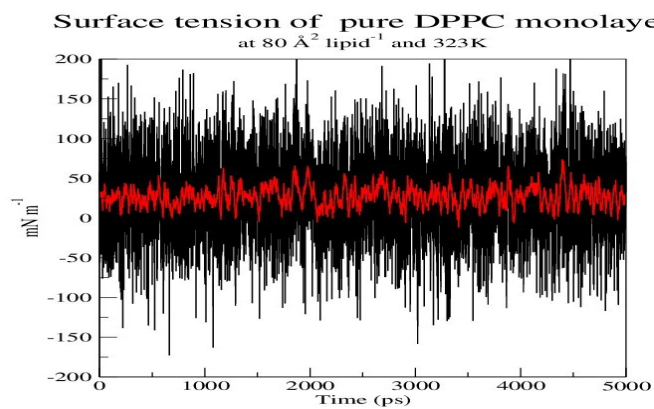


Figure 16. Showing the surface tension of air/lipid interface of DPPC monolayer at $80 \text{ \AA}^2 \text{ lipid}^{-1}$. Red line is the running average using 20 data points.

At $80 \text{ \AA}^2 \text{ lipid}^{-1}$ both DPPC and POPG simulation systems exhibit a low surface pressure, which is expected to be close to 0. Observation of higher surface tension of systems consists of DPPC, hence a negative surface pressure and a lower surface tension of pure POPG and POPG mixed with oxidised lipid is observed. A reduced surface tension, hence an increase in surface pressure of all systems upon the reduction of area per lipid from $80 \text{ \AA}^2 \text{ lipid}^{-1}$ to $63 \text{ \AA}^2 \text{ lipid}^{-1}$ is observed. The surface pressure of POPG systems are at much higher compared to systems consists of DPPC. At $63 \text{ \AA}^2 \text{ lipid}^{-1}$ pure DPPC simulation has surface pressure of 17 mN m^{-1} which is much lower than that of pure POPG monolayer of 26 mN m^{-1} . This trend in pressure area isotherm between DPPC and POPG has been reported previously. [92] When oxidised lipid is introduced to pure DPPC monolayers at 10%, there is a reduction of surface pressure observed from 17 to 14 mN m^{-1} at $63 \text{ \AA}^2 \text{ lipid}^{-1}$. An increased surface pressure of 1 mN m^{-1} with 20% oxidised lipid is observed when compared with mixed monolayer of 80% DPPC and 20% POPG, mixed monolayer with 80% DPPC and 10% POPG and 10% PonPG at $63 \text{ \AA}^2 \text{ lipid}^{-1}$. This trend is observed for most of the systems when oxidised lipid PonPG is present. At $80 \text{ \AA}^2 \text{ lipid}^{-1}$, surface pressure changes from -7 in pure DPPC to -6 mN m^{-1} in DPPC with 10% PonPG. Pure POPG from 1 to 4 mN m^{-1} . Mixed monolayer of 80% DPPC and 20% POPG also shows an increase in surface pressure from -10 to -9 mN m^{-1} when 10% of POPG is replaced with PonPG. This is further increased to -8 mN m^{-1} when the concentration of PonPG is increased to 20% in the system. At 100% oxidised system at $80 \text{ \AA}^2 \text{ lipid}^{-1}$, the surface pressure is highest at 4 mN m^{-1} .

System	Surface tension (mN m^{-1}) $80 \text{ \AA}^2 \text{ lipid}^{-1}$	Surface pressure (mN m^{-1}) $80 \text{ \AA}^2 \text{ lipid}^{-1}$	Surface tension (mN m^{-1}) $63 \text{ \AA}^2 \text{ lipid}^{-1}$	Surface pressure (mN m^{-1}) $80 \text{ \AA}^2 \text{ lipid}^{-1}$
Pure DPPC	54 +- 107	-7	30 +- 130	17
Pure POPG	46 +- 108	1	21 +- 133	26
DPPC with 10% PonPG	53 +- 105	-6	33 +- 130	14
POPG with 10% PonPG	43 +- 108	4	20 +- 134	27
DPPC 80% POPG 20%	57 +- 106	-10	30 +- 132	17
DPPC 80%, POPG 10%, PonPG 10%	56 +- 105	-9	30 +- 128	17
DPPC 70%, PonPG 20%, POPG 10%	55 +- 105	-8	29 +- 128	18
PonPG	43 +- 105	4	29 +- 123	18

Table 1. Showing the surface tension/pressure of simulations. For each area per lipid two columns of values are provided under surface tension. First is the average surface tension of the simulated system and the second one is the surface pressure calculation (see 2.4.4).

Due to a very large variability in surface tension calculation observed over the simulation time for both pure water/vacuum interface and lipid/vacuum interface, it is reasonable to assume that the negative average value of surface pressure observed for pure DPPC, DPPC with 10% PonPG, DPPC with 20% POPG, DPPC with 10% POPG and 10% PonPG, DPPC with 20% PonPG and 10% POPG at $80 \text{ \AA}^2 \text{ lipid}^{-1}$ is within the error of the calculation when comparing to experimental surface pressures.

To understand the effect of acyl chain reversal on the surface pressure properties, the surface tension and surface pressure calculation is carried out at regular intervals (0.5 ns) during simulation.

Time (ps)	DPPC with 10% PonPG Surface tension (mN m ⁻¹) 80 \AA^2 lipid ⁻¹	POPG with 10% PonPG Surface tension (mN m ⁻¹) $80 \text{ \AA}^2 \text{ lipid}^{-1}$	DPPC 80% POPG 10% PonPG 10% Surface tension (mN m ⁻¹) 80 \AA^2 lipid ⁻¹	DPPC 70% POPG 10% PonPG 20% Surface tension (mN m ⁻¹) $80 \text{ \AA}^2 \text{ lipid}^{-1}$	PonPG Surface tension (mN m ⁻¹) $80 \text{ \AA}^2 \text{ lipid}^{-1}$
500	49 +- 105	-2 22 +- 109	25 46 +- 107	1 1	49 +- 104 -2 25 +- 104 22
1000	50 +- 105	-3 30 +- 110	17 49 +- 106	-2 51 +- 105 -4	31 +- 104 16
1500	50 +- 105	-3 34 +- 109	13 52 +- 107	-5 52 +- 106 -5	35 +- 103 12
2000	52 +- 105	-5 36 +- 109	11 52 +- 107	-5 52 +- 106 -5	38 +- 103 9
2500	54 +- 105	-7 39 +- 109	8 53 +- 106	-6 53 +- 105 -6	40 +- 103 7
3000	53 +- 105	-6 42 +- 109	5 54 +- 106	-7 54 +- 105 -7	40 +- 103 7
3500	53 +- 105	-6 42 +- 109	5 55 +- 106	-8 54 +- 105 -7	41 +- 103 6
4000	53 +- 105	-6 43 +- 108	4 55 +- 106	-8 54 +- 105 -7	42 +- 103 5
4500	53 +- 104	-6 43 +- 108	5 55 +- 105	-8 54 +- 105 -7	42 +- 103 5
5000	53 +- 104	-6 44 +- 108	3 55 +- 105	-8 55 +- 105 -8	43 +- 103 4

Table 2. Showing the change in surface tension/pressure over regular interval (0.5 ns) of simulation at $80 \text{ \AA}^2 \text{ lipid}^{-1}$. For each simulation systems containing oxidised lipid, two columns are provided, first column is surface tension and second column is surface pressure.

Time (ps)	DPPC with 10% PonPG Surface tension (mN m ⁻¹) 63 Å ² lipid ⁻¹		POPG with 10% PonPG Surface tension (mN m ⁻¹) 63 Å ² lipid ⁻¹		DPPC 80% POPG 10% PonPG 10% Surface tension (mN m ⁻¹) 63 Å ² lipid ⁻¹		DPPC 70% POPG 10% PonPG 20% Surface tension (mN m ⁻¹) 63 Å ² lipid ⁻¹		PonPG Surface tension (mN m ⁻¹) 63 Å ² lipid ⁻¹	
500	40 +- 131	7	-12 +- 136	59	22 +- 129	25	22 +- 129	25	-2 +- 127	49
1000	36 +- 130	11	3+- 134	44	28 +- 129	19	22 +- 130	25	7 +- 126	40
1500	34 +- 130	13	8 +- 135	39	31 +- 129	16	22 +- 130	25	13 +- 125	34
2000	33 +- 130	14	12 +- 135	35	29 +- 130	18	23 +- 129	24	18 +- 125	29
2500	33 +- 130	14	15 +- 134	32	30 +- 130	17	26 +- 129	21	21 +- 124	26
3000	33 +- 129	14	16 +- 134	31	31 +- 130	16	26 +- 129	21	23 +- 124	24
3500	33 +- 129	14	18 +- 134	29	30 +- 130	17	25 +- 129	22	25 +- 123	22
4000	32 +- 129	15	18 +- 134	29	31 +- 130	16	26 +- 129	21	27 +- 123	20
4500	33 +- 128	14	20 +- 134	27	30 +- 130	17	27 +- 129	20	29 +- 124	18
5000	33 +- 128	14	20 +- 134	27	30 +- 130	17	29 +- 129	18	29 +- 123	18

Table 3. Showing the change in surface tension/pressure over regular interval (0.5 ns) of simulation at $63 \text{ \AA}^2 \text{ lipid}^{-1}$. For each simulation systems containing oxidised lipid, two columns are provided, first column is surface tension and second column is surface pressure.

As can be seen from table 2 and 3, the surface pressure values at intervals of 0.5 ns generally shows a large surface pressure value initially and gradually stabilizing over the simulation time to the value observed in table 1. This suggests that the acyl chain reversal might have already happened at 0.5 ns. This is found to be the case as shown in table 9 and 10, the aldehyde group instantly moves closer to the interface and remains within hydrogen bonding distance from the interface.

3.2.4. Monolayer thickness

In the presence of oxidised lipids, the monolayer is expanded as a result of acyl chain reversal in simulations using constant pressure. This results in the monolayers transitioning from a liquid-condensed phase to liquid-expanded phase. [47] Expanded monolayers are more fluid than the well packed monolayers, therefore the monolayer thickness is expected to be lower for the expanded phase. However this study uses a constant volume, hence monolayer expansion is not possible. Therefore a measure of the fluidity of the monolayer will depend on the orientation of the tail groups of lipid towards water. For instance does the lipid tail groups orient more towards the water effectively decreasing the monolayer thickness and hydrophobic region in the presence of oxidised lipid? Or does it cause an increase in monolayer thickness and hydrophobic region?. At $63 \text{ \AA}^2 \text{ lipid}^{-1}$, molecular dynamics simulations of DPPC monolayer at 310 K is reported to be in L_e phase, [69] therefore lipid tail group movement and rearrangement is possible at both area per lipid, more so at $80 \text{ \AA}^2 \text{ lipid}^{-1}$ where pore formation is reported. [69]

System	Monolayer thickness	
	At $80 \text{ \AA}^2 \text{ lipid}^{-1} (\text{\AA})$	At $63 \text{ \AA}^2 \text{ lipid}^{-1} (\text{\AA})$
DPPC	16.8 +- 0.9	16.8 +- 0.8
POPG	14.7 +- 0.9	18.9 +- 1.0
DPPC with 10% PonPG	14.7 +- 0.8	16.8 +- 0.9
POPG with 10% PonPG	16.8 +- 0.9	16.8 +- 1.0
DPPC 80%, POPG 20%	16.8 +- 0.8	16.8 +- 0.8
DPPC 80%,POPG 10%, PonPG 10%	14.7 +- 0.8	16.8 +- 0.8
DPPC 70%, PonPG 20%, POPG 10%	12.6 +- 0.8	16.8 +- 0.8
PonPG	12.6 +- 0.8	14.7 +- 0.7

Table 4. Monolayer thickness of different simulations. Calculations were carried out using DPPC electron density for all except pure POPG, POPG with 10% PonPG and PonPG. For POPG and POPG with 10% PonPG systems, electrons density of POPG is used calculate the monolayer thickness. Electron density profile of PonPG head and tail atoms were used to calculate the monolayer thickness of pure PonPG monolayers. For more details on calculation of monolayer thickness, see supplementary information (S10.1.1).

As can be seen from table 4, in the presence of oxidised lipid, the monolayer thickness decreases for all systems except for 10% oxidised lipid replaced with pure POPG system at $80 \text{ \AA}^2 \text{ lipid}^{-1}$. There is also evidence of decrease in monolayer thickness upon the increase in oxidised lipid concentration as increase of 10% oxidised lipid to 20% in the mixed monolayers at $80 \text{ \AA}^2 \text{ lipid}^{-1}$ results in a decrease from 14.7 to 12.6 \AA . At lower area per lipid of 63 \AA^2 , the effect of oxidised lipid on monolayer thickness is not evident. This maybe due to the way in which the monolayer thickness is calculated using only the difference in electron density peaks of DPPC head and tail groups, hence at $63 \text{ \AA}^2 \text{ lipid}^{-1}$ oxidised lipid may not affect the way DPPC molecules are packed. At $63 \text{ \AA}^2 \text{ lipid}^{-1}$, only reduction of monolayer thickness due to the presence of oxidised lipid is noticed in POPG with

10% PonPG. However the monolayer thickness calculated for this system is using the electron density profile of POPG as there are no DPPC present in the system. The monolayer thickness of POPG with 10% PonPG at $80 \text{ \AA}^2 \text{ lipid}^{-1}$ shows opposite effect as the thickness is observed to increase from 14.7 Å for pure POPG to 16.8 Å. Pure PonPG monolayer at $80 \text{ \AA}^2 \text{ lipid}^{-1}$ shows same value as with mixed system at 20% concentration. However the tail group atom used for monolayer thickness calculation is the CH_3 group of the *sn*-1 chain as opposed to the aldehyde group. *sn*-1 chains of PonPG are generally oriented towards the hydrophobic region remaining perpendicular to the monolayer, also reported previously. [47] At $63 \text{ \AA}^2 \text{ lipid}^{-1}$ simulation, the monolayer thickness of pure PonPG is lower than all other systems.

A more relevant measure of the fluidity of the lipids in the presence of oxidised lipids is the order parameter values of acyl chains of the lipids.

3.2.5. Order Parameter

Order parameter of the *sn*-1 acyl chain of the DPPC at 80 \AA^2 and $63 \text{ \AA}^2 \text{ area lipid}^{-1}$ is given in figure 17 and 18 respectively for all systems that contains DPPC. The order parameter of *sn*-2 chains of DPPC at $80 \text{ \AA}^2 \text{ lipid}^{-1}$ and $63 \text{ \AA}^2 \text{ lipid}^{-1}$ are given in figure 19 and 20 respectively. Order parameter values of *sn*-1 chains of POPG at 80 \AA^2 and $63 \text{ \AA}^2 \text{ lipid}^{-1}$ is given in figure 21 and 22 respectively. The order parameter values of *sn*-2 chains of POPG at 80 \AA^2 and $63 \text{ \AA}^2 \text{ lipid}^{-1}$ is given in figure 23 and 24 respectively. The behaviour of the acyl chains of DPPC and POPG assessed using order parameter shows number of observations depending on the simulation system. As expected the acyl chains become more ordered with a decrease in area per lipid for both chains of DPPC and POPG. When pure monolayers (systems 1&2) of DPPC and POPG were mixed with 10% of oxidised lipid (systems 3&4), a definite decrease in order parameter is observed at both area per lipid and for both acyl chains. This trend remains same for the mixed monolayers (systems 5&6) where the monolayers of 80% DPPC and 20% POPG is replaced with oxidised lipid to 80% DPPC 10% POPG and 10% PonPG. A sharp decrease in order parameter value of POPG *sn*-1 chain in 80 % DPPC, 20% POPG (figure 21, unfilled circle) compared to pure POPG (figure 21, filled circle) at $80 \text{ \AA}^2 \text{ lipid}^{-1}$. The *sn*-1 chain of POPG at 80 \AA^2 (figure 21, filled circle) have a significantly large difference in order parameter value compared to the *sn*-1 of POPG in DPPC:POPG:PonPG (figure 21, unfilled square). *sn*-1 of POPG in POPG:PonPG (figure 22, filled square) at $63 \text{ \AA}^2 \text{ lipid}^{-1}$ has a significantly larger value compared to *sn*-1 of POPG in DPPC:POPG:PonPG (figure 22, unfilled square), indicating either the concentration of POPG in the monolayer or the presence of DPPC in

monolayer have a direct effect on the order parameter of POPG *sn*-1 chain. A correlation of reduced order parameter values for lipid species in the presence of oxidised lipid species is also established.

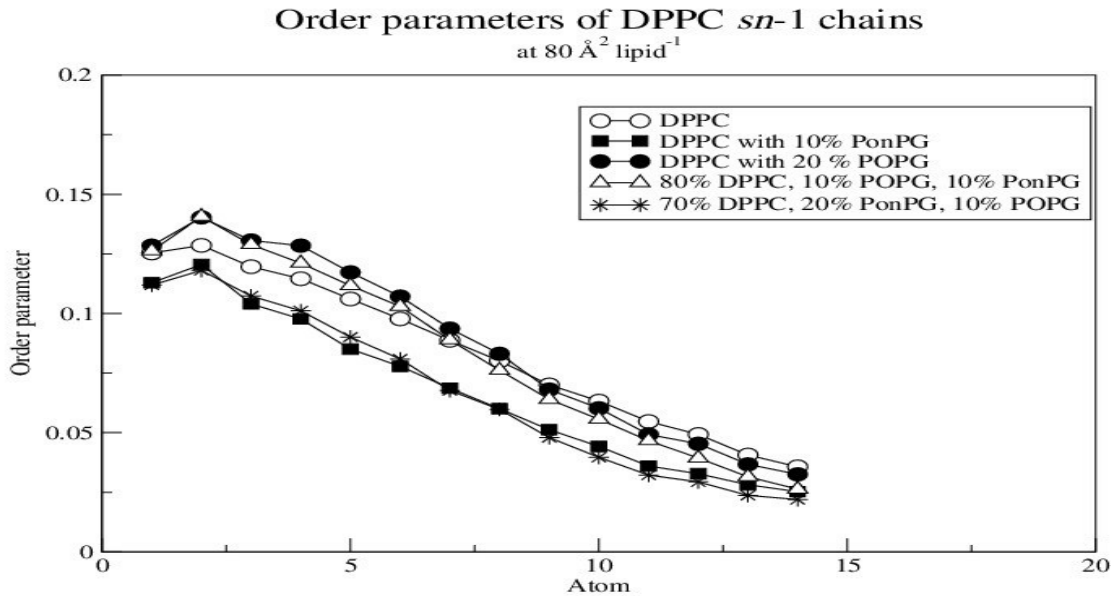


Figure 17. Showing the order parameter values of DPPC *sn*-1 chains in different systems at 80 \AA^2 area lipid $^{-1}$. Unfilled circle represents pure DPPC, filled circle represents DPPC with 20% POPG, filled square represents DPPC with 10% PonPG, unfilled triangle represents DPPC with 10% POPG and 10% PonPG, stars represent DPPC with 20% PonPG and 10% POPG. Atom 1 represents the first CH_2 carbon in the acyl chain that is close to the head group.

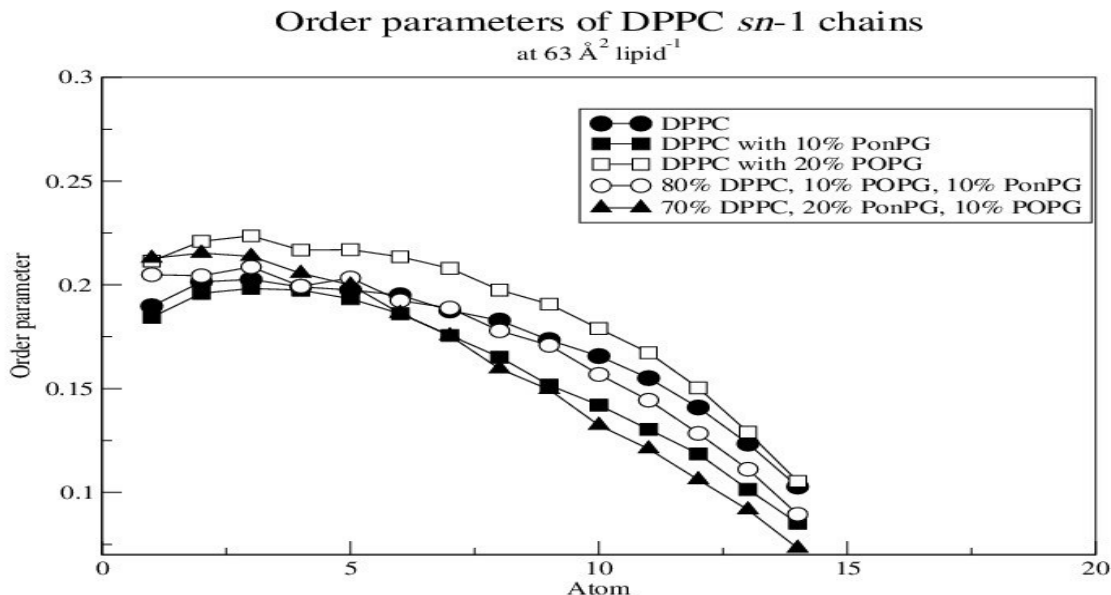


Figure 18. Showing the order parameter values of DPPC *sn*-1 chains in different systems at 63 \AA^2 area lipid $^{-1}$. Filled circle represents pure DPPC, filled square represents DPPC with 10% PonPG, unfilled square represents DPPC with 20% POPG, unfilled circle represents DPPC with 10% POPG and 10% PonPG, filled triangle represents DPPC with 20% PonPG and 10% POPG.

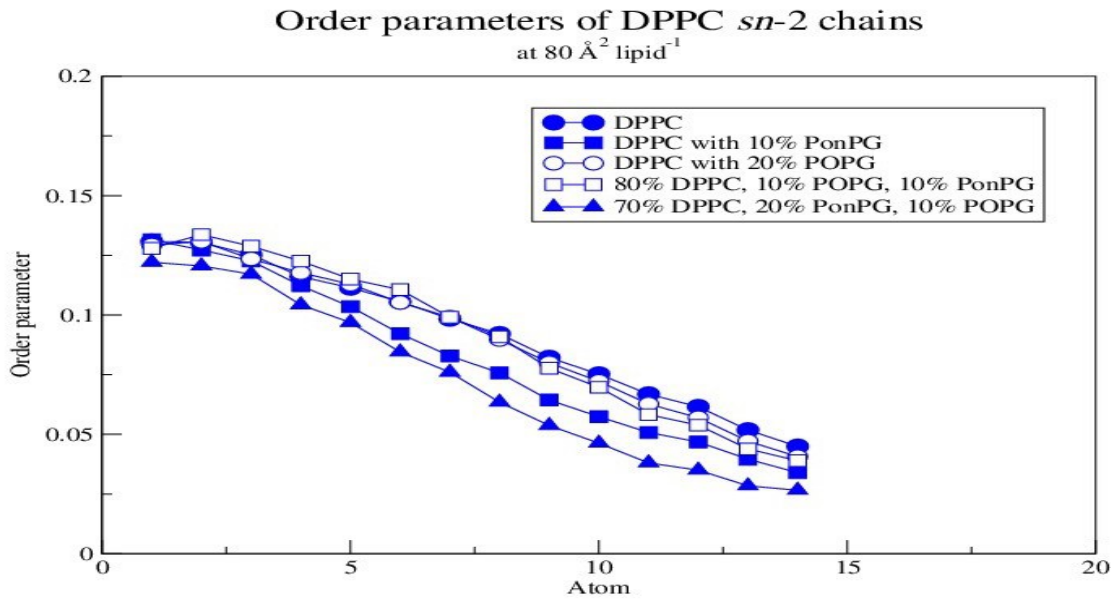


Figure 19. Showing the order parameter values of DPPC *sn*-2 chains in different systems at 80 \AA^2 area lipid $^{-1}$. Filled circle represents pure DPPC, filled square represents DPPC with 10% PonPG, unfilled circle represents DPPC with 20% POPG, unfilled square represents DPPC with 10% POPG and 10% PonPG, filled triangle represents DPPC with 20% PonPG and 10% POPG.

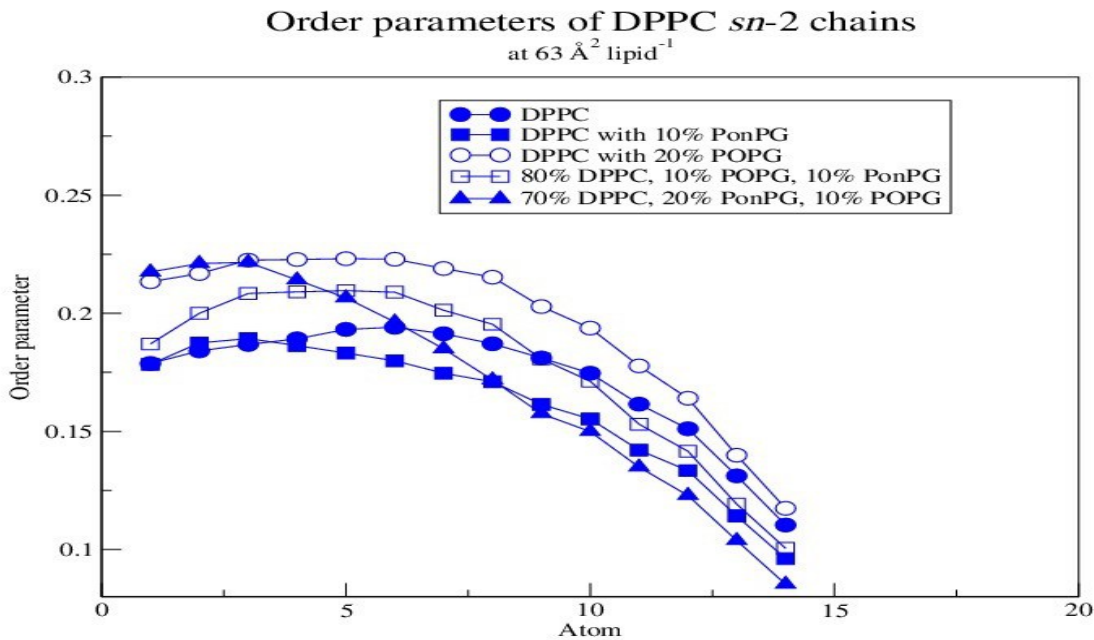


Figure 20. Showing the order parameter values of DPPC *sn*-2 chains in different systems at 63 \AA^2 area lipid $^{-1}$. Filled circle represents pure DPPC, filled square represents DPPC with 10% PonPG, unfilled circle represents DPPC with 20% POPG, unfilled square represents DPPC with 10% POPG and 10% PonPG, filled triangle represents DPPC with 20% PonPG and 10% POPG.

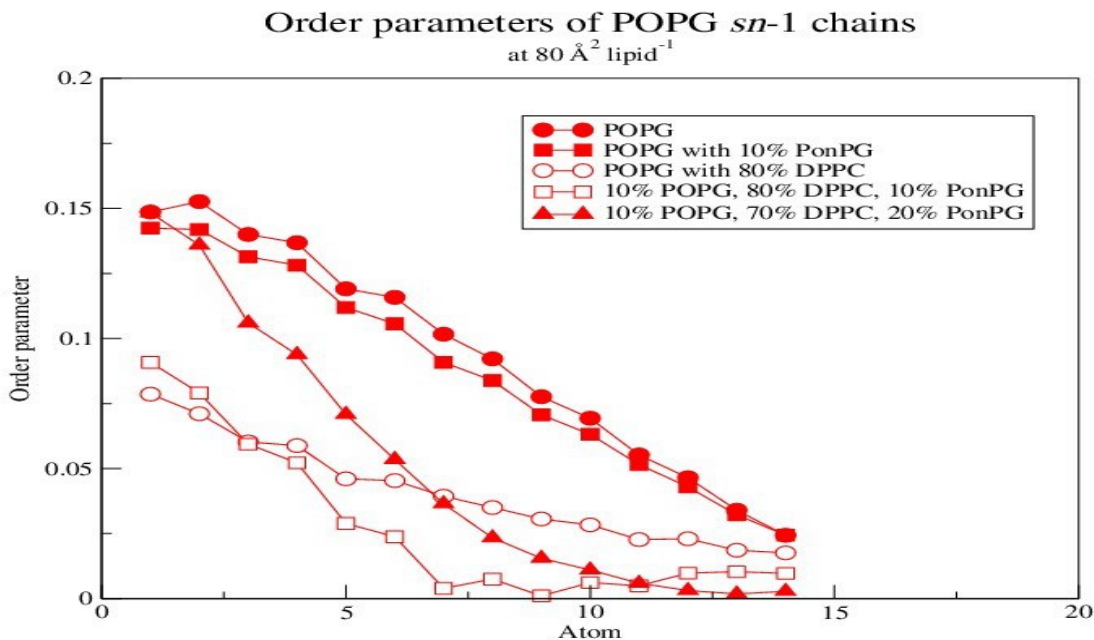


Figure 21. Showing the order parameter values of POPG *sn*-1 chains in different systems at 80 \AA^2 area lipid $^{-1}$. Filled circle represents pure POPG, filled square represents POPG with 10% PonPG, unfilled circle represents POPG with 80% DPPC, unfilled square represents POPG with 80% DPPC and 10% PonPG, filled triangle represents POPG with 70% DPPC and 20% PonPG.

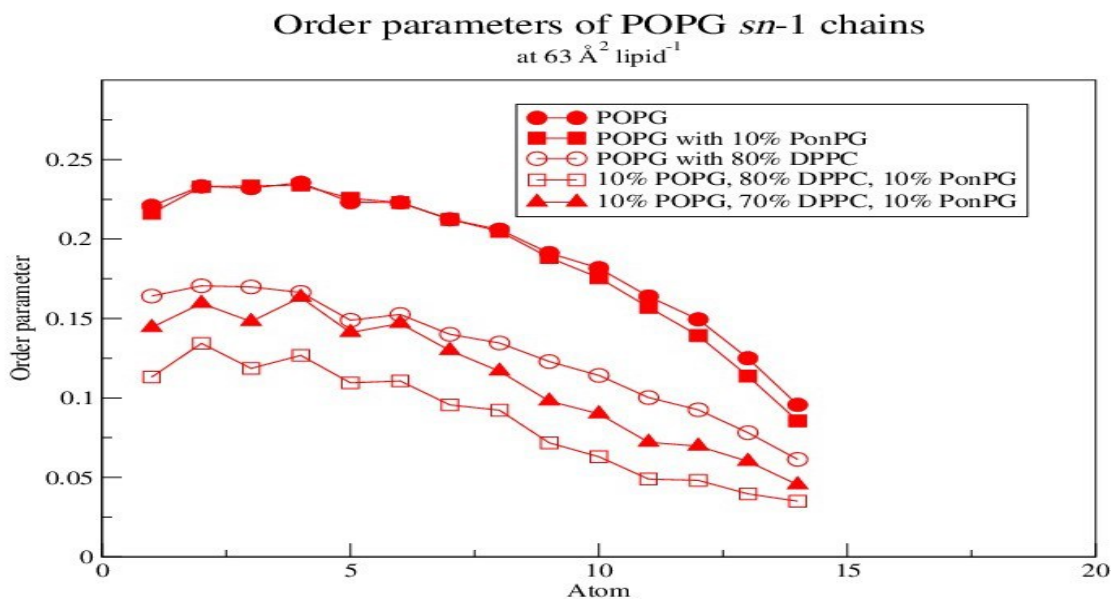


Figure 22. Showing the order parameter values of POPG *sn*-1 chains in different systems at 63 \AA^2 area lipid $^{-1}$. Filled circle represents pure POPG, filled square represents POPG with 10% PonPG, unfilled circle represents POPG with 80% DPPC, unfilled square represents POPG with 80% DPPC and 10% PonPG, filled triangle represents POPG with 70% DPPC and 20% PonPG.

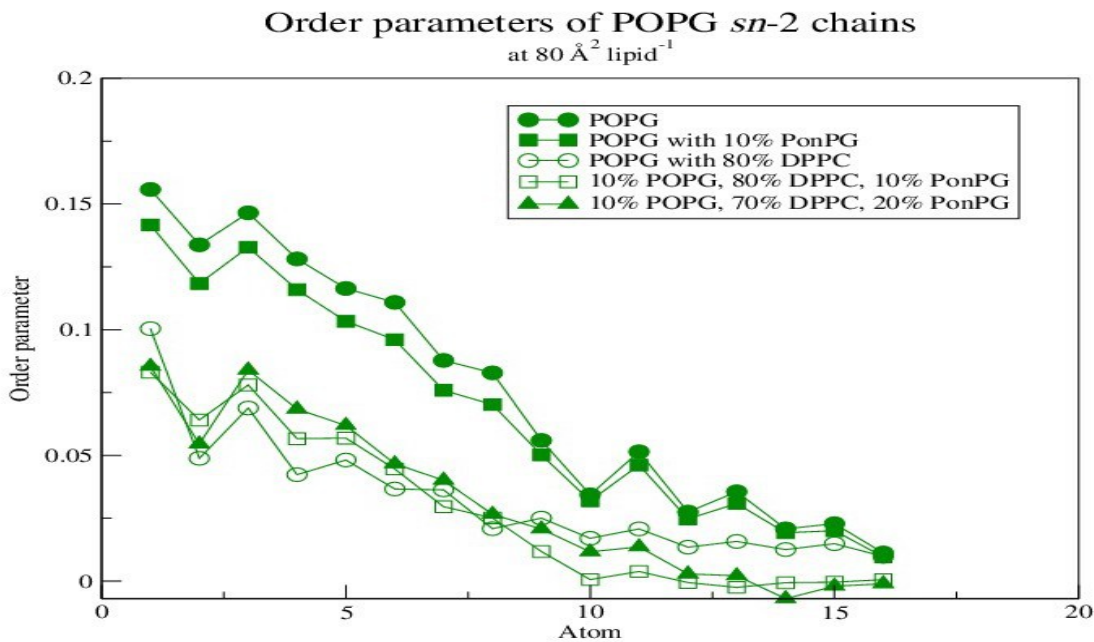


Figure 23. Showing the order parameter values of POPG *sn*-2 chains in different systems at $80 \text{ \AA}^2 \text{ area lipid}^{-1}$. Filled circle represents pure POPG, filled square represents POPG with 10% PonPG, unfilled circle represents POPG with 80% DPPC, unfilled square represents POPG with 80% DPPC and 10% PonPG, filled triangle represents POPG with 70% DPPC and 20% PonPG.

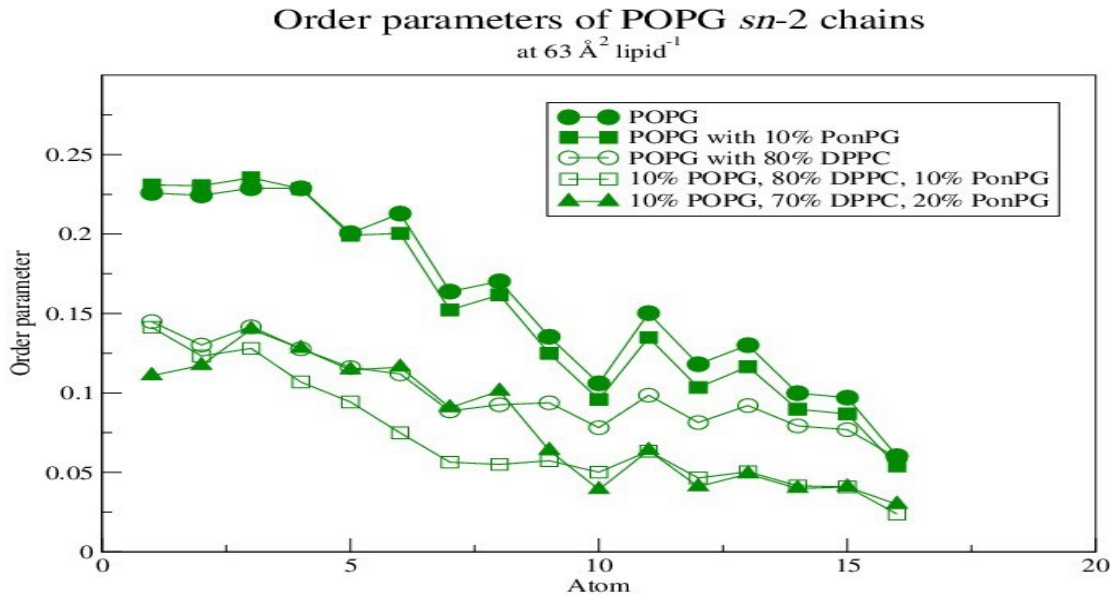


Figure 24. Showing the order parameter values of POPG *sn*-2 chains in different systems at $63 \text{ \AA}^2 \text{ area lipid}^{-1}$. Filled circle represents pure POPG, filled square represents POPG with 10% PonPG, unfilled circle represents POPG with 80% DPPC, unfilled square represents POPG with 80% DPPC and 10% PonPG, filled triangle represents POPG with 70% DPPC and 20% PonPG.

A good correlation of decrease in order parameter values of both DPPC and POPG monolayers upon introduction of 10% oxidised lipid is observed. This trend remains same for the *sn*-2 chain of DPPC in mixed monolayer. The decrease in order parameter value of *sn*-2 chain of

DPPC is correlated with the percentage of oxidised lipid, as observed by a lower value for 20% oxidised system compared to 10% oxidised system. Upper chain order parameter values of first few carbons of POPG *sn*-1 chain in mixed monolayer of 70% DPPC, 20% PonPG, 10% POPG (figure 21, filled triangle) at $80 \text{ \AA}^2 \text{ lipid}^{-1}$ are higher than mixed monolayer containing 80% DPPC, 20% POPG (figure 21, unfilled circle) and mixed monolayer containing 80% DPPC, 10% POPG, 10% PonPG (figure 21, unfilled square). At $63 \text{ \AA}^2 \text{ lipid}^{-1}$ first few carbon atoms of *sn*-1 of POPG in mixed monolayer of 70%, 20% PonPG, 10% POPG (figure 22, filled triangle) shows higher values when compared with 10% oxidation (figure 22, unfilled square). This trend is also observed in the first few carbons of *sn*-2 chains of POPG in mixed monolayer at $80 \text{ \AA}^2 \text{ lipid}$. Where 10% oxidation (figure 23, unfilled square) is higher than 80% DPPC, 20% POPG mixed monolayer (figure 23, unfilled circle) and the 20% oxidation shows higher values than both 80% DPPC, 20% POPG and 10% oxidation. This trend is also observed at $63 \text{ \AA}^2 \text{ lipid}^{-1}$ for 20% oxidation (figure 24, filled triangle) compared with 10% oxidation (figure 24, unfilled square).

From the order parameter calculations, it is clear that the presence of oxidised lipid affects the fluidity of the membranes. The systems simulated shows a decrease in order parameter values of acyl chains of lipids in the presence of PonPG, making the systems more fluid.

3.2.6. Movement of lipid head groups into water

Permeability of water is reported to be increased in the presence of oxidised lipids. The free energy increases from the water interface to the hydrophobic region of the membranes. The oxidised lipids decrease the free energy barrier for water penetration due to the position of the polar oxygen in the tails and therefore increase the water penetration which is correlated with area per lipid and concentration of the oxidised lipid. [51]

Since the water movement is found to be limited towards the hydrophobic region (see 3.1), an indirect way to measure the water permeability is to measure the immersion of lipid head groups into the water to detect possible decrease in hydrophobic region of the lipid tails.

Lipid headgroup (Phosphorus) of DPPC at 80 Å area/lipid

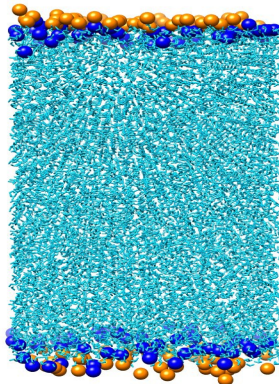


Figure 25. Snapshot of lipid head movement towards water. Orange balls represent the head groups before simulation. Blue balls represent the head groups after 5 ns simulation. Light blue sticks represent water molecules.

System at 80 Å ² lipid ⁻¹	Average distance moved (nm) DPPC	Max distance moved by a single DPPC (nm)	Average distance moved (nm) POPG	Max distance moved by a single POPG (nm)	Average distance moved(nm) PonPG	Max distance moved by a single PonPG (nm)
DPPC	0.47 +- 0.26	1.16				
POPG			0.46 +- 0.27	1.11		
DPPC with 10% PonPG	0.54 +- 0.26	1.19			0.46 +- 0.31	0.93
POPG with 10% PonPG			0.45 +- 0.29	1.33	0.55 +- 0.26	0.87
80% DPPC, 20% POPG	0.48 +- 0.26	1.18	0.28 +- 0.19	0.63		
80% DPPC, 10% POPG, 10% PonPG	0.54 +- 0.23	1.15	0.37 +- 0.31	0.86	0.47 +- 0.25	0.81
70% DPPC, 20% PonPG, 10% POPG	0.46 +- 0.23	1.13	0.39 +- 0.29	0.83	0.40 +- 0.20	0.77
PonPG					0.50 +- 0.28	1.28

Table 5. Showing the average head group movement for all lipid molecules at the end of 5 ns simulation. The average direction of movement is calculated to be towards water for all systems simulated. Table also presents the largest distance moved by each lipid type within simulation.

Movement of head group into the water is observed for all lipids at both area per lipid simulations. An increase in head group immersion was observed with the addition of 10% oxidised lipid for pure DPPC and mixed monolayer of 80% DPPC, 10% POPG, 10% PonPG at $80 \text{ \AA}^2 \text{ lipid}^{-1}$. However increasing the concentration of PonPG to 20% in the mixed monolayer seems to have a decrease in movement compared to 10% oxidised system and pure mixed monolayer of 80% DPPC, 20% POPG. Introduction of 10% oxidised lipids seems to have a slight decrease in movement compared to pure POPG monolayer. A significant increase $\sim 0.9 \text{ \AA}$ in head group immersion of POPG is observed with an addition of 10% oxidised lipid in the mixed monolayer of 80% DPPC, 10% POPG, 10% PonPG. This was further increased by $\sim 0.2 \text{ \AA}$ upon the increase in PonPG concentration. Head group immersion of PonPG is observed highest in POPG monolayer with 10% PonPG (system 4) and this is significantly larger $\sim 0.9 \text{\AA}$, than the DPPC with 10% PonPG system (system 3). No significant difference in PonPG head group movement is observed in mixed monolayer of 80% DPPC, 10% POPG, 10% PonPG compared with DPPC with 10% PonPG, however a reduction in movement is noted when compared with POPG monolayer with 10% PonPG. When the concentration of the PonPG is increased in the mixed system to 20%, a reduction is noticed compared to the 10% concentration system. Pure PonPG system shows a higher movement of the head groups when compared with DPPC with 10% PonPG, mixed monolayer with 10% PonPG and mixed monolayer with 20% PonPG. However the average distance moved by PonPG head groups in pure PonPG system is lower than the POPG with 10% system.

System at $63 \text{ \AA}^2 \text{ lipid}^{-1}$	Average distance moved (nm) DPPC	Max distance moved by a single DPPC (nm)	Average distance moved (nm) POPG	Max distance moved by a single POPG	Average distance moved (nm) PonPG	Max distance moved by a single PonPG
DPPC	0.53 +- 0.32	1.32				
POPG			0.45 +- 0.27	1.10		
DPPC with 10% PonPG	0.55 +- 0.30	1.24			0.23 +- 0.17	0.49
POPG with 10% PonPG			0.51 +- 0.25	1.10	0.35 +- 0.33	1.01
80% DPPC, 20% POPG	0.42 +- 0.26	1.11	0.33 +- 0.22	0.70		

80% DPPC, 10% POPG, 10% PonPG	0.49 +- 0.31	1.25	0.33 +- 0.16	0.59	0.49 +- 0.30	0.94
70% DPPC, 20% PonPG, 10% POPG	0.50 +- 0.32	1.26	0.48 +- 0.28	1.18	0.38 +- 0.22	0.81
PonPG					0.44 +- 0.27	1.36

Table 6. Showing the average head group movement for all lipid molecules at the end of 5 ns simulation. The average direction of movement is calculated to be towards water for all systems simulated. Table also presents the largest distance moved by each lipid type within simulation.

At $63 \text{ \AA}^2 \text{ lipid}^{-1}$ area, introduction of 10% oxidised lipid increases the distance moved by DPPC in pure monolayer and mixed monolayer. Increasing the percentage of oxidised lipid to 20% in mixed monolayer seems to increase the head group movement of DPPC, however this is lower than the value observed for pure DPPC monolayer with a difference of $\sim 0.5 \text{ \AA}$. Introduction of oxidised species increase the head group movement in pure POPG monolayer with a difference of $\sim 0.6 \text{ \AA}$. No difference is noted for the head group movement of POPG in mixed monolayer upon introduction of 10% oxidised lipid, however increasing the concentration results in an increase in head group movement compared to mixed monolayer, but as with DPPC this is lower than the pure POPG monolayer. Head group movement of oxidised lipid is greater in the presence of POPG at both area per lipid. In mixed monolayer of DPPC and POPG the head group of oxidised lipid shows an increased distance travelled into water, but this is reduced upon the increase in oxidised lipid concentration. A distinct correlation between the head group movement of any lipid against the difference in area per lipid is difficult to detect from the two tables. Increased movement is observed for DPPC in pure DPPC monolayer and monolayer contains DPPC and 10% oxidised lipid at $63 \text{ \AA}^2 \text{ lipid}^{-1}$. But this is reduced in the mixed monolayers of 80% DPPC, 20% POPG ,10% PonPG, except for with 20% oxidised lipid. POPG head movement shows a greater distance travelled into water at $63 \text{ \AA}^2 \text{ lipid}^{-1}$, except for mixed monolayer with 10% oxidised lipid.

The distance moved by oxidised lipid head group is higher at $80 \text{ \AA}^2 \text{ lipid}^{-1}$ except for mixed monolayer with 10% oxidised lipid. Overall there is some evidence of increases in lipid head group movement in the presence of PonPG, hence a decrease in hydrophobic region of the monolayers.

3.2.7. Movement of aldehyde group

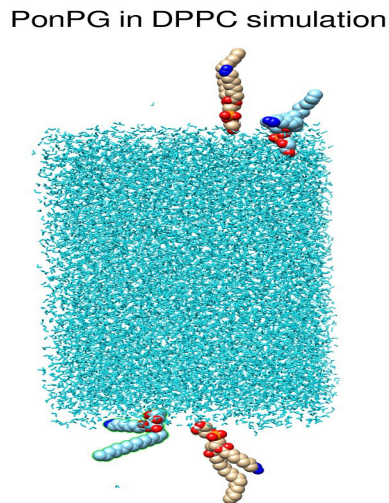


Figure 26. Showing the movement of aldehyde group after 5 ns simulation. One oxidised molecule from each lipid monolayers in the system is shown. Gold spheres represent the PonPG before simulation and the light blue spheres represent the PonPG after 5 ns of simulation. Aldehyde groups are shown in dark blue spheres. Water molecules are presented as light blue sticks. Oxygen atoms are coloured in red.

System	Average distance moved at 80 Å ² lipid ⁻¹ (Å)	Max distance moved by a single PonPG at 80 Å ² lipid ⁻¹ (Å)	Average distance moved at 63 Å ² lipid ⁻¹ (Å)	Max distance moved by a single PonPG at 63 Å ² lipid ⁻¹ (Å)
DPPC with 10% PonPG	19.1 +- 0.3	26.1	15.4 +- 0.36	20.2
POPG with 10% PonPG	16.6 +- 0.37	24.8	15.6 +- 0.52	24.3
80% DPPC, 10% POPG, 10% PonPG	18.2 +- 0.28	25.5	17.9 +- 0.78	30.5
70% DPPC, 20% PonPG, 10% POPG	18.7 +- 0.34	25.8	15.8 +- 0.48	22.8
PonPG	19.7 +- 0.46	37.1	17.4 +- 0.58	38.8

Table 7. Showing the average distance moved by the aldehyde oxygen towards water from the initial conformation. The average direction of movement was calculated to be towards water for all systems simulated. Table also showing the largest an oxidised lipid moved towards the water.

On average the distance moved by the aldehyde group towards the water at 80 Å² lipid⁻¹ is greater than at 63 Å² area lipid⁻¹. At 80 Å² area lipid⁻¹ DPPC system with 10% oxidised lipid has moved a greater distance than POPG with 10% oxidised lipids. The largest distance travelled by the aldehyde group at 80 Å² is the pure 100% oxidised lipid system with a value of 19.7 Å. A slight increase of ~0.5 Å is observed when the concentration of oxidised lipid is increased from 10% to 20% in the

mixed monolayer. At $63 \text{ \AA}^2 \text{ area lipid}^{-1}$ the largest distance travelled by the aldehyde group is in the mixed monolayer with 10% oxidised lipids. An increase of oxidised lipid concentration shows a decrease in aldehyde group movement towards water at lower area per lipid of 63 \AA^2 . 100% oxidised lipid shows an increase in distance moved compared to 20% oxidised mixed system, however the value is lower by $\sim 0.4 \text{ \AA}$ when compared to 10% oxidised mixed system.

3.2.8. Acyl-chain reversal

Acyl-chain reversal will be defined as a certain distance the aldehyde group moved towards the water from the initial configuration file. The threshold value will be 16 \AA which is the distance between the head group phosphate and the aldehyde chain of the oxidised lipid PonPG.

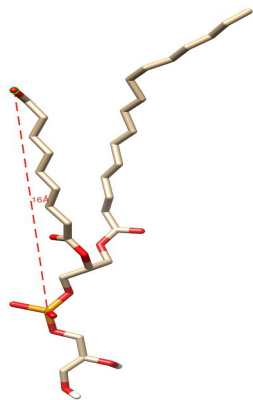


Figure 27. Showing the distance between the head group phosphate and aldehyde oxygen. The distance is 16 \AA .

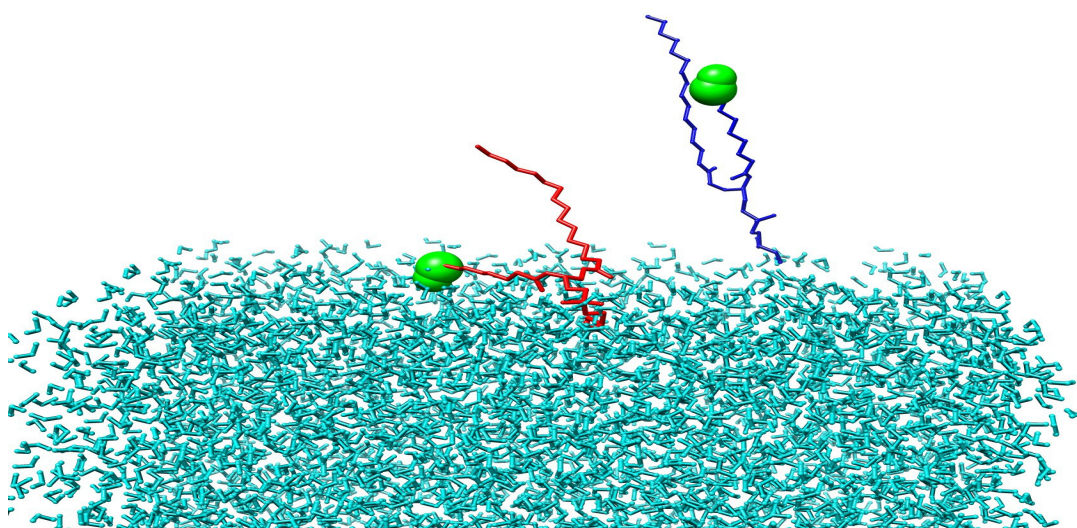


Figure 28. Showing a representative snapshot of acyl-chain reversal after 5 ns simulation. Blue residue represents PonPG at $t = 0 \text{ ns}$, red residue represents PonPG at $t = 5 \text{ ns}$, green spheres represent the aldehyde group of the PonPG molecule. Light blue sticks represent the water molecules.

System	Percentage of acyl-chain reversal at 80 Å ² lipid ⁻¹ (%)	Percentage of acyl-chain reversal at 63 Å ² lipid ⁻¹ (%)
DPPC with 10% PonPG	80	60
POPG with 10% PonPG	40	40
80% DPPC, 10% POPG, 10% PonPG	80	50
70% DPPC, 20% PonPG, 10% POPG	82	55
PonPG	83	57

Table 8. Showing the percentage of oxidised lipid molecules that carried out acyl-chain reversal after 5 ns simulation.

A clear decrease in acyl chain reversal is observed upon compression of monolayer from 80 Å² to 63 Å² area lipid⁻¹ for all systems, except POPG simulation with 10% oxidised lipid, which remains same. A slight increase in chain reversal is observed upon increase in concentration of oxidised lipid in mixed monolayer at 80 Å² lipid⁻¹. The change in percentage is increased from 50 to 57 at 63 Å² lipid⁻¹.

In order to make sure that the attraction of the polar aldehyde group to the water is stable, the acyl chain reversal is measured at regular intervals (0.5 ns) during simulation for all systems containing PonPG at both area per lipid.

Time (ps)	DPPC with 10% PonPG	POPG with 10% PonPG	80% DPPC, 10% POPG, 10% PonPG	70% DPPC, 20% PonPG, 10% POPG	PonPG
500	20.9	13.6	18.4	17.3	18.5
1000	18.7	16.4	19.5	17.4	18.9
1500	17.7	14.5	18.7	17.0	19.4
2000	18.0	16.2	18.6	18.5	19.2
2500	18.4	16.1	18.2	17.1	18.9
3000	19.1	17.7	18.4	18.0	18.6
3500	19.4	18.2	18.7	18.4	19.4
4000	18.4	19.1	20.0	17.7	18.8
4500	18.8	15.5	18.2	18.1	19.2
5000	19.1	16.6	18.2	18.6	19.7

Table 9. Showing the average movement of aldehyde group in angstroms (Å) from initial structure at regular intervals (0.5 ns) during the simulation. Systems presented is at 80 Å² lipid⁻¹.

Time (ps)	DPPC with 10% PonPG	POPG with 10% PonPG	80% DPPC, 10% POPG, 10% PonPG	70% DPPC, 20% PonPG, 10% POPG	PonPG
500	13.1	15.0	14.6	14.9	15.3
1000	14.2	16.2	15.6	15.9	16.0
1500	15.3	15.7	15.7	17.0	16.4
2000	14.5	14.6	18.6	16.5	16.3
2500	16.4	12.6	18.2	16.2	17.0
3000	15.3	14.7	17.8	17.5	17.4
3500	15.0	13.7	17.7	16.6	17.0
4000	16.7	13.0	18.2	16.9	17.0
4500	15.5	15.2	18.4	15.5	16.6
5000	15.4	15.6	17.9	15.8	17.4

Table 10. Showing the average movement of aldehyde group in angstroms (\AA) from initial structure at regular intervals (0.5 ns) during the simulation. Systems presented is at $63 \text{ \AA}^2 \text{ lipid}^{-1}$.

As can be seen from table 9 and 10, the aldehyde group stays close to the interface even at 500 ps. Although there is movement of the aldehyde group after the acyl chain reversal, it does not flip back into the hydrophobic region and is within 3-4 \AA (hydrogen bond distance) from the head group/interface. This shows that the acyl-chain reversal is due to the strong attraction of the polar aldehyde group in the oxidised lipid to the water.

4. Discussion

A good agreement of order parameter values of acyl chains of pure DPPC and POPG in mixed monolayer of 80% DPPC and 20% POPG is determined for both area per lipid values when compared with MD simulation of lipid monolayers of pure DPPC and mixed monolayer of 70% DPPC and 30% POPG from literature. The slight deviations may be explained by the difference in concentration of lipid, temperature (10 K difference) and other simulation parameters. [73] Due to large fluctuations in the surface tension calculation, deviation from the surface pressure calculations reported previously are expected. A reasonable agreement has been found for the values of surface pressure when compared with experimental and simulated systems of monolayers. At $80 \text{ \AA}^2 \text{ lipid}^{-1}$ surface pressure exhibited by pure DPPC monolayer is between $0 - 10 \text{ mN m}^{-1}$. At $63 \text{ \AA}^2 \text{ lipid}^{-1}$ this is between $20-40 \text{ mN m}^{-1}$ (see supplementary information S12.3). [90] Molecular dynamics study of pure DPPC at two different temperatures and area per lipid shows a good correlation when compared with the surface pressure obtained in this study (see supplementary information S12.3.2). A good agreement has been found for a simulated mixed monolayer of DPPC:POPG in

7:3 ratio at 310 K [93] (see supplementary information S12.3.3). At higher temperature of 323 K the surface pressure is expected to be higher than at 310 K, however it is reasonable to assume that deviations of values may be attributed to the large fluctuations in the calculated surface tension values and/or different simulation protocols used for the simulations.

An increased order parameter values observed with a reduction in area per lipid can be explained by the conformational space available for the chains at different area per lipid. At $63 \text{ \AA}^2 \text{ lipid}^{-1}$ the monolayer is more compressed than at $80 \text{ \AA}^2 \text{ lipid}^{-1}$, hence both molecular species will have a restriction of space available for its chains to move around freely normal to the monolayer interface. Acyl chain length determines the interchain van der Waals attraction, hence a longer chain decreases the area per lipid and keep the head groups closer together. [93] DPPC chains show a higher order parameter than the POPG, this is explained by the kink introduced by the *sn*-2 double bond in POPG increasing the interchain distance, hence a reduced van der Waals attraction preventing a tight packing. An explanation for the decrease in *sn*-1 chain order parameter for POPG in the presence of 80% DPPC when compared to pure POPG monolayer can be the increased space available for the POPG chains to orient in the presence of more compact DPPC molecules than itself.

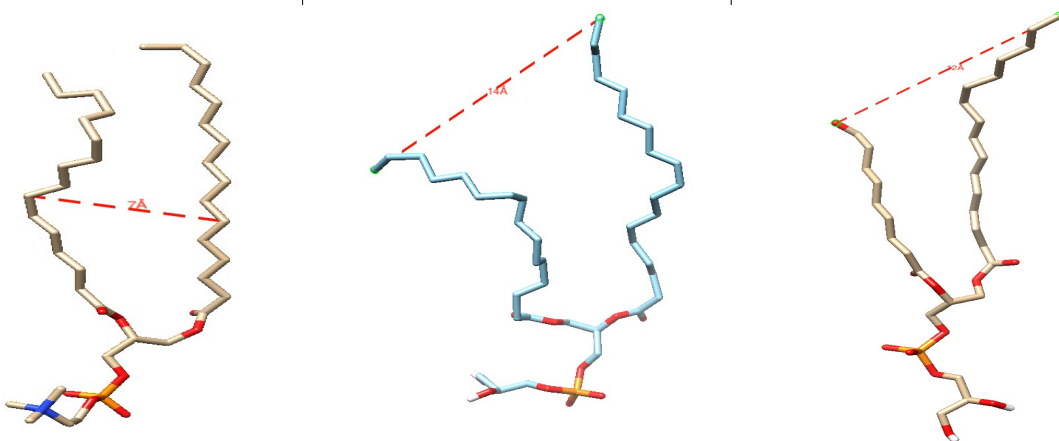


Figure 29. Showing the maximum distance between the acyl chains for the lipids used in simulations. DPPC has a distance of 7 Å, POPG (14 Å) and PonPG (12 Å).

The presence of oxidised lipid is correlated with a decrease in order parameter values and monolayer thickness. Both acyl chains of lipids studied are affected by the presence of oxidised species. The order parameter values suggest that increase in the concentration from 10% to 20% oxidised lipids in the monolayer decreases the acyl chain ordering of lipids. This effect is more evident in the monolayer thickness at $80 \text{ \AA}^2 \text{ lipid}^{-1}$, where the monolayer thickness reduced from

16.7 Å in mixed monolayer to 12.6 Å in mixed monolayer with 20% oxidised lipid. The reversal of the oxidatively modified acyl chains towards water decreases its length, therefore increasing the free space available for *sn*-1 chain, with the chain remaining perpendicular to the interface. This could result in an increase in volume available for the lipid chains which results in a decrease in order parameter values observed. [94]

Increase in monolayer thickness observed for POPG with 10% oxidised lipid when compared with pure POPG monolayer at $80 \text{ \AA}^2 \text{ lipid}^{-1}$ and a decrease observed at $63 \text{ \AA}^2 \text{ lipid}^{-1}$, suggests a differential effect of oxidised lipid on anionic lipid POPG. Furthermore the order parameter value of first few acyl chain carbons of POPG with 20% oxidised lipid is increased when compared with 10% oxidised lipid (see 3.2.5), suggesting at higher concentrations, the oxidised lipid improve the packing of POPG and negatively affect the packing of DPPC. Monolayer thickness calculated using POPG head and tail groups for the two concentrations of oxidised lipids in mixed monolayer at $63 \text{ \AA}^2 \text{ area lipid}^{-1}$ further compounds this evidence as the monolayer thickness was increased from 14.7 Å to 16.8 Å.

Area per lipid decrease in simulated systems with different salt concentrations are reported in POPG, DPPC and POPG bilayers. Increased concentrations of salt reduces the area per lipid. [95] [96][97] Area per lipid values in the presence of salt have greater reduction on PG lipids than PC lipids, and this is thought to be caused by the interaction between Na^+ ions and negatively charged lipids. [38] As can be seen from figure 30, the systems containing more negatively charged lipids show less spread in partial density across the simulation and are concentrated at the interface after 1 ns of simulation. For example DPPC with 10% PonPG system which only contains 5 ions show no observable peak in density, whereas systems containing only negatively charged lipids such as pure POPG and pure PonPG simulations show two clear peaks at box coordinates which correspond to the interfaces of the monolayers. Experimental determination of surface pressure as a function of area per lipid where the change in surface pressure for different concentrations of NaCl is monitored under a constant area per lipid is reported to increase the surface pressure as the concentration of NaCl increase. This is thought to be as a result of several interactions such as polar head group – solvent, polar head group-electrolyte and solvent-electrolyte interactions. [98] From figure 30 it is also observed that the higher the ion concentration the better separation of peaks, hence localisation of ions at the interface. A distinct formation of peaks is observed for systems containing higher concentrations of ions after 1 ns of simulation at both area per lipid, therefore the attraction of ions towards the interface is immediate and any effect induced by the ion interaction at the interface is relevant. The density peak of the ion remained same throughout the simulation time

(data not shown) and little movement of ion is observed away from the interface once it has localised near the interface. Experimental observation of dioleoylphosphatidylglycerol (DOPG) in the presence of counter ions is reported to have closer packing of the lipids and lack of fluidity in the upper chain region. [99] An increase in order parameter values in the upper chain in the presence of NaCl is reported and the motion of carbon-carbon bonds near head group is found to be restricted in the presence of NaCl. This is thought to be as a result of Na⁺ ions interacting with carbonyl oxygen atoms. [100] Systems simulated with Na⁺ ions show the movement of the ions towards the lipid head groups (figure 31).

Increase in monolayer thickness observed for POPG monolayers with 10% oxidised lipids at 80 Å² area lipid⁻¹ when compared to POPG only monolayer maybe attributed to the interaction of POPG or PonPG with Na⁺ improving the packing of the lipids as observed by an increase ordering of acyl chain carbons near the interface. This suggests that the interaction of Na⁺ ions with negatively charged lipids increase the packing capability of those lipids in a fluid system, hence the surface pressure. Monolayer thickness increase observed in the mixed monolayers with 10% and 20% oxidised lipid using POPG head and tail parameters can also be attributed to this effect. At 63 Å² lipid⁻¹ is still in the LE phase and at 323 K the system is expected to be in fluid state.

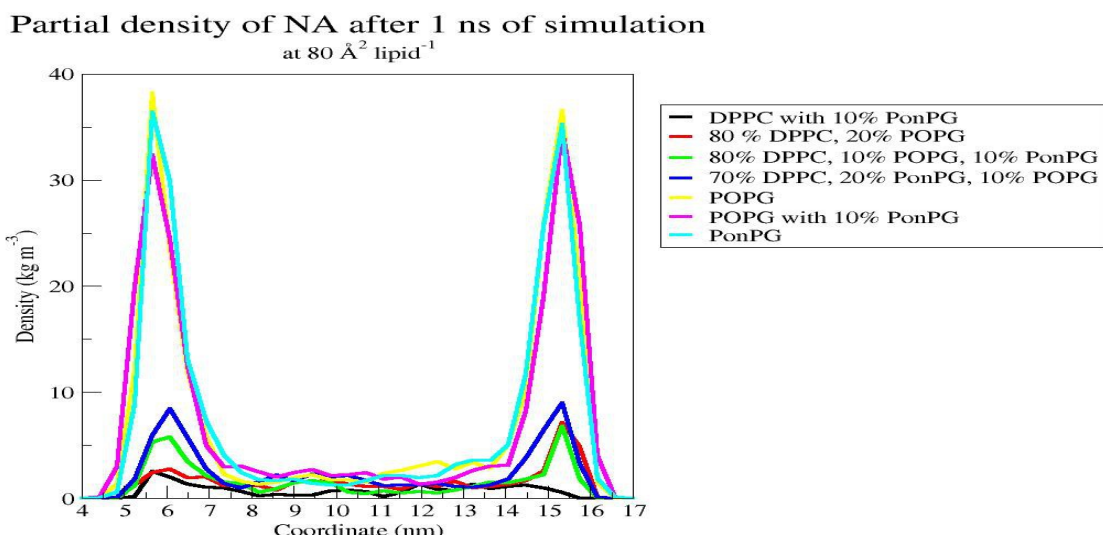


Figure 30. Showing the partial density of sodium atoms of simulated systems at 80 Å² lipid⁻¹ after 1 ns of simulation. Black line represents DPPC with 10% PonPG which contains 5 ions. Red line represents 80% DPPC, 20% POPG and contains 11 ions. Green line represents 80% DPPC, 10% POPG system and contains 11 ions. Blue represents 70% DPPC, 20% PonPG, 10% POPG and contains 17 ions. Yellow represents pure POPG simulation and contains 53 ions. Magenta represents POPG with 10% PonPG and contains 53 ions. Cyan line represents pure PonPG simulation and contains 53 ions.

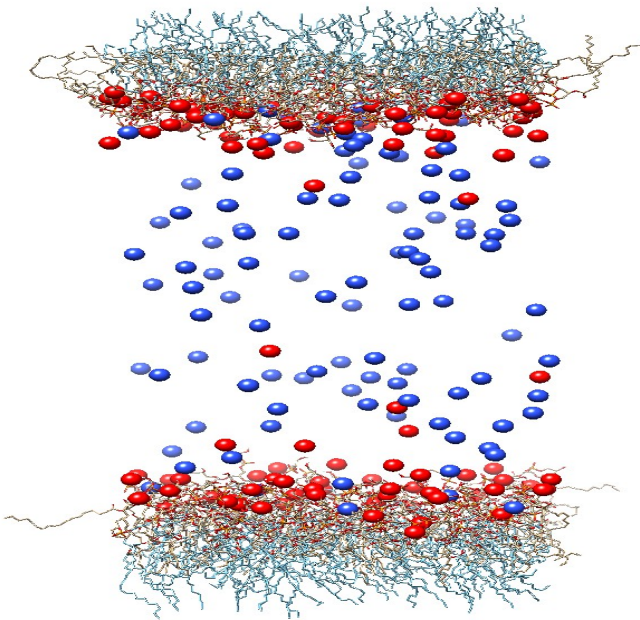


Figure 31. Showing the movement of Na^+ ions of POPG only system at $80 \text{ \AA}^2 \text{ lipid}^{-1}$. Blue ribbon represents the lipids before simulation and blue spheres represents the Na^+ ions before simulation. Gold ribbon represents lipids after simulation and red spheres represent Na^+ ions after 5 ns simulation.

Overall it has been observed that the introduction of oxidised lipid increases the surface pressure of monolayers, except for the DPPC only system compared to 10% oxidised system at $63 \text{ \AA}^2 \text{ lipid}^{-1}$ (table 1). Experimental determination of surface area of monolayers containing oxidised POPC under constant surface pressure using Langmuir trough results in a greater mean area per molecule for PonPC compared to pure POPC or DPPC. This is considered to be as a result of the acyl chain reversal of the oxidised chain containing a hydrophilic functional group bent towards the water surface taking more space than the ordered structure. [52] Experimental determination of surface pressure change as a function of area per molecule where the lipid monolayer is compressed at $4 \text{ \AA}^2 \text{ chain}^{-1} \text{ lipid}^{-1}$ results in higher surface pressure as the concentration of PonPC increases. Presence of oxidised lipids is thought to lower the surface potential of the monolayers due to reorganization of intra-molecular electric dipoles upon the accumulation of polar groups in the interfacial region. [47] Following this line of thought one would expect the pressure-area isotherm to increase in the presence of oxidised lipid. If the surface potential of the monolayer is lowered then the surface tension of the water at the interface is also lowered. Reduction in surface potential maybe attributed to the increase in hydrogen bonds between the newly available polar groups and water molecules. By the relation of surface tension and surface pressure (see 2.4.4), a reduction in surface tension will result in an increase in the surface pressure.

Oxidatively modified chains of phospholipids can change conformation within the monolayer by extending the chain into the aqueous phase (figure 26). Introduction of oxidatively modified lipids with polar functional groups at the end of acyl chain increases the water penetration, hence reducing the average hydrophobicity of the hydrocarbon chains. [47] Oxidised lipids are reported to expand the monolayers under constant surface pressure. [52][101] Acyl chain reversal leads to accumulation of polar groups in the interfacial region, hence the reorganization of the intramolecular electric dipoles of the head groups. [94] The head group movement increase noticed with the introduction of oxidised lipid may be attributed to the increased polar moieties available at the interface that can interact with the lipid head groups. From table 6 and 7, it is clear that, at higher area per lipid the aldehyde groups of the oxidised lipids move more close to the interfacial region. This may be attributed to the area available for the *sn*-2 chain to move at higher area per lipid. Another possible explanation for increased head group movement observed for lipids may be due to the ion-dipole interaction caused by the Na^+ ions in the system. The increased head group movement maybe attributed to the alignment of the molecules to increase the attraction to the ion. An increase in water penetration in the monolayers in the presence of oxidised lipid is established and this can be rationalised by the decrease in free energy barrier for water penetration as a result of increased polar moieties available at the interface.

A definite evidence for acyl chain reversal is observed at both are per lipid after 5 ns simulation and a general trend of increased movement of aldehyde group towards water with increasing concentration. Acyl chain reversal and increased lipid head movement can therefore be rationalised by the attraction of polar functional group in the *sn*-2 to the interface causing increased surface available for water penetration and decreased hydrophobic interaction of the acyl-chains. Figure 28 shows a representative snapshot of acyl-chain reversal, and this conformation is noted for many oxidised lipids in the simulated systems. To be able to define the acyl chain reversal and degree of reversal, the distance between the head group and the aldehyde group is used to find the percentage of acyl chain reversal, given in table 7. An interesting observation of reduced acyl-chain reversal in the presence of POPG suggest that the interaction of the polar functional group in the *sn*-2 chain of the oxidised lipid is reduced with the interface region. This could be due to the reduced electrostatic interaction of the aldehyde group to the negatively charged lipid head group.

5. Conclusion

This study was aimed to find the effect of lipid oxidation on the function of the lung surfactant monolayer. As previously reported, modified functions of lung surfactant monolayers in the presence of oxidised lipid species such as increased surface pressure [50], increased fluidity of the membrane, increased water penetration into the hydrophobic region [51] and monolayer deformation through acyl chain reversal [47] have been established using various molecular dynamics simulations of monolayers containing different lipid species and concentrations. An agreement to the standard observations of monolayer functions with experimental data and molecular dynamics data suggest that the modified functions observed during this study can be attributed to the oxidative species present in the monolayers. Furthermore, many of the modified functions can be attributed to the pattern of behaviour of the modified chain of the oxidative species relative to other molecules. As a previously reported behaviour of oxidised phospholipids, acyl-chain reversal of the modified chain may contribute to much of the effect such as increased surface pressure, fluidity and leakiness of the monolayer seen in this study. This is thought to be as a result of physical and electrochemical change introduced by the oxidised lipids. Since all simulation parameters such as number of particles, temperature, pressure, volume and area per lipid remained equivalent for the representative simulations under study, the observation related to the lipid oxidation can be regarded as valid. The systems simulated for this study is on the smaller side of molecular dynamics simulations with 53 lipid molecules per monolayer as well as on a shorter time scale of 5 ns as opposed to 100's of ns or micro seconds. Biological functions of lung surfactant molecules can range from micro seconds to hours and involve many more molecules such as lipids and proteins, therefore future studies can be improved by including the aforementioned variables to predict and better understand the effect of oxidation on the lung surfactant. For example, an experimentally reported behaviour of oxidised lipid under constant surface pressure is that the oxidised lipids start to dissolve into the aqueous phase after 120 minutes. [52] The time scale of 120 minutes is not feasible with current computing powers, however molecular dynamics at microsecond time scale using all or most the reaction products predicted to be formed from the oxidation reaction of phospholipids may give new insights. Dissolving of the oxidised lipid is not observed during this study after 5 ns simulation, however, acyl chain reversal reported experimentally and computationally have been observed for oxidised lipids during this study, suggesting that molecular dynamics can be used to understand some of the functions of lung surfactant which may not be possible to examine experimentally. Based on the results of this study, it can be proposed that the presence of oxidised lipid can negatively affect the lung surfactant functions at atomic level as well as structural level. Observation of increased fluidity and membrane

leakiness as a result of decreased hydrophobic region of the surfactant due to the presence of oxidised lipid indicates a negative impact on the biological role of the surfactant function to reduce the surface tension of the liquid/air interface. Increased number of polar groups introduced by the oxidised lipids can hinder the amphiphilic nature of the lung surfactant lipids, hence change the intermolecular interaction between other lipids or proteins. For example SP-B has a net positive charge and is thought to interact with negatively charged lipids, therefore an increase in polar residues may cause the function of the SP-B to change or its interaction with lipids.

References

- [1] R.H.Notter. Lung Surfactants: Basic Science and Clinical Applications. Marcel Dekker,Inc 149. pp. 2-10 (2000).
- [2] U. Pison, R. Herold, S. Schurch. The pulmonary surfactant system: biological functions, components, physicochemical properties and alterations during lung disease Colloids Surf., A Physicochem. Eng. Asp 114. pp. 165–184 (1996)
- [3] S. Orgeig, P.S. Hiemstra, E.J. Veldhuizen, C. Casals, H.W. Clark, A.Haczku, L.Knudsen, F. Possmayer. Recent advances in alveolar biology: Evolution and function of alveolar proteins. Respir Physiol Neurobiol 173. pp.43-54 (2010).
- [4] A.B. Lumb, J.F. Nunn
Nunn's Applied Respiratory Physiology
Elsevier/Butterworth Heinemann, Edinburgh (2005)
- [5] M. Ikegami, T.E. Weaver, S.N. Grant, J.A. Whitsett. Pulmonary Surfactant Surface Tension Influences Alveolar Capillary Shape and Oxygenation. American Journal of Respiratory Cell and Molecular Biology 41. pp.433-439 (2009).
- [6] I. Frerking, A. Gunther, W. Seeger, U. Pison. Pulmonary surfactant: functions, abnormalities and therapeutic options. Intensive Care Med., 27 (2001), pp. 1699–1717
- [7] D.L. Brown, E.N. Pattishall
Other uses of surfactant
Clin. Perinatol., 20 (1993), pp. 761–789
- [8] Y.Zuo, R.A. Veldhuizen, A.W.Neumann, N.O. Pteresen, F.Possmayer. Current perspective in pulmonary surfactant – Inhibition, enhancement and evaluation. Biochimica et Biophysica Acta 1778. pp 1947-1977 (2008)
- [9] E.Parra, J.Perez-Gil. Composition, structure and mechanical properties define performance of pulmonary surfactant membranes and films. Chemsitry and Physics of Lipids 185. pp.153-

175(2015).

- [10] S. Orgeig, W. Bernhard, S.C. Biswas, C.B. Daniels, S.B. Hall, S.K. Hetz, C.J. Lang, J.N. Maina, A.K. Panda, J. Perez-Gil, F. Possmayer, R.A. Veldhuizen, W. Yan. The anatomy, physics, and physiology of gas exchange surfaces: is there a universal function for pulmonary surfactant in animal respiratory structures?. *Integr. Comp. Biol* 47 .pp. 610–627 (2007)
- [11] L. F Voss et al. Oxidation of Oleic Acid at Air/Liquid Interfaces. *J.Geophys. Res.*112. (2007)D06209.
- [12] R.J. Mason, K.Greene, D.R.Voelker. Surfactant protein A and surfactant protein D in health and disease. *American Journal of Physiology* 275. pp.1-13 (1998).
- [13] E.C. Crouch. Structure, biologic properties, and expression of surfactant protein D (SP-D). *Biochim. Biophys. Acta*, 1408 (1998), pp. 278–289.
- [14] P.S. Kingma, J.A. Whitsett. In defense of the lung: surfactant protein A and surfactant protein D. *Curr. Opin. Pharmacol.*, 6 (2006), pp. 277–283
- [15] M.L. Ruano, E. Miguel, J. Perez-Gil, C. Casals. Comparison of lipid aggregation and self-aggregation activities of pulmonary surfactant-associated protein A. *Biochem. J.*, 313 (Pt 2) (1996), pp. 683–689
- [16] L.A.D. Worthman, K. Nag, N. Rich, M.L.F. Ruano, C. Casals, J. Perez-Gil, K.M.W. Keough. Pulmonary surfactant protein A interacts with gel-like regions in monolayers of pulmonary surfactant lipid extract. *Biophys. J.*, 79 (2000), pp. 2657–2666
- [17] M.L.F. Ruano, K. Nag, L.A. Worthman, C. Casals, J. Perez-Gil, K.M.W. Keough. Differential partitioning of pulmonary surfactant protein SP-A into regions of monolayers of dipalmitoylphosphatidylcholine/dipalmitoylphosphatidylglycerol. *Biophys. J.*, 74 (1998), pp. 1101–1109.
- [18] U.Kishore, T. J. Greenhough, P. Waters, A.K. Shrive, Rohit Ghai, M. F. Kamran, A. L. Bernal,

K.B.M. Reid, T.Madan, T. Chakraborty. Surfactant proteins SP-A and SP-D: Structure, function and receptors. *Molecular Immunology* 43. pp. 1293-1315 (2006).

[19] L.M. Nogee. Abnormal Expression of surfactant Protein C and Lung disease. *American journal of Respiratory Cell and Molecular Biology* 26 (6). pp. 641-644 (2001).

[20] K. Nag, S.G. Taneva, J. Perez-Gil, A.Cruz, K.M. Keough. Combinations of fluorescently labeled pulmonary surfactant proteins SP-B and SP-C in phospholipid films. *Biophys. J.*, 72 (1997), pp. 2638–2650

[21] L.A. Creuwels, E.H. Boer, R.A. Demel, L.M.G. Van Golde, H.P. Haagsman. Neutralization of the positive charges of surfactant protein C. Effects on structure and function. *J. Biol. Chem.*, 270 (1995), pp. 16225–16229

[22] M. Ross, S. Krol, A. Janshoff, H.J. Galla. Kinetics of phospholipid insertion into monolayers containing the lung surfactant proteins SP-B or SP-C. *Eur. Biophys. J.*, 31 (2002), pp. 52–61

[23] A. Cruz, L.A. Worthman, A.G. Serrano, C. Casals, K.M.W.Keough, J. Perez-Gil. Microstructure and dynamic surface properties of surfactant protein SP-B/dipalmitoylphosphatidylcholine interfacial films spread from lipid–protein bilayers. *Eur. Biophys. J.*, 29 (2000), pp. 204–213

[24] J. Perez-Gil, C. Casals, D. Marsh. Interactions of hydrophobic lung surfactant proteins SP-B and SP-C with dipalmitoylphosphatidylcholine and dipalmitoylphosphatidylglycerol bilayers studied by electron spin resonance spectroscopy. *Biochemistry*, 34 (1995), pp. 3964–3971

[25] K. Nag, S.G. Taneva, J. Perez-Gil, K.M. Keough. Combinations of fluorescently labeled pulmonary surfactant proteins SP-B and SP-C in phospholipid films. *Biophys. J.*, 72 (1997), pp. 2638–2650

[26] V. Schram, S.B. Hall. Thermodynamic effects of the hydrophobic surfactant proteins on the early adsorption of pulmonary surfactant. *Biophys. J.*, 81 (2001), pp. 1536–1546.

[27] J. Goerke. Pulmonary surfactant: functions and molecular composition. *Biochim. Biophys.*

Acta, 1408. pp. 79–89 (1998)

- [28] R. Wustneck, J. Perez-Gil, N. Wustneck, A. Cruz, V.B. Fainerman, U. Pison. Interfacial properties of pulmonary surfactant layers. *Adv. Colloid. Interface Sci.*, 117 (2005), pp. 33–58
- [29] R. Veldhuizen, K. Nag, S. Orgeig, F. Possmayer. The role of lipids in pulmonary surfactant. *Biochimica et Biophysica Acta(BBA)- Molecular Basis of Disease* 1408. pp.90-108(1998).
- [30] K. Nag, K.M. Keough. Epifluorescence microscopic studies of monolayers containing mixtures of dioleoyl- and dipalmitoylphosphatidylcholines. *Biophys. J.*, 65 (1993), pp. 1019–1026
- [31] R.C. MacDonald, S.A. Simon. Lipid monolayer states and their relationships to bilayers. *Proc. Natl. Acad. Sci. U. S. A.*, 84 (1987), pp. 4089–4093
- [32] L.A.D. Worthman, K. Nag, P.J. Davis, K.M.W. Keough. Cholesterol in condensed and fluid phosphatidylcholine monolayers studied by epifluorescence microscopy. *Biophys. J.*, 72 (1997), pp. 2569–2580
- [33] J.P. Gill. Structure of pulmonary surfactant membranes and films: The role of proteins and lipid-protein interactions.
- [34] S.H. Yu, F. Possmayer. Lipid compositional analysis of pulmonary surfactant monolayers and monolayer-associated reservoirs. *Journal of Lipid research* 44. pp.621-629(2003).
- [35] L.D. Susan, R.G Larson. Folding of lipid monolayers containing lung surfactant proteins SP-B₁₋₂₅ and SP-C studied via coarse-grained molecular dynamics simulations. *Biochimica et Biophysica Acta* 1798. pp.1632-1650(2010).
- [36] F. Possmayer. *Biophysical Activities of Pulmonary Surfactant in Fetal and Neonatal Physiology*. WB Saunders Co, Philadelphia, pp. 949–962 (1991)
- [37] J. Goerke, J.A. Clements. *Alveolar Surface Tension and Lung Surfactant*. American Physiological Society, Bethesda, MD, pp. 247–261 (1986).

- [38] A.Dickey, R.Faller. Examining the Contributions of Lipid Shape and Headgroup Charge on Bilayer Behavior. *Biophysical J* 95(6). pp. 2636-2646(2008).
- [39] J.Perez-Gil, K.M. Keough. Interfacial properties of surfactant proteins. *Biochim. Biophys. Acta* 1408, 203–217 (1998)
- [40] Wright SM, Hockey PM, Enhoring G, et al. Altered airway surfactant phospholipid composition and reduced lung function in asthma. *J. Appl. Physiol.* 2000;89(4):1283–1292
- [41] M.Numata, P.Kandasamy, D.R.Voelker. Anionic pulmonary surfactant lipid regulation of innate immunity. *Expert Rev Respir Med* 6(3).pp. 243-246 (2012).
- [42] O.Blanco, J.Perez-Gil. Biochemical and pharmacological differences between preparations of exogenous natural surfactant used to treat Respiratory Distress syndrome: Role of the different components in an efficient pulmonary surfactant. *European journal of pharmacology* 568. pp.1-15(2007).
- [43] J.F.Chapman, DrPH, W.N.P.Herbert,MD. Current Methods for Evaluating Fetal Lung Maturity. *Laboratory medicine* 17(10). pp. 597-602(1986)
- [44] R. Schmidt, U. Meier, P. Markart, F. Grimminger, H. G. Velcovsky, H. Morr, W. Seeger, A. Günther. Altered fatty acid composition of lung surfactant phospholipids in interstitial lung disease. *American Journal of Physiology - Lung Cellular and Molecular Physiology* 283(5). pp. L1079-L1085 (2002).
- [45] K.Rodriguez-Capote, D. Manzanares, T. Haines, F. Possmayer. Reactive Oxygen Species Inactivation of surfactant Involves Structural and Functional Alterations to Surfactant Proteins SP-B and SP-C. *Biophysical Journal* 90. pp.2808-2821(2006).
- [46] M . M . Lee , F.H.Y.Green, S.Schürch, S.Cheng, S.G.Bjarnason, S.Leonard, W.Wallace,F.Possmayer, V.Vallyathan. Comparison of inhibitory effects of oxygen radicals and calf serum protein on surfactant activity. *Mol.Cell.Biochem* 259. pp.15-22(2004).

- [47] K.Sabatini, J. Mattila, F.M. Megli, P.A.J. Kinnunen. Characterization of Two Oxidatively Modified Phospholipids in Mixed Monolayers with DPPC. Biophysical Journal 90. pp.4488-4499(2006).
- [48] http://apps.who.int/iris/bitstream/10665/69477/1/WHO_SDE_PHE_OEH_06.02_eng.pdf
 Date accessed : 08/08/2017
<http://www.sciencemag.org/news/2017/03/here-are-some-world-s-worst-cities-air-quality>
 Date accessed : 08/08/2017
- [49] Christian Geletneky and Stefan Berger. The mechanism of ozonolysis by ¹⁷O-NMR Spectroscopy. Eur.J.Org.Chem. pp.1625-1627 (1998).
- [50] K.C.Thompson, A.R. Rennie, M.D. King, S.J.O. Hardman, C.O.M. Lucas, C.Pfrang, B.R. Hughes, A.V. Hughes. Reaction of a Phospholipid Monolayer with Gas-Phase Ozone at the Air-Water Interface: Measurement of Surface Excess and Surface Pressure in Real Time. Langmuir 26. pp.17295-17303(2010).
- [51] J. Wong-ekkabut, Z. Xu, W. Triampo, I.M. Tang, D. P. Tieleman, L. Monticelli. Effect of Lipid peroxidation on the Properties of Lipid Bilayers: A Molecular Dynamics Study. Biophysical Journal 93. pp.4225-4236(2007).
- [52] L.Qiao et al. Oxidative Degradation of the Monolayer of 1-Palmitoyl-2-Oleoyl-sn-Glycero-3-Phosphocholine (POPC) in Low-Level Ozone. J.Physical Chemistry. pp.14188-14199(2015).
- [53] J.F.D. Lijeblad et al. Phospholipid monolayers Probed by Vibrational Sum Frequency Spectroscopy: Instability of Unsaturated Phospholipids. Biophysical Journal 98. pp. 50-52(2010).
- [54] E.Boisselier, P.Calvez, E.Demers, L. Cantin, C. Salesse. Effect of oxidation of polyunsaturated phospholipids on the binding of proteins in monolayers. Colloids and Surfaces B: Biointerfaces 109. pp. 109-114 (2013).
- [55] A. Korytowski, W. Abuillan, A.Makky, O. Konovalov,M. Tanaka. Impact of Lipid Oxidization on Vertical Structures and Electrostatics of Phospholipid Monolayers Revealed by Combination of Specular X-ray Reflectivity and Grazing-Incidence X-ray Fluorescence. Journal of Physical

Chemistry B, 119. pp. 9787-9794 (2015).

- [56] M.Khabiri, M.Roeselova, L.Cwiklik. Properties of oxidised phospholipid monolayers: An atomistic molecular dynamics study. *Chemical Physics Letters* 519-520. pp. 93-99 (2012).
- [57] W.F. Van Gunsteren, H.J.C. Berendsen. A leap-frog Algorithm for Stochastic Dynamcis. *Mol.Sim* 1. pp. 173-185(1988).
- [58] W. van Gunsteren, S. Billeter, A. Eising, P. Hunenberger, P. Kruger, A. Mark, W. Scott, I. Tironi, *Biomolecular Simulation: The GROMOS96 Manual and User Guide*, Vdf Hochschulverlag AG an der ETH Zürich, Zürich, Switzerland, 1996, 1-1042.
- [59] O.Berger et al. Molecular dynamics simulations of a fluid bilayer of dipalmitoylphosphatidylcholine at full hydration, constant pressure, and constant temperature. *Biophysical J* 72. pp. 2002-2013(1997).
- [60] A.Kukol. Lipid Models for United-Atom Molecular Dynamics Simulations of Proteins. *J.Chem.Theory.Comput* 5. pp.615-626 (2009).
- [61] W.L.Jorgensen, J. Tirado-Rives. The OPLS [optimised potentials for liquid simulations] potential functions for proteins , energy minimizations for crystals of cyclic peptides and crambin. *J.Am.Chem.Soc* 110(6).pp.1657-1666(1988).
- [62] Electroporation of the *E. coli* and *S. aureus* Membranes: Molecular Dynamics Simulations of Complex Bacterial Membranes. Thomas J. Piggot, Daniel A. Holdbrook, and Syma Khalid. *The Journal of Physical Chemistry B* 2011 115 (45), 13381-13388.
- [63] J.Henin et al. Models for Phosphatidylglycerol Lipids put to a Structural Test. *J.Phys.Chem* 113. pp.6958-6963(2009).
- [64] <ftp://ftp.gromacs.org/pub/manual/manual-5.0.4.pdf>
- [65] Y.N. Kaznessis, S. Kim, R.G. Larson. Simulations of Zwitterionic and Anionic Phospholipid

Monolayers. Biophysical Journal 82. pp. 1731- 1741 (2002).

- [66] Y.N. Kaznessis, S. Kim, R.G. Larson. Specific Mode of Interaction Between Components of Model Pulmonary Surfactants Using Computer Simulations. Journal of Molecular Biology 322. pp.569-582 (2002).
- [67] J.A. Freites, Y. Choi, D.J. Tobias. Molecular Dynamics Simulations of a Pulmonary Surfactant Protein B Peptide in a Lipid Monolayer. Biophysical Journal 84. pp.2169-2180 (2003).
- [68] S.O. Nielsen, C.F. Lopez, P.B. Moore, J.C. Shelly, M.L. Klein. Molecular Dynamics Investigations of Lipid Langmuir Monolayers Using a Coarse-Grain Model. Journal of Physical Chemistry B. 107. pp. 13911-13917 (2003).
- [69] S. Baoukina, L. Monticelli, M. Amrein, D.P. Tieleman. The Molecular Mechanism of Monolayer-Bilayer Transformations of Lung Surfactant from Molecular Dynamics Simulations. Biophysical Journal 93. pp. 3775 – 3782 (2007).
- [70] H. Lee, S.K. Kandasamy, R.G. Larson. Molecular Dynamics Simulations of the Anchoring and Tilting of the Lung-Surfactant Peptide SP-B₁₋₂₅ in Palmitic Acid Monolayers. Biophysical Journal 89 (6). pp. 3807-3821 (2005).
- [71] S.K. Kandasamy, R.G. Larson. Molecular Dynamics Study of the Lung Surfactant Peptide SP-B₁₋₂₅ with DPPC Monolayers: Insights into Interactions and Peptide Position and Orientation. Biophysical Journal 88. pp.1577-1592 (2005)
- [72] F. Rauch, M. Schicht, L. Brauer, F. Paulsen, W. Brandt. Protein modeling and molecular dynamics simulation of the two novel surfactant proteins SP-G and SP-H. J Mol Model 20:2513. pp.1-12 (2014).
- [73] D.Rose, J.Rendall, D.Lee,K.Nag,V.Booth. Molecular dynamics simulations of lung surfactant lipid monolayers. Biophysical Chemistry 138. pp.67-77(2008).
- [74] S.J. Marrink, O. Berger, P. Tieleman, F. Jähnig, Adhesion forces of lipids in a phospho-lipid

membrane studied by molecular dynamics simulations, *Biophys. J.* 74 (1998) 931–943.

[75] Electroporation of the *E. coli* and *S. aureus* Membranes: Molecular Dynamics Simulations of Complex Bacterial Membranes. Thomas J. Piggot, Daniel A. Holdbrook, and Syma Khalid. *The Journal of Physical Chemistry B* 2011 115 (45), 13381-13388.

[76] L. Martínez, R. Andrade, E. G. Birgin, J. M. Martínez. Packmol: A package for building initial configurations for molecular dynamics simulations. *Journal of Computational Chemistry*, 30(13):2157-2164, 2009.

[77] Hanwell, Marcus D; Curtis, Donald E; Lonie, David C; Vandermeersch, Tim; Zurek, Eva; Hutchison, Geoffrey R (2012). "*Avogadro: An advanced semantic chemical editor, visualization, and analysis platform*". *J. Cheminform.* 4 (1): 17.

[78] A.K. Rappe, C.J. Casewit, K.S. Colwell, W.A. Goddard III, W.M. Skiff. UFF, a Full Periodic Table Force Field for Molecular Mechanics and Molecular Dynamics Simulations. *J. Am. Chem. Soc.* 114. pp.10024–10035 (1992).

[79] Electroporation of the *E. coli* and *S. aureus* Membranes: Molecular Dynamics Simulations of Complex Bacterial Membranes. Thomas J. Piggot, Daniel A. Holdbrook, and Syma Khalid. *The Journal of Physical Chemistry B* 2011 115 (45), 13381-13388.

<https://lipidbook.bioch.ox.ac.uk/package/show/id/58.html>

[80] J.W.Ekkabut et al. Effect of Lipid peroxidation on the properties of Lipid bilayers: A molecular dynamics study. *Biophysical Journal* 93. pp.4225-4236(2007).

[81] M.I.Hoops, et al. Bilayer Structure and Lipid Dynamics in a Model Stratum Corneum with Oleic Acid. *Journal of Physical Chemistry B* 115,3164-3171(2011)

<https://ucdavis.app.box.com/v/fallergroupdownloads>

[82] <ftp://ftp.gromacs.org/pub/manual/manual-5.0.4.pdf>

[83] D.J.Evans and B.L.Holian. The Nose-Hoover thermostat. *The Journal of Chemical Physics* 83.

pp.4069 (1985).

[84] J.F.Nagle. Area/lipid of bilayers from NMR. Biophysical journal 64. pp 1476-1481(1993)

[85] B.Hess, H.Bekker, H.J.C.Berendsen, J.G.E.M.Fraaije. LINCS: A linear constraint solver for molecular simulations. Journal of computational Chemistry 18. pp.1463-1472(1997)

[86] U. Essmann, L. Perela, M.L. Berkowitz, T. Darden, H. Lee, L.G. Pedersen, A smooth particle mesh Ewald method, J. Chem. Phys. 103 (1995) 8577–8592.

[87] G.Bussi, D.Donadio and M.Parrinello. Canonical sampling through velocity-rescaling. Journal of Chemical Physics 126,014101(2007)

[88] L.S.Vermeer, B.L. De Groot, V. Reat, A. Milon, J.Czaplicki. Acyl chain order parameter profiles in phospholipid bilayers: computation from molecular dynamics simulations and comparison with ²H NMR experiments. Biophysical Journal Eur 36. pp. 919-931(2007)

[89] C. Hofsaß, E.Lindahl and O.Edholm. Molecular Dynamics Simulations of Phospholipid Bilayers with Cholesterol. Biophysical Journal 84. pp.2192-2206 (2003).

[90] B.Liu et al. Molecular Dynamics Simulations of DPPC/CTAB Monolayers at the Air/Water Interface. J.Physical Chemistry B 118. pp.11723-11737(2014)

[91] R.A.Zubillaga et al. Surface Tension of Organic Liquids Using the OPLS/AA Forcefield. JCTC 9. pp.1611-1615(2013).

[92] AF, Mingotaud, C.Mingotaud, L.K. Patterson. (1993). Handbook of Monolayers. London. Academic Press Limited. 786-965.

[93] H.I.Petrache et al. Area per Lipid and Acyl Length Distributions in Fluid Phosphatidylchlines Determined by ²H NME Spectroscopy. Biophysical Journal 79.pp.3172-3192(2000).

[94] M.C. Phillips, D. Chapman. Monolayer characteristics of saturated 1,2-diacyl

phosphatidylcholines (lecithins) and phosphatidylethanolamines at the air-water interface. *Biochim. Biophys. Acta.* 163. pp.301-313(1968).

[95] D.E. Elmore. Molecular dynamics simulation of a phosphatidylglycerol membrane. *FEBS Lett.* 580:pp.144–148(2006)

[96] S. A. Pandit, D. Bostick, and M. L. Berkowitz. Molecular dynamics simulation of a dipalmitoylphosphatidylcholine bilayer with NaCl. *Biophys. J.* 84. pp.3743–3750(2003).

[97] Böckmann, R. A., A. Hac, T. Heimburg, and H. H. Grubmüller. 2003. Effect of sodium chloride on a lipid bilayer. *Biophys. J.* 85:1647–1655.

[98] A.K. Chattopadhyay et al. Salt Effects on Monolayers and Their Contribution to surface Viscosity. *J.Phys.Chem* 96. pp.6509-6513(1992).

[99] M.M.Claessens et al. Opposing effects of cation binding and hydration on the bending rigidity of anionic lipid bilayers. *J Phys Chem B* 111(25). pp. 7127-7132(2007).

[100] P.L. Mukhopadhyay et al. Molecular dynamics simulation of a palmitoyl-oleoyl phosphatidylserine bilayer with Na^+ counterions and NaCl. *Biophys. J.* 86. pp.1601-1609(2004).

[101] R.A. Demel. Relation between various phospholipase actions on human red cell membranes and the interfacial phospholipid pressure in monolayers. *Biochim. Biophys. Acta.* 406. pp.97-107(1975)

Supplementary information

Contents

S1. Forcefield and parameters	76
S1.1 Forcefield	76
S1.2 Topology file	76
S2. Forcefield editing to include lipid parameters	78
S3. Monolayer building	80
S3.1. Monolayer building of DPPC	80

S3.2. Monolayer building of POPG	81
S4. Box dimensions	82
S4.1. Define box for the monolayers	82
S4.2.1 Energy minimization	82
S4.2.2 Energy information of the simulation	84
S4.2.3 F_{max}	84
S5. Water box of the simulation	85
S5.1. Solvate with water	85
S5.2 Removing water molecules above lipid heads using a script	86
S6. Adding ions	86
S6.1. Input parameter file for adding ions	87
S7. Equilibration of the system	88
S7.1 equilibration parameters	88
S7.2 Coupling and centre of motion groups	89
S8. Short MD run	90
S.8.1 Short MD run parameters	91
S9. Final MD run	92
S9.1. Final MD run parameters	92
S10. Analysis	94
S10.1 Monolayer thickness	94
S10.1.1 Electron.dat file to include partial charges of molecules	94
S10.1.2 Monolayer thickness calculation in GROMACS	95
S10.1.3 Monolayer thickness using POPG head and tail electron density	96
S10.2 Order parameter	97
S10.3. Diffusion of lipids into the water	97
S10.4. Acyl-chain reversal	98
S11. In house scripts	98
S11.1 Python script used for head group movement and acyl-chain reversal	98
S11.2. Perl script used to remove water molecules above the head groups	104
S12. Experimental comparison	105
S12.1. Pure water simulation	105
S12.2. Surface tension value from simulations	106

S12.3.1 Comparison of pressure-area isotherms	107
S12.4.1. Comparison of order parameter values	108
S13. Forcefield parameter file of PonPG	109

S1. Forcefield and parameters

GROMACS tutorial for bilayer membrane-protein provided by Dr. Justin A. Lemkul was used as a guidance to set up the monolayer systems used in this study. Further information can be found on his website at http://www.bevanlab.biochem.vt.edu/Pages/Personal/justin/gmx-tutorials/membrane_protein/.

S1.1. Forcefield

The forcefield used for this study is GROMOS96 53a6, which is a united atom forcefield.

S1.2. Topology file

A topology file (topol.top) contains all the information such as non bonded and bonded parameters needed to define the molecule within a simulation such as atom types, charges, bonds, angles and dihedrals. Position restrain file (posre.itp) contains information that is used to restrain the positions of atoms.

The topology file (topol.top) contains some important information.

```
#include "gromos53a6.ff/forcefield.itp"
```

This line calls the parameters within the gromos53a6 forcefield, therefore all subsequent parameters are derived from this forcefield. The forcefield.itp contains important parameter that describes chemical groups and interactions. All biological molecules are parameterised using a forcefield along with ffbonded.itp and ffnonbonded.itp. Since GROMACS does not contain parameters that defines the atom types in lipids, these are added to the ffbonded.itp and ffnonbonded.itp by editing these files by using parameters for a large class of lipids (lipid.itp), explained in the next section. For each lipid types, a topology (.itp) file that parameterise the molecule that is compatible with the forcefield is used.

```
[ moleculetype ]
```

```
; Name      nrexcl
```

'nrexcl' is the number of neighbour atoms that are excluded in the Lennard-Jones interaction for an atom. For example five atoms which are covalently bonded(i,i+1,i+2,i+3,i+4), only the interaction between I and i+4 is used.ie. I+1,i+2,i+3 interactions are excluded with respect to I. It is assumed that the interaction between I and i+1 is modelled by harmonic bond term or constraint and harmonic angle term(i+1,i+2).

The [atoms] directive defines the atoms of the molecule. Most are self explanatory such as atom type, mass and charge. 'cgnr' is a charge group number which define units of integer charge that speeds up calculation. 'qtot' is the running total of the charge on the molecule.

[bonds], [pairs] and [dihedral] directives defines the atoms bonded and non-bonded interaction in a molecule. These parameters can be found for the atom type in the forcefield directory with file name 'ffbonded.itp' and 'ffnonbonded.itp'. Special 1-4 interactions are defined under 'pairs'.

There are various information that can be found in the topology(.top) file that describes the protocols of the simulation.

; Include Position restraint file

```
#ifdef POSRES
#include "posre.itp"
#endif
```

This defines a force constant to keep atoms in place during equilibration.

; Include water topology

```
#include "gromos53a6.ff/spc.itp"
```

The next molecule type is the solvent (water) and its parameters are derived from 'spc.itp' from the gromos53a6 forcefield.

```
#ifdef POSRES_WATER
; Position restraint for each water oxygen
[ position_restraints ]
```

```
; i funct    fcx    fcy    fcz
  1   1    1000    1000    1000
#endif
```

The water oxygen is restrained using a force constant of 1000kJ mol⁻¹ nm⁻².

```
; Include topology for ions
#include "gromos53a6.ff/ions.itp"
```

Parameters for ions is derived from 'ions.itp'.

```
[ system ]
; Name
DPPC monolayers in water
```

This directive defines the name of the system.

```
[ molecules ]
; Compound    #mols
DPPC          53
DPPC          53
SOL           4000
```

[molecules] directive lists all the molecules within the system. The order of the molecules in the topology file must match the order in the .gro file to avoid fatal errors and warnings when using grompp.

S2. Forcefield editing to include lipid parameters

Since GROMACS can only parametrise proteins, nucleic acids and some cofactors, lipids are parameterised using Berger lipids and modified GROMOS forcefield. Berger lipid forcefield is a hybrid between GROMOS atom types and OPLS partial charges. DPPC (dipalmitoyl phosphatidylcholine) are parametrised using “Berger lipids” parameters. [1]

These parameters can be combined with GROMOS representation of the protein for simulations that contain both lipid and protein. The parameter (dppc.itp, lipid.itp) and the structure (dppc128.pdb) files were obtained from <http://wcm.ucalgary.ca/tieleman/downloads>, where dppc.itp is the molecule type definition for DPPC, lipid.itp is Berger lipid parameters and dppc128.pdb is the structure of a 128-lipid bilayer.

Similar to how gromos53a6/forcefeld.itp describes a protein, lipid.itp contains all the atom types, nonbonded parameters and bonded parameters for a large class of lipids. To use the parameters in lipid.itp, some changes to the gromos53a6/forcefield.itp needs to be made as they both have same precedence. This is done by making a directory called “gromos53a6_lipid.ff” in the working directory and copying following files from gromos53a6.ff into it.

aminoacids.rtp, aminoacids.hdb, aminoacids.c.tdb, aminoacids.n.tdb, aminoacids.r2b, aminoacids.vsd, ff_dum.itp, ffnonbonded.itp, ffbonded.itp, forcefield.itp, ions.itp, spc.itp, watermodels.dat.

A file that contains the description of the forcefield parameters called forcefield.doc was created. The description is “GROMOS96 53A6 force field, extended to include Berger lipid parameters”.

The entries in [atomtypes], [nonbond_params], and [pairtypes] sections in lipid.itp were copied and pasted into the appropriate headings within ffnonbonded.itp. [atomtypes] section in lipid.itp lacks atomic numbers, therefore these were also added. The new lines are:

LO	8	15.9994	0.000	A	2.36400e-03	1.59000e-06	;carbonyl O, OPLS
LOM	8	15.9994	0.000	A	2.36400e-03	1.59000e-06	;carboxyl O, OPLS
LNL	7	14.0067	0.000	A	3.35300e-03	3.95100e-06	;Nitrogen, OPLS
LC	6	12.0110	0.000	A	4.88800e-03	1.35900e-05	;Carbonyl C, OPLS
LH1	6	13.0190	0.000	A	4.03100e-03	1.21400e-05	;CH1, OPLS
LH2	6	14.0270	0.000	A	7.00200e-03	2.48300e-05	;CH2, OPLS
LP	15	30.9738	0.000	A	9.16000e-03	2.50700e-05	;phosphor, OPLS
LOS	8	15.9994	0.000	A	2.56300e-03	1.86800e-06	;ester oxygen, OPLS
LP2	6	14.0270	0.000	A	5.87400e-03	2.26500e-05	;RB CH2, Bergers LJ
LP3	6	15.0350	0.000	A	8.77700e-03	3.38500e-05	;RB CH3, Bergers LJ
LC3	6	15.0350	0.000	A	9.35700e-03	3.60900e-05	;CH3, OPLS
LC2	6	14.0270	0.000	A	5.94700e-03	1.79000e-05	;CH2, OPLS

In the [nonbon_params], the line “;;parameters for lipid-GROMOS interaction.” and all subsequent lines in this section are deleted as these combinations are for deprecated ffgrmx forcefield. Therefore removing it allows the standard combination rules of gromos53a6 for protein and lipid. In [nonbond_params] section atomtype HW is renamed to H to be consistent with GROMOS96 53A6 naming convention. The [dihedraltypes] contents were appended to the corresponding section in the ff bonded.itp. The [dihedraltypes] in lipid.itp is Ryckaert-Bellemans dihedrals whereas the GROMOS 53A6 forcefield uses standard periodic dihedrals.

To use the newly edited parameters, the #include statements in topology file (.top) needs to be changed from “#include 'gromos53a6.ff/forcefield.itp'” to “#include gromos53a6_lipid.ff/forcefield.itp”. To use the molecule specific parameters for DPPC, an include statement “#include dppc.itp” needed to be added to the topology file

The newly added section of the topology looks like this:

; Include DPPC chain topology

```
#include "dppc.itp"
```

; Include water topology

```
#include "gromos53a6_lipid.ff/spc.itp"
```

S3. Monolayer building

S3.1. Monolayer building of DPPC

Next step is to create a monolayer of DPPC. This simulation is performed using slab geometry where two monolayers are created on each side of the water slab. Equal number of DPPC molecules were placed on both sides. The monolayers were created using Packmol. [2]

One DPPC molecule coordinates and one water coordinates were copied from the dppc128.pdb structure file downloaded previously to create dppc.pdb and water.pdb. These files are used as the structure files for Packmol to create the initial configuration file of the monolayer. Packmol uses geometry based packing method to put the molecules in place. The input file for the DPPC monolayers on a slab of water is provided:

```

structure dppc.pdb
number 53
inside box 0. 0. -74. 65. 65. 0.
atoms 50
below plane 0. 0. 1. -24.
end atoms
atoms 1
over plane 0. 0. 1. -2.
end atoms
end structure

```

```

structure dppc.pdb
number 53
inside box 0. 0. 100. 65. 65. 174.
atoms 1
below plane 0. 0. 1. 102.
end atoms
atoms 38
over plane 0. 0. 1. 124.
end atoms
end structure

```

```

structure water.pdb
number 4000
inside box 0. 0. 0. 65. 65. 100.
end structure

```

This input file packs 4000 water molecules in $6.5 * 6.5 * 10$ nm³ box. 53 DPPC molecules were packed above the slab of water, with the lipid head (atom C1) being inserted no more than 1 nm within the water and the lipid tail (atom C50) to be 24 nm above the water. The output file is dppc106.pdb.

S3.2. Monolayer building of POPG

The popg topology(.itp) file and coordinate(.pdb) files were downloaded from

<https://lipidbook.bioch.ox.ac.uk/package/show/id/58.html>. The coordinate file derived from a 200 ns bilayer structure[3]. The d-popc lipids are used in this simulation.

The monolayers using slab geometry were built with packmol. The atomic co-ordinate of a single POPG molecule was extracted from the bilayer structure to be used as the input file for Packmol. Each monolayer contains 53 residues of D-POPG in 6.5*6.5*7.4 nm box and the water slab contains 4000 water molecules in 6.5*6.5*10 nm box. This creates area per lipid of $\sim 80\text{\AA}^2$ ($65*65/53$) or 0.8 nm^2 . GROMACS uses nm as the default unit of measurement for distance.

S4. Box dimensions

S4.1 Define box for the monolayers

The box size needs to be increased on the direction normal to the monolayers (z-axis) to make sure there is a vacuum layer large enough such that the movement of the lipid tails are not restricted. All simulation systems have 21 nm along the normal direction of the monolayers, which means there is a vacuum layer of 3 nm above the monolayers. Run energy minimization on the new system. An example of pure POPG system at $80 \text{ \AA}^2 \text{ lipid}^{-1}$ consisting of two monolayers is given below

```
$ gmx editconf -f popg80.pdb -o popg80.gro -box 6.5 6.5 21.0
```

S4.2.1 Energy minimization

Energy minimization is a process in which the structure is relaxed or the potential energy of the atoms are reduced by arranging the atoms in the system by finding the local minimum of potential energy in geometry for each atom.

Use grompp to assemble the structure topology and simulation parameters into binary file (.tpr). Here another .mdp (minim.mdp) file is used to describe the energy minimization parameters.

```
; minim.mdp - used as input into grompp to generate em.tpr
; Parameters describing what to do, when to stop and what to save
integrator    = steep      ; Algorithm (steep = steepest descent minimization)
emtol        = 1000.0     ; Stop minimization when the maximum force < 1000.0 kJ/mol/nm
emstep       = 0.01       ; Energy step size
nsteps       = 50000      ; Maximum number of (minimization) steps to perform

; Parameters describing how to find the neighbors of each atom and how to calculate the interactions
```

```

nstlist      = 1          ; Frequency to update the neighbor list and long range forces
ns_type      = grid       ; Method to determine neighbor list (simple, grid)
rlist        = 1.0        ; Cut-off for making neighbor list (short range forces)
coulombtype  = PME        ; Treatment of long range electrostatic interactions
rcoulomb    = 1.0        ; Short-range electrostatic cut-off
rvdw         = 1.0        ; Short-range Van der Waals cut-off
pbc          = xyz        ; Periodic Boundary Conditions

```

\$ gmx grompp -f minim.mdp -c popg80.gro -p topol.popg80.top -o em

topol.popg80.top is the topology file for the monolayer.

```

;      File 'topol.popg80.top'
;      By : Merril

;

; Include chain topologies
#include "gromos53a6_lipid.ff/forcefield.itp"
#include "POPG-D_GROMOS-CKP.itp"

; Include water topology
#include "gromos53a6_lipid.ff/spc.itp"

; Include ion topologies
#include "gromos53a6_lipid.ff/ions.itp"

; System specifications
[ system ]
POPG Lipid monolayer

[ molecules ]
; molecule name nr.
DPOG 106
SOL 4000

```

The .tpr file is passed into module mdrun for energy minimization.

```
$ gmx mdrun -v -deffnm em -nb gpu -nt 1 &
```

Here, -v command is for verbose to see the stage of the process and -nb and -nt defines the processor and the unit assigned.

The output of this process is four files. An ASCII-text log file of the EM process (em.log), binary energy file (em.edr), binary full precision trajectory (em.trr) and energy minimised structure file (em.gro).

Assessing if the EM was successful can be done in two ways. One is to look at the potential energy of the system, which can be extracted from the energy file. E_{pot} is expected to be negative and in the order of $10^4 - 10^6$.

S4.2.2 Energy information of the simulation

Energy status of the system can be collected from the em.edr file using energy module.

```
$ gmx energy -f em.edr -o potential.xvg
```

The .xvg file is plotted using Xmgrace tool.

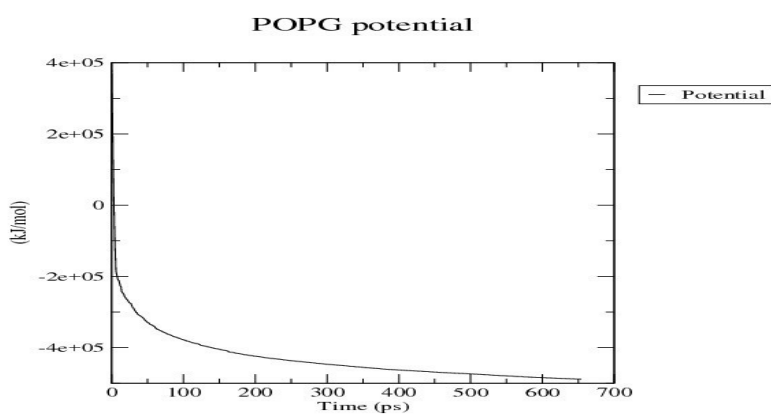


Figure S1. Showing a steady convergence of potential energy of the system.

S4.2.3 F_{max}

Another factor is the F_{max} , or maximum force which was the target set in minim.mdp. “emtol = 1000”. This means the target potential of the system must be less than $1000 \text{ KJ mol}^{-1} \text{ nm}^{-1}$. F_{max} is

printed to the screen at the end of the EM process.

Use trjconv to fix any broken molecules:

```
$ gmx trjconv -s em.tpr -f em.gro -o em_whole.gro -pbc whole -ur compact
```

S5. Water box of the simulation

S5.1. Solvate with water

In this step the 'solute' module is taking in (-cp em_whole.gro) the configuration of energy minimised monolayer from the previous step and using GROMACS standard water configuration (-cs spc216.gro) to output the new configuration that includes water molecules in 'solute.gro'.

```
$ gmx solvate -cp em_whole.gro -cs spc216.gro -o solvate.gro -p topol.popg80.top
```

15875 water molecules were added.

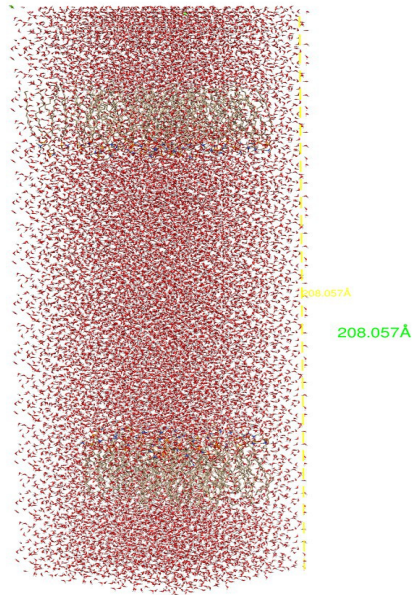


Figure S2. Solvate adds water molecules to the whole box.

S5.2 Removing water molecules above lipid heads using a script

As can be seen, solvate adds water to the whole box. The waters above and in-between the monolayers needs to removed. A script written for this project (see **In house script in section S11.2**) was used to delete the water molecules above the lipid head on both layers.

The script has three output files. One which contains all the lipid molecules (solv.gro), and the other two (solv1.gro, solv_removed.gro) which contains the water molecules between certain coordinates of z-plane (normal to monolayers). The file solv1.gro contains the water molecules that satisfy the water slab and the file solv_removed.gro contains water molecules above the lipid head. The scripts also prints the number of water molecules the water slab (solv1.gro) has, therefore update the topology for number of SOL.

Remove the water molecules above the monolayers (see S11.2 for the script):

```
$ ./solvate.pl solvate.gro
```

concatenate the output files:

```
$ cat solv.gro solv1.gro > solvated.gro
```

Cut and paste the box vectors found after the coordinates of lipids to the end of the file. Update the number of atoms for the new system, which is equal to number of lines minus header information and box vector lines. The topology file needs to be edited before the next step. Previous system contained 4000 water molecules and changing the box dimension and solvating changes the number of molecules

S.6. Adding ions

The next step after solvating the system is to add ions using 'genion'. Looking at the 'qtot' from the topology file from [atoms] directive, the net charge of the POPG lipid is -1e. Adding ions balances the charge on the system. The genion module replaces the water molecules with ions specified. The input file for genion is produced by another module called grompp, which has an extension of .tpr. Grompp process the co-ordinate file from the previous step(solvated.gro) and topology file to

generate an atomic level input. To produce a .tpr file using grompp, an additional file with extension .mdp is required which describes the parameters for the molecular dynamics. Grompp assembles the parameters from .mdp file with the information from the coordinate and topology file to generate the .tpr file.

POPG lipid have a net charge of -1e. Therefore 106 positive ions must be added to neutralise the system. Choose the solvent to be replaced with the ions.

S6.1. Input parameter file for adding ions

; ionsmdp – Input file for grompp to generate .tpr file

; Simulation parameters for adding ions

```
integrator    = steep      ; Algorithm (steep = steepest descent minimization)
emtol        = 1000.0     ; Maximum force < 1000.0 kJ/mol/nm and stop minimization when this is achieved
emstep       = 0.01       ; Energy step size
nsteps       = 50000      ; Maximum number of steps to perform energy minimization
```

; Parameters for finding the neighbours of each atom and how to calculate the interactions

```
nstlist      = 1          ; Frequency for updating the neighbour list and long range forces
ns_type      = grid        ; Neighbour list determining method
rlist        = 1.2         ; Cut-off of short-range forces for making neighbour list
coulombtype  = PME        ; method for computing long range electrostatic interactions
rcoulomb     = 1.2         ; Cut-off for short-range electrostatic interactions
rvdw         = 1.2         ; Cut-off for short-range Van der Waals cut-off
pbc          = xyz        ; Periodic Boundary Conditions
```

\$ gmx grompp -f ionsmdp -c solvated.gro -p topol.popg80.top -o ions

Now that the atomic level description of the system is in the ions.tpr, it can be used as an input to genion.

\$ gmx genion -s ions.tpr -o solvated_ions.gro -p topol.popg80.top -np 106 -pname NA -nname CL

The solvated electro neutral system must be checked for steric clashes or inappropriate geometry.

Run energy minimization:

```
$ gmx grompp -f minimmdp -c solvated_ions.gro -p topol.popg80.top -o confout
$ gmx mdrun -v -deffnm confout -nb gpu -nt 1 &
```

Again trjconv is used to fix the broken molecules. Select the system when prompted

```
$ gmx trjconv -s confout.tpr -f confout.gro -o confout_whole.gro -pbc whole -ur compact
```

Now the system is at an energy minimum, the next step is to equilibrate the system.

S7. Equilibration of the system.

Equilibration involves equilibrating the solvent around the solute, in this case the head groups of the monolayer lipids. The solvent is mostly optimized within itself therefore it needs to be brought to the chosen temperature and properly oriented about the lipid. An NVT ensemble or “Isothermal-isochoric” ensemble is conducted under constant number of particles, volume and temperature. The temperature of the system is expected to stabilize and reach a plateau. An additional .mdp file describing the parameters for the NVT equilibration is needed for this step. The explanation of the parameters can be found on GROMACS manual.

S7.1 equilibration parameters

```
Title      = NVT equilibration of 106 POPG monolayer.
; Run parameters
integrator = md      ; leap-frog integrator
nsteps     = 50000   ; 2 * 50000 = 100 ps
dt         = 0.002   ; 2 fs
; Output control
nstxout    = 100    ; saving coordinates at 0.2 ps interval
nstvout    = 100    ; saving velocities at 0.2 ps interval
nstenergy  = 100    ; saving energies at 0.2 ps interval
nstlog     = 100    ; updating log file at 0.2 ps interval
; Bond parameters
continuation = no    ; first dynamics run
constraint_algorithm = lincs ; holonomic constraints
constraints   = all-bonds ; all bonds are constrained
lincs_iter   = 1      ; LINCS accuracy
lincs_order  = 4      ; also related to accuracy
```

; Neighborsearching

```
ns_type      = grid      ; search neighbouring grid cells
nstlist      = 5          ; 10 fs
rlist        = 1.2        ; short-range neighbour list cutoff (in nm)
rcoulomb    = 1.2        ; short-range electrostatic cutoff (in nm)
rvdw         = 1.2        ; short-range van der Waals cutoff (in nm)
```

; Electrostatics

```
coulombtype = PME       ; Particle Mesh Ewald for long-range electrostatics
pme_order    = 4          ; cubic interpolation
fourierspacing = 0.16     ; grid spacing for FFT
```

; Temperature coupling is on

```
tcoupl      = V-rescale   ; modified Berendsen thermostat
tc-grps     = DPOG SOL_NA ; two coupling groups for increased accuracy
tau_t       = 0.1 0.1      ; time constant, in ps
ref_t       = 323 323      ; reference temperature for each coupling group in Kelvin
```

; Pressure coupling is off

```
pcoupl      = no          ; no pressure coupling in NVT
```

; Periodic boundary conditions

```
pbc         = xyz        ; 3-D PBC
```

; Dispersion correction

```
DispCorr    = EnerPres   ; account for cut-off vdW scheme
```

; Velocity generation

```
gen_vel     = yes         ; assign velocities from Maxwell distribution
gen_temp    = 323         ; temperature for Maxwell distribution
gen_seed    = -1          ; generate a random seed
```

; COM motion removal

; These options remove motion of the monolayer relative to the solvent/ions

```
nstcomm     = 1
```

```
comm-mode   = Linear
```

```
comm-grps   = DPOG SOL_NA
```

NPT equilibration is not used in this simulation to preserve the system size and geometry as the barostat can cause molecules to be distorted and break the monolayer structure.

S7.2 Coupling and centre of motion groups

Index groups for solvent+ions and lipids are created using make_index module:

Create an index for all atoms of the lipids by choosing lipid1|lipid2 etc.. and SOL|NA for all atoms of water and ions, such that it can be used as coupling groups and centre of motion groups.

```
$ gmx make_ndx -f confout_whole.gro -o index.ndx
```

Create a solvate+ions group and a lipid/s group. The new groups are called SOL_NA and DPOG
DPOG is used as the centre of mass motion removal.

Create .tpr file as in EM. Equilibration runs for 100 ps.

- Rcoulmb, rvdw = 1.2: 1.2-nm short range cutoff for electrostatics and van der Walls interaction.
- ref_t,gen_temp = 323, this temperature is above the phase transition temperature for DPPC
- tc-grps = DPOG SOL_NA: each group is coupled separately to increase accuracy. Solvent and ions are coupled together as there insufficient number of degrees of freedom to couple ion separately.
- Centre of mass(COM) motion removal is used for interfacial systems(membrane-water). The motion of the monolayers COM and the solvent COM is reset separately to avoid the phases moving in opposite direction.

Similar to the EM step, .tpr file is created using grompp before invoking mdrun.

```
$ gmx grompp -f nvtmdp -c confout_whole.gro -p topol.popg80.top -n index.ndx -o nvt
```

```
$ gmx mdrun -v -deffnm nvt -nb gpu -nt 1 &
```

As with the EM step, the energy status of the system can be analysed using nvt.edr file. The temperature of the system can be analysed by following command and when prompted by selecting the temperature option.

```
$ gmx energy -f nvt.edr -o temperature_popg80.xvg
```

As can be seen from the plot. The temperature has stabilized about 323 K

S.8. Short MD run

The short MD run for 10 ps is conducted to allow the water molecules to orient around the lipid

heads. Therefore the movement of the monolayers are restrained using strong position restraints $1000000 \text{ kJ mol}^{-1} \text{ nm}^{-2}$ on xyz coordinates. This position restraint is applied to the topology file by including the lines:

```
#ifdef STRONG_POSRES
#include "posre.itp"
#endif
```

And .mdp file:

```
define = -DPOSRES
$ gmx genrestr -f nvt.gro -o posre.itp -fc 100000 100000 100000
```

Choose lipids or non-water as the atoms to be restrained.

S.8.1 Short MD run parameters

```
title      = Pure POPG short MD
define     = -DPOSRES ; position restrain the protein
; Run parameters
integrator = md       ; leap-frog integrator
nsteps     = 5000    ; 2 * 5000 = 10 ps (0.01 ns)
dt         = 0.002   ; 2 fs
; Output control
nstxout    = 1000    ; saving coordinates at 2 ps interval
nstvout    = 1000    ; saving velocities at 2 ps interval
nstxtcout  = 1000    ; xtc compressed trajectory output at 2 ps interval
nstenergy  = 1000    ; saving energies at 2 ps interval
nstlog     = 1000    ; updating log file at 2 ps interval
; Bond parameters
continuation = yes     ; Restarting after NVT
constraint_algorithm = lincs ; holonomic constraints
constraints   = all-bonds ; all bonds are constrained constrained
lincs_iter   = 1        ; LINCS accuracy
lincs_order  = 4        ; also related to accuracy
; Neighborsearching
ns_type     = grid     ; search neighboring grid cels
nstlist     = 5        ; 10 fs
rlist       = 1.2      ; short-range neighborlist cutoff (in nm)
rcoulomb   = 1.2      ; cutoff (in nm) for short-range electrostatic
rvdw        = 1.2      ; cutoff (in nm) for short-range van der Waals interaction
```

```

; Electrostatics
coulombtype = PME      ; Particle Mesh Ewald method for computing long-range electrostatics interactions
pme_order   = 4          ; cubic interpolation
fourierspacing = 0.16    ; grid spacing for FFT

; Temperature coupling is on
tcoupl     = Nose-Hoover      ; More accurate thermostat
tc-grps    = DPOG SOL_NA ; Two coupling groups for increased accuracy
tau_t      = 0.5 0.5        ; time constant, in ps
ref_t      = 323 323        ; reference temperature for each coupling group in Kelvin

; Periodic boundary conditions
pbc        = xyz           ; 3-D PBC

; Dispersion correction
DispCorr   = EnerPres      ; account for cut-off vdW scheme

; Velocity generation
gen_vel    = no            ; Velocity generation is off

; COM motion removal
; These options remove motion of the monolayer relative to the solvent/ions
nstcomm    = 1
comm-mode   = Linear
comm-grps  = DPOG SOL_NA

```

\$ gmx grompp -f pre_md.mdp -c nvt.gro -t nvt.cpt -p topol.popg80.top -n index.ndx -o pre_md

A check point file(nvt.cpt) from the previous step which contains temperature coupling information is included to generate the run input file.

flag -t includes the checkpoint file from the NVT equilibration and -c the coordinate file.

\$ gmx mdrun -v -deffnm pre_md -nb gpu -nt 1 &

S9. Final MD run

After equilibration, the system is stable at the desired temperature,volume and the head groups are immersed in the solvent. The final MD run involves releasing the position restraint on the monolayer and running the simulation for 5 ns. Again a .mdp file that contains parameters for running the simulation is used.

S9.1. Final MD run parameters

```

title      = Pure POPG monolayer at 80 Å²
; Run parameters

```

```

integrator    = md      ; leap-frog integrator
nsteps       = 5000000   ; 1 * 5000000 = 5000 ps (5 ns)
dt          = 0.001    ; 1 fs

; Output control
nstxout     = 1000    ; saving coordinates at 2 ps interval
nstvout     = 1000    ; saving velocities at 2 ps interval
nstxtcout   = 1000    ; xtc compressed trajectory output at 2 ps interval
nstenergy   = 1000    ; saving energies at 2 ps interval
nstlog      = 1000    ; updating log file at 2 ps interval

; Bond parameters
continuation = yes     ; Restarting after short MD run.
constraint_algorithm = lincs ; holonomic constraints
constraints    = all-bonds ; all bonds are constrained
lincs_iter    = 1        ; LINCS accuracy
lincs_order   = 4        ; also related to accuracy

; Neighborsearching
ns_type      = grid    ; search neighboring grid cels
nstlist      = 5        ; 10 fs
rlist        = 1.2      ; short-range neighborlist cutoff (in nm)
rcoulomb    = 1.2      ; cutoff (in nm) for short-range electrostatic interactions
rvdw         = 1.2      ; cutoff (in nm) for short-range van der Waals interactions

; Electrostatics
coulombtype = PME     ; Particle Mesh Ewald method for computing long-range electrostatic interactions
pme_order    = 4        ; cubic interpolation
fourierspacing = 0.16   ; grid spacing for FFT

; Temperature coupling is on
tcoupl      = Nose-Hoover ; More accurate thermostat
tc-grps     = DPOG SOL_NA ; two coupling groups for increased accuracy
tau_t       = 0.5 0.5    ; time constant, in ps
ref_t       = 323 323    ; reference temperature for each coupling groups in Kelvin

; Periodic boundary conditions
pbc         = xyz      ; 3-D PBC

; Dispersion correction
DispCorr    = EnerPres  ; account for cut-off vdW scheme

; Velocity generation
gen_vel     = no       ; Velocity generation is off

; COM motion removal
; These options remove motion of the monolayer relative to the solvent/ions
nstcomm     = 1
comm-mode   = Linear
comm-grps   = DPOG SOL_NA

```

As previously a check point file from the previous step of short MD run.

\$ gmx grompp -f md.mdp -c pre_md.gro -t pre_md.cpt -p topol.popg80.top -n index.ndx -o md

```
$gmx mdrun -v -deffnm md -nb gpu -nt 1 &
& gmx trjconv -s md.tpr -f md.gro -o md_whole.gro -pbc whole -ur compact
```

S10. Analysis

S10.1 Monolayer thickness

S10.1.1 Electron.dat file to include partial charges of molecules

Monolayer thickness can be calculated by obtaining electron density for the head group and tail group of the molecule of interest and calculating the difference between the peaks of the head group and tail. GROMACS density requires an additional file (eg. electrons.dat) that define the number of electrons in each atom for that molecule. Partial charges for the atoms needs to be included, which can be obtained from the topology (.itp) file for the molecule. The first line in electrons.dat is the number of atoms for the specific molecule. POPG has 53 atoms and the rest of the lines defines the atom identifier from the .itp file and the corresponding partial charge is added or subtracted from the number of electrons for each atom. For example H0 has 0.417 in the .itp file therefore the electrons.dat file has the line 'H0 = 1.417'

53

H0 = 1.417

O1 = 7.426

C2 = 6.157

C3 = 6.157

O4 = 7.426

H5 = 1.417

C6 = 6.4

O7 = 7.2

P8 = 16.7

O9 = 7.2

O10 = 7.2

O11 = 7.3

C12 = 6.4

C13 = 6.3

O14 = 7.3

C15 = 6.7

O16 = 7.3

.....

.....

C44 = 6

C45 = 6

C46 = 6

C47 = 6

C48 = 6

C49 = 6

C50 = 6

\$ gmx make_ndx -f md.tpr -o monolayer_thickness.ndx

S10.1.2 Monolayer thickness calculation in GROMACS

Type '2 & a P8' for phosphate headgroup and type 'headgroup' to name the index.

Type '2 & a CA2' for the 34th carbon which is at the farthest from the phosphate for POPG. Type 'tail group' to name the index. For DPPC atom 'N4' is used as the head group and 'C49' as the tail group. For pure PonPG monolayer thickness caluclation, H37 and C45 is used as the head and tail group respectively.

All other index groups in the system can be deleted by typing using 'del' command to leave the just the head groups and tail groups. Optionally any atom can be selected to represent headgroup and tail group.

**\$ gmx density -s md.tpr -f md.xtc -n popg80_thick.ndx -ei electrons_popg.dat -o popg80_head.xvg -d Z
-dens electron**

choose option 11 for the head group indexed in the monolayer_thickness.ndx. Repeat the step to make an electron density for tail group by choosing option 12 this time.

For pure monolayers of DPPC and POPG (system 1&2) electron.dat will contain the corresponding molecule type partial charges.DPPC electrons.dat and POPG are used to calculate the monolayer thickness.

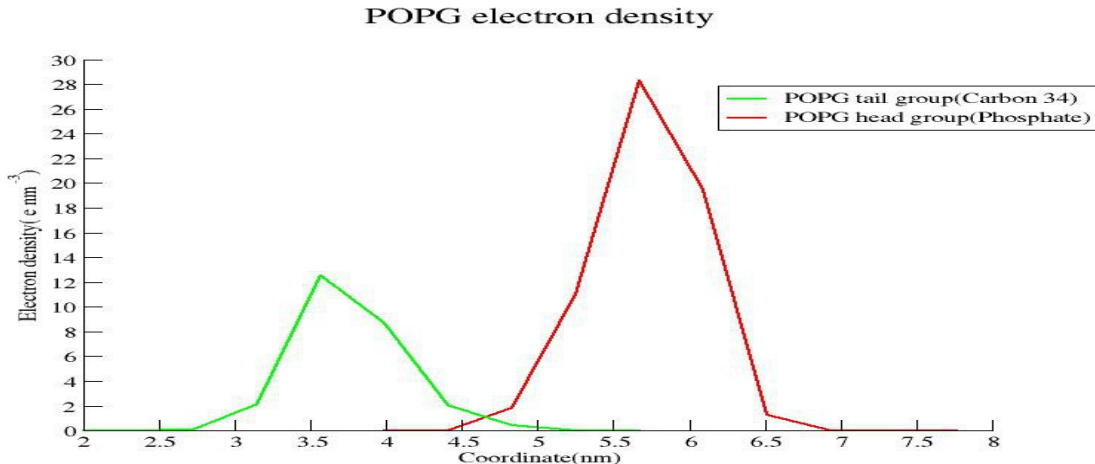


Figure S3. Showing the electron density of selected head group and tail group atom for POPG. There are two pairs of lines for two monolayers of a system.

The average of the pairs of peak difference will be taken to calculate the monolayer thickness.

nm	POPG head	nm	POPG tail
4.83	0.04947	3.15	0.00108178
5.25	3.178	3.57	0.374701
5.67	26.2205	3.99	6.4238
6.09	12.9065	4.41	7.755
6.51	0.350641	4.83	2.59241
6.93	0.00547876	5.25	0.741627
		5.67	0.0319125

Table S1. Showing the coordinates and the electron density of the head and tail atoms for the first pair of peaks in the figure above.

The highest peak for the head group phosphate is at 5.67 nm and for tail Carbon 34 is 4.41. Therefore the monolayer thickness is $5.67 - 4.41 = 1.26$ nm or 12.6 \AA . For the second pair of peaks, this was $15.33 - 17.01 = -1.68$ nm or 16.8 \AA . Therefore the average monolayer thickness for this simulation is $(12.6+16.8)/2 = 14.7 \text{ \AA}$.

S10.1.3. Monolayer thickness using POPG head and tail electron density

System	Monolayer thickness	
	At 80 Å² lipid⁻¹(Å)	At 63 Å² lipid⁻¹(Å)
DPPC:POPG	16.8 ± 0.8	16.8 ± 0.8
DPPC:POPG:OPO	14.7 ± 0.7	14.7 ± 0.7
DPPC:OPO:POPG	14.7 ± 0.8	16.8 ± 0.8

Table S2. Showing the monolayer thickness calculated using the POPG electron density.

S10.2 Order parameter

For deuterium order parameter analysis, the carbons in the acyl chains needs to be indexed separately. The double bonds are not well calculated therefore this will be avoided when indexing.

```
$ gmx make_ndx -f md.tpr -o sn1.ndx
```

Choose atom numbers, which can be found from the topology file that belongs to each chain when prompted by typing:

```
> a C15
> a C17
> a C18
.....
.....
> a C31
> a CA1
> a CA2
del 0-21 ; this deletes all other groups in the system.
> q
```

Do the same for the second chain.

To measure deuterium order parameters with the normal to the monolayers along the Z-axis:

```
$ gmx order -s md.tpr -f md.xtc -n sn1.ndx -d z -od deuter_popg_sn1.xvg
```

repeat the step for the second chain.

S10.3. Diffusion of lipids into the water

A python script (see **In house scripts** in appendix) was written to calculate the movement of atoms

from before and after simulation. The script takes two files as input one for before simulation and one for after simulation. User is required to specify the residue of interest and the atom of interest at the terminal separated by a space. The user is required to specify the normal plane (Z-dimension) at which the selected atom type is located for the before simulation file. This is because there are two monolayers for the slab geometry and there is a range (1 nm) for the atoms to be spread around in the before simulation file. This is useful if initial configuration files are made using geometric packing tools such as Packmol which randomly places the atoms within a range specified.

S10.4. Acyl-chain reversal

Used the same script in S10.3, but with a minor modification of changing the Z-dimension of the interphase plane and renaming the output (.csv) file.

S11. In house scripts

S11.1 Python script used for head group movement and acyl-chain reversal

The user can use the script by typing as follows (example):

\$ python script.py -r DPPC -a P8 -l 5.4 -u 15.8 -d Z -o script.csv

The script requires specific order to its command-line arguments. They are:

-r – reference residue, DPPC in the case above

-a – reference atom, P8 in the case above

-l – lower reference plane where the atoms are expected in the initial configuration file, 5.4 nm in the case above

-u – upper reference plane where the atoms are expected in the intial configuration file, 15.8 nm in the case above

-d – dimension for computing the difference of atom coordinates, Z in the case above

-o – output file

When computing the difference in X and Y dimension -l and -u is not used. The user will also have to specify the data directory (data_dir) and input files (solvated_file_name, md_file_name) manually.

```
#!/usr/bin/python
```

```
import numpy as np
```

```

import re
import csv
import sys,getopt

# Directory and input files for comparison
data_dir = '/Users/merrilmathew/Dropbox/md/dppc_opo80/'

solvated_file_name = 'solvated_ions.gro'
md_file_name = 'md.gro'

solvated_f = open(data_dir + solvated_file_name,'rb')
md_f = open(data_dir + md_file_name,'rb')
solvated_lines = solvated_f.readlines()[2:-1]
md_lines = md_f.readlines()[2:-1]
assert len(solvated_lines)==len(md_lines)

# Declaring variables and methods to store user input values from command line
lower_z_atom_plane = ""
upper_z_atom_plane = ""
outfile = ""
dimension = ""
ref_residue = ""
ref_atom = ""

# Declaring lists to store specific lines of the residue and atom from the two files to compare. Declaring lists to store the
coordinates of the XYZ dimension of interest from the files.
solvated_list = []
md_list = []
solvated_cord = []
md_cord = []

# Command line user input argument fetching and storing
def main(argv):
    try:
        opts,args = getopt.getopt(argv,"hr:a:l:u:d:o:",
["help","res","atom","lower_plane","upper_plane","dimension","ofile="])
        except getopt.GetoptError:
            print 'test.py -o <outputfile>'
            sys.exit(2)
        for o, a in opts:

```

```

if o == '-h':
    print 'test.py -o <outputfile>'

elif o in ("-r","--res"):
    global ref_residue
    ref_residue = a

elif o in ("-a","--atom"):
    global ref_atom
    ref_atom = a

elif o in("-l","--lower_plane"):
    global lower_z_atom_plane
    lower_z_atom_plane = float(a)

elif o in("-u","--upper_plane"):
    global upper_z_atom_plane

elif o in("-d","--dimension"):
    global dimension
    dimension = a

elif o in ("-o", "--ofile"):
    global outfile
    outfile = a

if __name__ == "__main__":
    main(sys.argv[3:])

# Regular expression to match all the lines contains the reference residue and atom
def reg_search(str):

    my_regex = r'^.*' + re.escape(ref_residue) + r'.*\b' + re.escape(ref_atom) + r'\b.*$'

    match = re.search(my_regex,str,re.IGNORECASE)
    return match;

for atom_idx_sol, atom_idx_md in zip(solvated_lines,md_lines):

    matchObj_sol = reg_search(atom_idx_sol)
    matchObj_md = reg_search(atom_idx_md)
    if matchObj_sol:
        solvated_list.append(atom_idx_sol)
    if matchObj_md:

```

```

    md_list.append(atom_idx_md)

# Store all the xyz coordinates of solvated_list into solvated_cord
for atom_idx in range(len(solvated_list)):
    solvated_line = solvated_list[atom_idx].split()
    solvated_cord.append(map(lambda x:float(x),solvated_line[3:6]))

# Store all the xyz coordinates of md_list into md_cord

for atom in range(len(md_list)):
    md_line = md_list[atom].split()
    md_cord.append(map(lambda x: float(x),md_line[3:6]))


# If the user input for the dimension is X then compute the difference between the coordinates of the same atom and
# store into x_diffs.
x_diffs =[]

if dimension == 'X':
    for atom_idx in range(len(md_cord)):
        x_diffs.append(md_cord[atom_idx][0]-solvated_cord[atom_idx][0])
        f = open(str(outfile),'a')
        wtr = csv.writer(f,delimiter= '\t')
        for atom_idx in range(len(x_diffs)):
            atom_num = atom_idx
            dist = x_diffs[atom_idx]
            wtr.writerow((atom_num, "%.3f" % dist))

# If the user input for the dimension is Y then compute the difference between the coordinates of the same atom and
# store into x_diffs
elif dimension == 'Y':
    for atom_idx in range(len(md_cord)):
        x_diffs.append(md_cord[atom_idx][1]-solvated_cord[atom_idx][1])
        f = open(str(outfile),'a')
        wtr = csv.writer(f,delimiter= '\t')
        for atom_idx in range(len(x_diffs)):
            atom_num = atom_idx
            dist = x_diffs[atom_idx]
            wtr.writerow((atom_num, "%.3f" % dist))

```

```
# If the user input for dimension (-d) is Z then split the coordinates into lower monolayer/plane (-l) and upper monolayer/plane(-u) and store into lists.
```

```
elif dimension == 'Z':
```

```
    lower_idxs = []
    for atom_idx in range(len(solvated_cord)):
        if np.abs(solvated_cord[atom_idx][2]-lower_z_atom_plane)<1:
            lower_idxs.append(atom_idx)
```

```
# Checking if the z-coordinates of the atoms is within a range of the upper plane, i.e the second plane of the slab and storing into list.
```

```
    upper_idxs = []
    for atom_idx in range(len(solvated_cord)):
        if np.abs(solvated_cord[atom_idx][2]-upper_z_atom_plane)<1:
            upper_idxs.append(atom_idx)
```

```
# Checking if all atoms are stored into upper and lower plane lists from the previous two steps
```

```
assert len(lower_idxs) + len(upper_idxs) == len(solvated_cord)
```

```
lower_solvs = [solvated_cord[idx] for idx in lower_idxs]
```

```
upper_solvs = [solvated_cord[idx] for idx in upper_idxs]
```

```
lower_mds = [md_cord[idx] for idx in lower_idxs]
```

```
upper_mds = [md_cord[idx] for idx in upper_idxs]
```

```
lower_dists = []
```

```
lower_trans = []
```

```
# Computing and storing the distance between the atom coordinates from the two files in the lower monolayer/plane and storing the sign of change to detect the direction of movement.
```

```
for atom_idx in range(len(lower_solvs)):
    z_solv = lower_solvs[atom_idx][2]
    z_md = lower_mds[atom_idx][2]
    lower_dists.append(np.abs(z_solv-z_md))
    lower_trans.append([(z_solv-lower_z_atom_plane),(z_md-lower_z_atom_plane)])
```

```
# Printing the average distance moved by the reference residue and atom and the direction of the movement to standard output.
```

```
print"\nAverage movement in lower monolayer: ", sum(lower_dists)/len(lower_dists)
```

```

x = np.asarray(lower_trans)
initial_pos = sum(x[:,0])
final_pos = sum(x[:,1])
if initial_pos < 0:
    print " Atom started from Air/Water interface"
elif initial_pos > 0:
    print " Atom started from Air/Water interface"
if final_pos < 0:
    print "Atom moved towards Air"
elif final_pos > 0:
    print "Atom moved towards Water"

# Computing and storing the distance between the atom coordinates from the two files in the upper monolayer/plane
and storing the sign of change to detect the direction of movement.

upper_dists = []
upper_trans = []
for atom_idx in range(len(upper_solv)):
    z_solv = upper_solv[atom_idx][2]
    z_md = upper_mds[atom_idx][2]
    upper_dists.append(np.abs(z_solv-z_md))
    upper_trans.append([(z_solv-upper_z_atom_plane),(z_md-upper_z_atom_plane)])  

print"\nAverage movement in upper monolayer: ", sum(upper_dists)/len(upper_dists)
y = np.asarray(upper_trans)
initial_pos1 = sum(y[:,0])
final_pos1 = sum(y[:,1])
if initial_pos1 < 0:
    print " Atom started from Air/Water interface"
elif initial_pos1 > 0:
    print " Atom started from Air/Water interface"
if final_pos1 < 0:
    print "Atom moved towards Water"
elif final_pos1 > 0:
    print "Atom moved towards the Air"

# writing the atom number, distance moved, intial position and final position to a CSV file.
f = open(str(outfile),'a')
wtr = csv.writer(f,delimiter='\t')
for atom_idx in range(len(lower_solv)):
    atom_num = atom_idx

```

```

dist_lower = lower_dists[atom_idx]
initial = x[atom_idx][0]
final = x[atom_idx][1]
wtr.writerow((atom_num, "%.3f" % dist_lower, "%.3f" % initial, "%.3f" % final))
for atom_idx in range(len(upper_solv)):
    dist_upper = upper_dists[atom_idx]
    initial1 = y[atom_idx][0]
    final1 = y[atom_idx][1]
    wtr.writerow((atom_idx, "%.3f" % dist_upper, "%.3f" % initial1, "%.3f" % final1))

```

S11.2. Perl script used to remove water molecules above the head groups

```

#!/usr/bin/perl -w
use strict;
use File::Slurp;

# Declaring file names for the out files
my $output = 'solv.gro';
my $output1 = 'solv1.gro';
my $output2 = 'sol_removed.gro';

# Opening file handlers for output files
open my $outfile,'>', $output or die "Cant write to $output: $!";
open my $outfile1,'>', $output1 or die "Cant write to $output: $!";
open my $outfile2,'>', $output2 or die "Cant write to $output: $!";

# Reading all the lines from the file and storing into an array
my @array = read_file('solute.gro');

# Avoiding all the lines that contains SOL atoms and printing the rest to an outfile named solv.gro. This stores the
# number of atoms line, all the lines of lipid atoms, and box dimension.
for my $line(@array){
    next if($line =~ m/^ *SOL */);
    print $outfile $line;
}

# All the lines that contain SOL is searched using regular expression to identify the z coordinates that is within the intial
# water box. If the water atom line has z coordinate less than 15.8 nm or greater than 5.4 nm, it is pushed to a hash. All
# other water atom lines are printed to another file named sol_removed.gro.

```

```

my %count;
for my $line(@array){

    if($line =~ m/^$s*(\d+)SOL\s+[HW|OW].*$s+-?\d+\.d+\s+-?\d+\.d+\s+(-?\d+\.d+)\$/){
        if(($2 <= 15.8) && ($2 >= 5.4)){
            push(@{$count{$1}}, $line);
        }
        else{
            print $outfile2 $line;
        }
    }
}

# From the Hash structure that stored all the water atom line within the set of z planes, water molecules that have three atoms is printed to an outfile named solv1.gro, the rest is printed to an outfile names sol_removed.gro. This make sure that there are no broken water molecules for next steps.

my $count = 0;
foreach my $key(keys %count){
    if(scalar(@{$count{$key}})==3){
        print $outfile1 @{$count{$key}};
        $count++;
    }
    elsif(scalar(@{$count{$key}})<3){
        print $outfile2 @{$count{$key}};
    }
}
# Printing the total number of water molecule atoms that is kept. i.e the number of lines in solv1.gro
print $count;

```

S12. Experimental comparison

S12.1. Pure water simulation

The surface tension of the SPC water model at 300K equals 54.7mN m⁻¹[1], therefore the surface pressure acting at the lipid monolayer. Another study reported surface tension of water at 53.4mN m⁻¹.[2] SPC-F and SPC-G water models by Tironi et al and SPC-Fw model by Wu et al incorporated harmonic bond-stretching and angle potentials into SPC water model. SPC-Fd by Dang and Pettitt used a harmonic bond-stretching potential and the Urey-Bradley angle potential with SPC. SPC-G and SPC-F shows a reasonable agreement of surface tension at 300 K at 54 and 52.5 mN m⁻¹ respectively. Whereas SPC-Fw and SPC-Fd does note with 63.4 and 62.1 mN m⁻¹

respectively. [3] A system of water with 5nm XYZ is simulated at 300 K for 10 ns. The average surface tension over 10 ns is 50.78 mN m^{-1} , which is lower than the values found in literature, however the surface tension calculated has a large fluctuation during the simulation time frame.

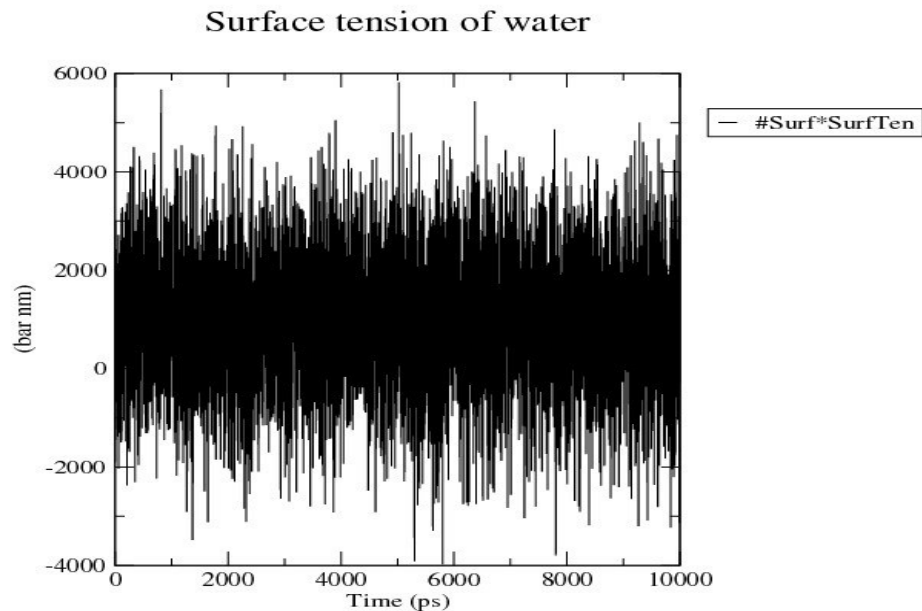


Figure S4. Showing the fluctuations in the surface tension of the pure Air/water interface at 300 K. The measurement is in bar/nm for two interfaces. The average value is obtained by the average of the surface tension in the figure and dividing by 2 and multiplying by 0.1 for mN/m.

The surface pressure of pure Air/Water interface depends on the temperature. There are no water model that can reproduce the experimental data across the whole temperature range, however some are closer to the experimental values.

S12.2. Surface tension value from simulations

Surface tension value can be extracted from the energy file(.edr) using the energy module in GROMACS.

```
$ gmx energy -f md.edr -o surface_tension.xvg
```

choose the number for the Surface tension value, alternatively the pressure tensor in the XYZ dimensions can be used to calculate the surface tension value. Gromacs uses bar nm^{-1} . Since the simulated system contains tow interphases normal to monolayer, a conversion is used to derive mN

m^{-1} . The value calculated by GROMACS has been devided by two and then times by 0.1.

S12.3.1 Comparison of pressure-area isotherms

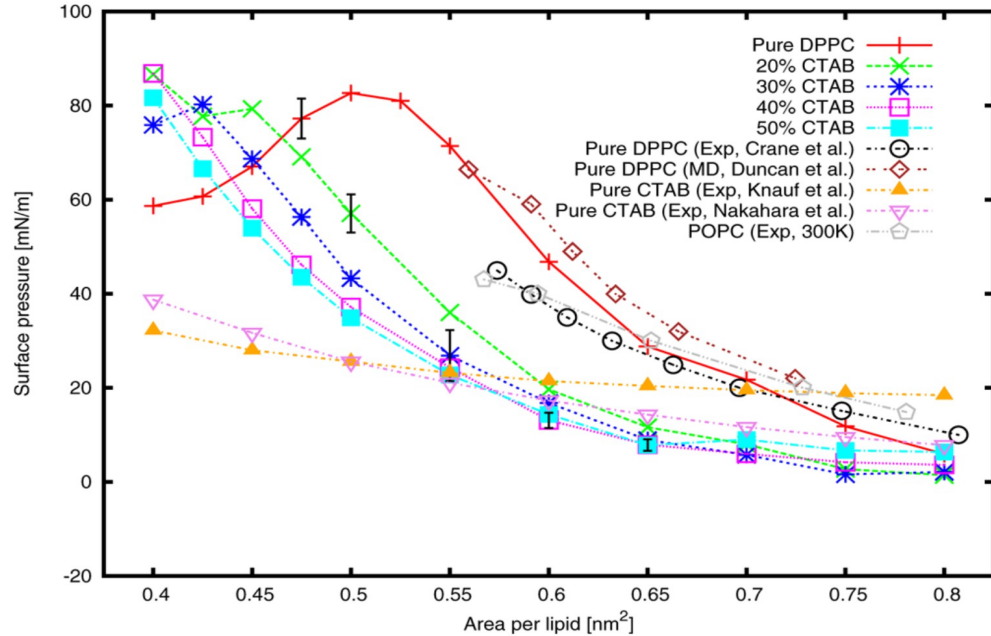


Figure S5. Shows the surface pressure isotherm for the pure DPPC monolayers from experimental and MD studies at 323 K except POPC (Exp,300 K), image taken from B.Liu et al, 2014. [4]

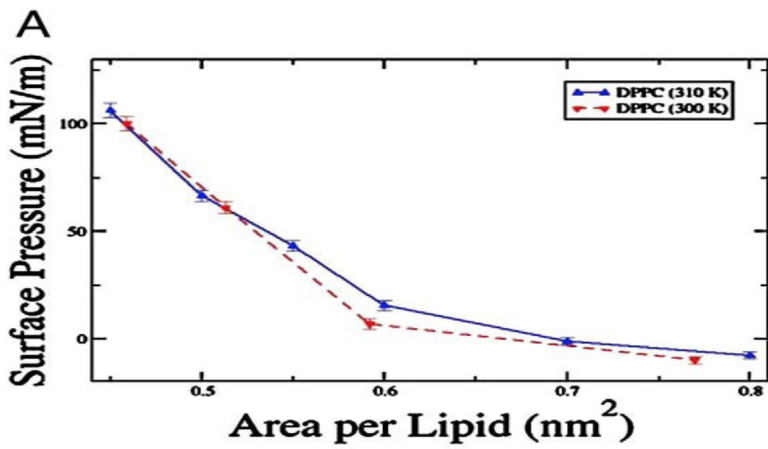


Figure S6. Showing the effect of temperature on surface pressure on DPPC monolayers. Image taken from D.Rose et al, 2008. [5]

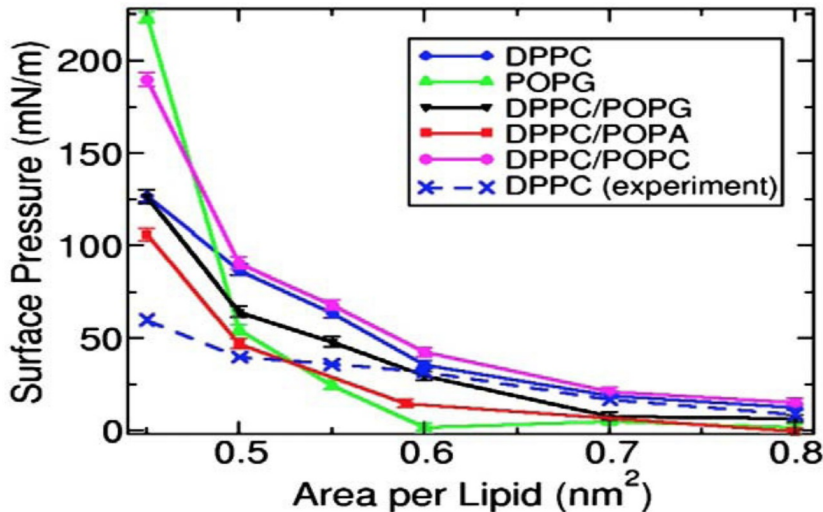


Figure S7. Pressure area isotherms for different lipid groups at 310 K. Image taken from D.Rose et al, 2008. [5]

S12.4.1. Comparison of order parameter values

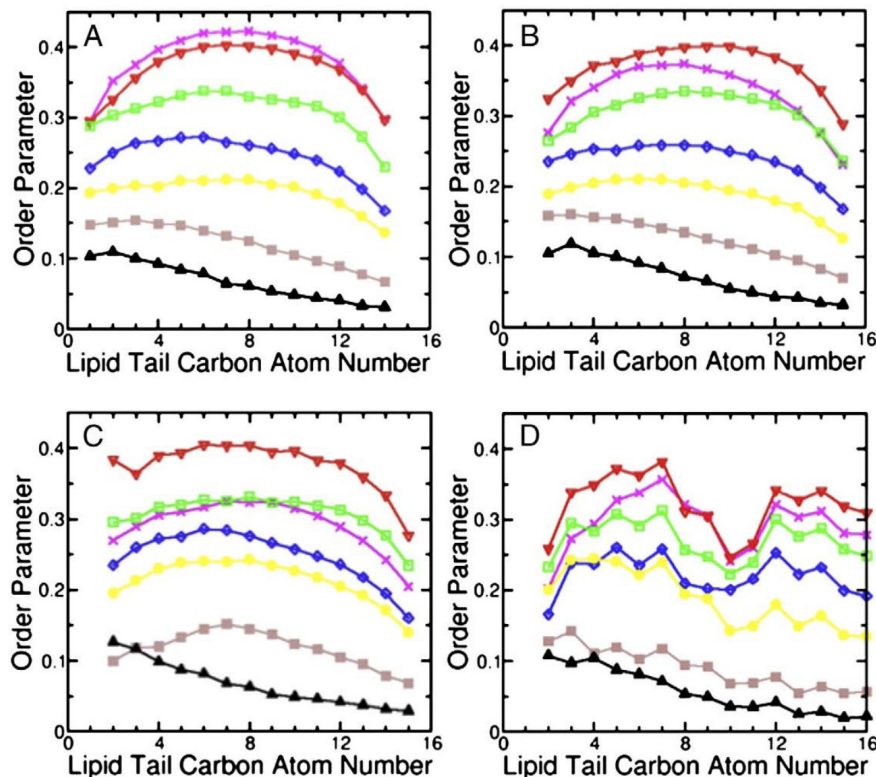


Fig. 5. Lipid chain order parameter profiles for lipids at 0.40 (magenta), 0.45 (red), 0.50 (green), 0.55 (blue), 0.60 (yellow), 0.70 (brown), 0.80 (black) nm²/lipid. A) DPPC in the pure DPPC monolayer and B) DPPC, C) POPG chain 1, D) POPG chain 2 in the 7:3 DPPC/POPG monolayer. (For interpretation of the references to colour in this figure legend, the reader is referred to the web version of this article.)

Figure S8. Showing the order parameter values of DPPC and POPG acyl-chains in 7:3 concentration. Image taken from D.Rose et al, 2008. [5]

S13. Forcefield parameter file of PonPG**[moleculetype]**

; Name nrexcl

OPO 3

[atoms]

;	nr	type	resnr	residu	atom	cgnr	charge	mass
1	LH1	1	OPO	C1	1	0.1570	13.0190 ; qtot:0.76	
2	LH1	1	OPO	C2	1	0.1570	13.0190 ; qtot:0.76	
3	OA	1	OPO	O3	0	-0.5740	15.9994 ; qtot:0.72	
4	OA	1	OPO	O4	0	-0.5740	15.9994 ; qtot:0.72	
5	LC2	1	OPO	C5	2	0.4000	14.0270 ;	
6	LOS	1	OPO	O6	2	-0.800	15.9994 ; qtot:0.54	
7	LP	1	OPO	P7	2	1.700	30.9738 ; qtot:2.3	
8	LOM	1	OPO	O8	2	-0.800	15.9994 ; qtot:1.5	
9	LOM	1	OPO	O9	2	-0.800	15.9994 ; qtot:1.5	
10	LOS	1	OPO	O10	2	-0.700	15.9994 ; qtot:0	
11	LC2	1	OPO	C11	3	0.400	14.0270 ; qtot:0.08	
12	LH1	1	OPO	C12	3	0.300	13.0190 ; qtot:0.52	
13	LC2	1	OPO	C13	21	0.50	14.0270 ; qtot:	
14	LOS	1	OPO	O14	3	-0.700	15.9994 ; qtot:-0.14	
15	LOS	1	OPO	O15	21	-0.70	15.9994 ; qtot:	
16	LC	1	OPO	C16	21	0.70	12.0110 ; qtot:	
17	LO	1	OPO	O17	21	-0.70	15.9994 ; qtot:	
18	LC	1	OPO	C18	3	0.80	12.0110 ; qtot:0.56	
19	LO	1	OPO	O19	3	-0.600	15.9994 ; qtot:0.0	
20	LP2	1	OPO	C20	4	0.0	14.0270 ; qtot:	
21	LP2	1	OPO	C21	9	0	14.0270 ; qtot:	
22	LP2	1	OPO	C22	10	0	14.0270 ; qtot:	
23	LP2	1	OPO	C23	22	0	14.0270 ; qtot:	
24	LP2	1	OPO	C24	23	0	14.0270 ; qtot:	
25	LP2	1	OPO	C25	24	0	14.0270 ; qtot:	
26	LP2	1	OPO	C26	25	0	14.0270 ; qtot:	
27	LP2	1	OPO	C27	26	0	14.0270 ; qtot:	
28	LP2	1	OPO	C28	27	0	14.0270 ; qtot:	
29	LP2	1	OPO	C29	28	0	14.0270 ; qtot:	
30	LC	1	OPO	C30	18	0.530	12.0110 ; Khabiri et al	
31	LP2	1	OPO	C31	29	0	14.0270 ; qtot:	
32	LP2	1	OPO	C32	30	0	14.0270 ; qtot:	
33	LP2	1	OPO	C33	31	0	14.0270 ; qtot:	

34 LP2 1 OPO C34 5 0 14.0270 ; qtot:
 35 LP2 1 OPO C35 6 0 14.0270 ; qtot:
 36 H 1 OPO H36 0 0.4170 1.0080 ; qtot:0.36
 37 H 1 OPO H37 0 0.4170 1.0080 ; qtot:0.36
 38 LO 1 OPO O38 19 -0.530 15.9994 ; from Khabiri et al
 39 LP2 1 OPO C39 8 0 14.0270 ; qtot:
 40 LP2 1 OPO C40 33 0 14.0270 ; qtot:
 41 LP2 1 OPO C41 34 0 14.0270 ; qtot:
 42 LP2 1 OPO C42 35 0 14.0270 ; qtot:
 43 LP3 1 OPO C43 36 0 15.0350 ; qtot:
 44 LP3 1 OPO C44 36 0 15.0350 ; qtot:
 45 LP3 1 OPO C45 36 0 15.0350 ; qtot:

[bonds]

; ai aj funct c0 c1 c2 c3

36 3 2 gb_1
 37 4 2 gb_1
 1 2 2 gb_27
 2 4 2 gb_18
 1 3 2 gb_18
 1 5 2 gb_27
 5 6 2 gb_18
 6 7 2 gb_28
 7 8 2 gb_24
 7 9 2 gb_24
 7 10 2 gb_28
 10 11 2 gb_18
 11 12 2 gb_27
 12 13 2 gb_27
 12 14 2 gb_18
 14 16 2 gb_10
 16 17 2 gb_5
 16 23 2 gb_23
 23 24 2 gb_27
 24 25 2 gb_27
 25 26 2 gb_27
 26 27 2 gb_27
 27 28 2 gb_27
 28 29 2 gb_27
 29 30 2 gb_27
 30 38 1 0.12300E+00 502080.0 ; from oliec.itp

```

13 15 2 gb_18
15 18 2 gb_10
18 19 2 gb_5
18 20 2 gb_23
20 32 2 gb_27
32 33 2 gb_27
33 34 2 gb_27
34 35 2 gb_27
35 21 2 gb_27
21 22 2 gb_27
22 31 2 gb_27
31 39 2 gb_27
39 40 2 gb_27
40 41 2 gb_27
41 42 2 gb_27
42 43 2 gb_27
43 44 2 gb_27
44 45 2 gb_27

```

[pairs]
; ai aj funct

```

3 4 1
4 5 1 5.670071e-04 9.118883E-07 ;ffgmxnb.itp
2 6 1
3 6 1 2.827125e-04 1.321084e-07 ;ffgmxnb.itp
1 7 1

```

```

5 8 1
5 9 1
5 10 1
6 11 1
7 12 1
8 11 1
9 11 1
10 14 1
10 13 1
11 16 1
11 15 1
12 18 1

```

12 17 1
 12 23 1
 14 24 1
 14 15 1
 16 25 1
 16 13 1
 17 24 1
 23 26 1
 24 27 1
 25 28 1
 26 29 1
 27 30 1
 28 38 1 ; pair with new carbonyl oxygen
 13 19 1
 13 20 1
 15 32 1
 18 33 1
 19 32 1
 20 34 1
 32 35 1
 33 21 1
 34 22 1
 35 31 1
 21 39 1
 22 40 1
 31 41 1
 39 42 1
 40 43 1
 41 44 1
 42 45 1

[angles]

	ai	aj	ak	funct	c0	c1	c2	c3
36	3	1	2	ga_12				
37	4	2	2	ga_12				
3	1	2	2	ga_13				
1	2	4	2	ga_13				
2	1	5	2	ga_13				
3	1	5	2	ga_13				
1	5	6	2	ga_13				

5 6 7 2 ga_26
6 7 8 2 ga_14
6 7 9 2 ga_14
6 7 10 2 ga_5
7 10 11 2 ga_26
8 7 9 2 ga_29
8 7 10 2 ga_14
9 7 10 2 ga_14
10 11 12 2 ga_15
11 12 14 2 ga_13
11 12 13 2 ga_13
12 14 16 2 ga_22
12 13 15 2 ga_15
14 12 13 2 ga_13
14 16 17 2 ga_31
14 16 23 2 ga_16
16 23 24 2 ga_15
17 16 23 2 ga_35
23 24 25 2 ga_15
24 25 26 2 ga_15
25 26 27 2 ga_15
26 27 28 2 ga_15
27 28 29 2 ga_15
28 29 30 2 ga_15
29 30 38 1 121.0 502.1 ; from oleic.itp
13 15 18 2 ga_22
15 18 19 2 ga_31
15 18 20 2 ga_16
18 20 32 2 ga_15
19 18 20 2 ga_35
20 32 33 2 ga_15
32 33 34 2 ga_15
33 34 35 2 ga_15
34 35 21 2 ga_15
35 21 22 2 ga_15
21 22 31 2 ga_15
22 31 39 2 ga_15
31 39 40 2 ga_15
39 40 41 2 ga_15
40 41 42 2 ga_15

```

41 42 43 2 ga_15
42 43 44 2 ga_15
43 44 45 2 ga_15
[ dihedrals ]
; ai aj ak al funct c0          c1          c2          c3          c4          c5
37 4 2 1 1 gd_23
36 3 1 5 1 0.0 1.255 3 ; standard Gromacs parameter
3 1 5 6 1 0.0 2.092 2 ; standard Gromacs parameter
4 2 1 3 1 0.0 2.092 2 ; standard Gromacs parameter
4 2 1 5 1 gd_34
4 2 1 5 1 0.0 0.418 2 ; standard Gromacs parameter
2 1 3 36 1 gd_23
2 1 5 6 1 gd_34
2 1 5 6 1 gd_34

```

References for supplementary information

- [1] C.Vega, E. de Miguel. Surface tension of the most popular models of water by using the test-area simulation method. *The Journal of Chemical Physics* 126. pp.1-10(2007).
- [2] F. Chen, P.E. Smith. Simulated surface tensions of common water models. *J.Chem. Phys.* 126 (2007) 221101.
- [3] P.K.Yuet, D.Blankschtein. Molecular Dynamicis Simulation Study of Water Surfaces: Comparison of Flexible water Models. *J.Phys.Chem.B* 114.pp.13786-13795(2010)
- [4] B.Liu et al. Molecular Dynamics Simulations of DPPC/CTAB Monolayers at the Air/Water Interface. *J.Physical Chemistry B* 118. pp.11723-11737(2014)
- [5] D.Rose et al. Molecular dynamics simulations of lung surfactant lipid monolayers. *Biophysical Chemistry* 138.pp 67-77(2008)